The Role of the Human Nasal Cavity in Patterns of Craniofacial Covariation and Integration

by

Joshua A. Lindal

A Thesis submitted to the Faculty of Graduate Studies of

The University of Manitoba

in partial fulfilment of the requirements of the degree of

MASTER OF ARTS

Department of Anthropology

University of Manitoba

Winnipeg

Copyright © 2015 by Joshua Lindal

Abstract

Climate has a selective influence on nasal cavity morphology. Due to the constraints of cranial integration, naturally selected changes in one structure necessitate changes in others in order to maintain structural and functional cohesion. The relationships between climate and skull/nasal cavity morphology have been explored, but the integrative role of nasal variability within the skull as a whole has not. This thesis presents two hypotheses: 1) patterns of craniofacial integration observed in 2D can be reproduced using 3D geometric morphometric techniques; 2) the nasal cavity exhibits a higher level of covariation with the lateral cranial base than with other parts of the skull, since differences in nasal morphology and basicranial breadth have both been linked to climatic variables. The results support the former hypothesis, but not the latter; covariation observed between the nasal cavity and other cranial modules may suggest that these relationships are characterized by a unique integrative relationship.

Acknowledgments

Thanks to: my committee, Mirjana Roksandic, Robert Hoppa, and Bruce Bolster; Dr. Djurdja Bracanovic (Radiology Department, Belgrade University); Dr. F. Gigi Osler (St. Boniface Hospital); Jeff Babb (Department of Mathematics and Statistics, University of Winnipeg); Dejana Nikitovic (University of Toronto); and to the subjects who agreed to the use of their scans. This research was supported by an NSERC Alexander Graham Bell Canadian Graduate Scholarship (reference no. 155719599) and an NSERC Discovery Grant held by Mirjana Roksandic (371077-2010).

Table of Contents

List of Tables

List of Figures

Chapter 1: Introduction

The skull is an extremely complex structure that is implicated in virtually all of a vertebrate's vital functions on a day-to-day and minute-to-minute basis. In the human lineage, the cranial components responsible for these vital roles have been shaped by natural selection and other evolutionary forces into the distinct and unique human morphology, which can be described in general terms as the result of evolutionary trends towards increasing encephalization, reduction of the dentition and masticatory apparatus, and reduction and retraction of the face. However, due to the compact and spatially-efficient nature of the skull, evolutionary forces cannot act to change the shape of one part of the skull without necessitating shape changes in connected parts, in order to maintain structural and functional cohesion. This concept is referred to as *cranial integration*, and it has been the subject of substantial anthropometric scrutiny in recent decades (e.g. Ross and Henneberg 1995; Lieberman and McCarthy 1999; McCarthy 2001; Lieberman et al. 2000a, 2000b, 2002, 2004, 2008; Lieberman 2011; Bastir and Rosas 2006, Bastir et al. 2008, 2009, 2011, 2013). For this reason, interpretations of evolutionary shape changes in particular cranial structures must be made within the context of their integrative relationships with the rest of the skull.

Because of humans' wide geographic range and occupation of diverse environments, it is reasonable to expect that differences in climate, and especially temperature, have exerted selective pressures on our cranial anatomy. The physical implications of size/volume relationships on body heat conservation have been long understood (Allen's and Bergman's rules; Bernstein 2010), and have been invoked to explain differences in body proportions between modern human populations, as well as to explain body proportions of the Neanderthals, who occupied Ice-Age Eurasia.

Heat conservation has been put forward to explain population differences in cranial

proportions among modern humans (Beals et al. 1983, 1984), and the relationship between temperature/climate and other aspects of skull shape has been explored with mixed results (Steegman 1970; Harvati and Weaver 2006). Among the structures of the skull, it can be argued that the internal nasal cavity should be under the greatest selective pressure from climate/temperature, since its role is to mediate interactions between the external environment (air) and the inside of the body (lungs) by warming and humidifying inspired air (Lieberman 2011). Significant covariation between nasal cavity morphology and temperature has been reported (Noback et al 2011), and adaptation to cold climates has also been proposed to explain the unique morphology of the Neanderthal cranial airways (Holton and Franciscus 2008; Franciscus 2003). However, without considering nasal cavity variation in the context of its integrative relationships with the rest of the skull, functional selective explanations are at risk of being merely "just so" stories.

The relationship between brain size, cranial base morphology, and facial shape have been studied elsewhere, and it is apparent that ontogenetic and epigenetic interactions between the brain and the cranial base have a significant influence on the shape of the developing face (Boughner et al. 2008; Young et al. 2010; Bastir et al. 2010). Additionally, the relationship between the nasal airways and the midface has been explored, in order to address questions of modularity in the nasal cavity (Bastir ad Rosas 2013). However, the integrative relationship between the nasal airways and the cranial base has not been explored. In order to investigate the integrative context of the nasal cavity within the skull overall, as well as the potential relationships between cold-climate morphologies in the nasal cavity and cranial base, this study will consist of a series of landmark-based geometric morphometric analyses (principal components analysis and partial least squares) on a sample of modern human cranial CT scans from medical contexts. These analyses are aimed

at testing two hypotheses:

1. *Patterns of integration between the face and cranial base that have been demonstrated in 2D can be replicated in 3D*. Bastir and Rosas (2006) and Gkantidis and Halazonetis (2011), using 2D lateral radiographs, found higher levels of integration between the lateral cranial base and face than between the midline cranial base and face. While the midline cranial base is traditionally conceptualized as a two dimensional angle in the anteroposterior plane, the lateral cranial base and face may both comprise substantial variation in the breadth dimension, which is not observable using lateral radiographs; 2D analyses of integration may overemphasize these integrative relationships if the covariation observable in the anteroposterior and superoinferior dimensions is much stronger than covariation in the mediolateral dimension. Furthermore, understanding the 3D shape relationships between the cranial fossae (endocranial lateral cranial base) and the face can help elucidate the integrative relationships between the brain and face.

2. *The integrative relationship between the lateral cranial base and the internal nasal cavity is stronger than the relationships either module share with either the face or with the midline cranial base*. Since the cranial breadth (across the lateral cranial base) and nasal cavity morphology have been independently linked to adaptation to cold climates, it is likely that these shape changes could be the result of physical or developmental integrations between the two modules. Face shape has been shown to covary more strongly with the lateral cranial base then the midline base, but the degree of covariation between the nasal cavity alone and the lateral cranial base has not been established. This hypothesis is based on the premise that these purported cold adaptation morphologies are either a) independent adaptations, which may be ontogenetically unrelated and may not exhibit any pattern of covariation, or b) result from a common integrative pathway,

possibly representing an adaptation and spandrel, or the pleiotropic effects of some regulator gene (i.e. selection may only be operating on one module, while secondary shape changes in the other result from physical or developmental integration).

This hypothesis can only establish the patterns of covariation between the nasal cavity and cranial base; in the absence of a specific cold-climate sample population or Pleistocene hominin population, if any pattern of covariation is observed, it will not be possible to address the evolutionary or selective basis for that pattern. However, the results of this study can serve as a foundation to address these questions in the future: establishing the integrative relationship between these modules will help to determine the way natural selection should be expected to be able to operate – whether apparent cold-climate morphologies could be expected to be the result of selection operating on different modules independently, or whether we should be expecting adaptations in one module to be accompanied by secondary integrative changes in another.

Finally, because this thesis will draw from several different geometric morphometric analyses, substantial space will be devoted to assessing morphometric methodologies. With advances in computer technologies in recent decades, landmark-based geometric morphometric techniques have become commonplace in osteometry, but due to the nature of skeletal variation, there has been little standardization regarding landmark selection. The potential implications of differences in landmark selection methodology, in previous studies as well as this one, will be discussed.

Chapter 2: Literature Review

Modularity and Integration

The cranium is composed of many individual bones, and it is easy to think of a skeleton in terms of its skeletal components alone, but to do so is to lose sight of the forest for the trees. Heads are composed of skeletal, muscular, epithelial, nervous, and all manner of other tissues, which combine to form *functional modules* (Moss and Salentijn 1969) that perform specific vital roles – vision, olfaction, respiration, mastication, speech, etc. – and these units are tightly and seamlessly packed into a relatively small space. The term *modularity* is used in biology to describe the relative independence of a group of anatomical components, which collectively serve a common functional role, from other such modules (Mitteroecker and Bookstein 2008), and the morphology of skeletal components is inseparable from the overall morphologies of these modules of which they are a part. Somewhat counterintuitively, perhaps, to the biological anthropologist who spends the majority of time considering dry bones in isolation, the morphology of cranial bones is the secondary result of shape changes in their functional modules (Moss and Salentijn 1969); cranial bones largely grow passively in response to primary shape changes within functional modules, providing structure and support almost as an (evolutionary) afterthought, as growth in the module as a whole determines their overall shape. Because several distinct bones may contribute to the structure of a single module, and different parts of a single bone may contribute to the structures of more than one functional module, it is more biologically meaningful to consider the skeletal contributions to each module collectively, rather than to consider individual bones in isolation.

Modularity is implicated in both ontogenetic and evolutionary processes. During ontogeny, it is well established that different parts of the head follow different growth trajectories: the brain

and associated bones grow very rapidly, attaining roughly 90% of adult size by six years of age (Moore and Lavelle 1974:5), while the face in general grows much more slowly, in a parallel trajectory to the postcranial skeleton, reaching adult proportions ten years or more later (Lieberman et al. 2000a; Lieberman 2011). Due to the relative independence of facial and neural modules, they are allowed to change in shape and size relative to one another throughout growth and development.

The modularity of the cranium is also crucial for its *evolvability* – its capacity for evolutionary change (Lieberman 2011). The relative independence of cranial modules allows selection to operate on functional modules independently, tinkering with the performance of certain modules without confounding the performance of others. This phenomenon is referred to as *mosaic evolution* (e.g. Bastir and Rosas 2009), which describes evolutionary processes which occur at different rates in different parts of the body, and which has been invoked to account for the different patterns of traits observed across human taxa over time (e.g. Rosas et al. 2008).

Despite the relative independence of cranial modules, and due to the compact nature of the head, adjacent modules tend to share spaces and structures – for example, the same bones that make up the roof of the orbit also constitute the floor of the anterior cranial fossa, and the bones of the palate also make up the floor of the nasal cavity. Therefore functionally and genetically independent cranial modules must also be highly integrated with one another (Lieberman 2011), such that a change in the morphology of one module necessitates a change in the morphology of another, in order to maintain structural cohesion in the skull as a whole, and to ensure the functions of all modules are not impeded. Thus, *integration* can be defined as "...the association of elements through a set of causal mechanisms so that change in one element is reflected by change in another..." (Smith 1996:70).

Integration is therefore the counterpart to modularity (Lieberman 2011). Whereas the morphology of different modules can change across ontogeny and evolution, integration between modules mediates their morphological relationships at both these levels. *Developmental* integration describes the interactions that result in coordinated growth between modules during ontogeny. These processes may be genetic, resulting from the pleiotropic effects of regulator genes and related growth factors influencing growth and development in different modules (Moss 1997c; Lieberman 2011), or from genetic linkage, whereby genes related to growth or morphological patterning are located at adjacent loci and are inherited together (Lieberman 2011). They may also be epigenetic, resulting from local responses to growth factors induced by ontogenetic processes in adjacent tissues/modules (Lieberman 2011), from mechanical forces induced in bones due to muscle loading, or forces of tension or pressure between and within modules undergoing shape changes (Moss 1997a,b), or from other environmental stimuli (Moss 1997d). The result of coordinated shape changes across ontogeny through these mechanisms is that the head maintains *functional integration* – while the head is undergoing local shape and size changes within modules, the ability of these modules to perform their vital roles must remain unimpeded at every step along the way. Functional integration between modules mediates evolutionary change, as selective pressures towards morphological change within one module are only advantageous insofar as they do not have a maladaptive morphological influence on other modules.

Cranial Base

Ontogeny

Approaching the skull from the perspective of modularity and integration, in the most basic sense the skull can be considered in terms of three main functional components: the vault or

neurocranium, which represents essentially a protective case for the brain; the face or *viscerocranium*, which is a highly integrated structure composed of many functional modules, most of whose functions are essential to the organism's continued life; and the cranial base or *basicranium*, which is not easily observed ectocranially and which can be difficult to visualize. Essentially, the cranial base serves as a platform atop which the brain rests, below which the face hangs, and which connects both to each other and to the postcranial body via its articulation with the spinal column and its perforations by numerous foramina for the cranial nerves and blood vessels. As mentioned above, the brain and neurocranium follow an accelerated neural growth trajectory while the face follows a slower skeletal growth trajectory; as the interface between the two, the cranial base serves as an "adjustment zone" that follows an intermediate trajectory (Moore and Lavelle 1974:6), maintaining structural cohesion between the vital systems of the face and the brain, and between the head as a whole and the rest of the body. The cranial base has thus been the subject of a deep history of research concerning its important role in the functional integration of the head.

The cranial base also plays an important role in the developmental integration of the head due to its unique embryogenetic origins. The ontogeny of the cranial base differs from that of the rest of the skull, in that it ossifies endochondrally from mesodermal, in addition to neural crest, precursors, whereas most of the face and vault derive from neural crest cells and ossify intramembranously. In the intramembranous cranial bones, bone growth is induced in periosteal membranes that enclose organs or spaces (i.e. functional modules); as a result, the morphology of these bones is dependent on, and reflects, the shape of the soft-tissue modules that these membranes surround. In contrast, endochondral bones develop from an initial condensation of mesenchymal cells called an *anlage*, which subsequently differentiates into cartilage (Lieberman

2011). This cartilage serves as a template or prototype for the future bone, and a periosteal membrane surrounding this osseous precursor eventually induces chondroclastic and osteoblastic activity, replacing the cartilage with bone from the outside in. Thus, endochondral bone morphology results from the morphology of these cartilage precursors, which is under strong genetic control (Lieberman 2011: Sperber et al. 2010).

In the skull, the endochondral bones of the cranial base ossify from within a single cartilage structure called the *chondrocranium* (which itself develops from multiple cartilages which later fuse into a single plate). The chondrocranium represents the first part of the skull to appear: mesenchymal condensations at the rostral end of the notochord differentiate into the parachordal cartilages, which form a floor for the already-developing brain, at around 40 days post-conception. The intramembranous facial bones develop later, starting in the 6^{th} to 7^{th} week post-conception, induced by an interaction between mesenchyme in the facial prominences and an ectodermal epithelium (Sperber et al. 2010). These different embryological origins reflect different evolutionary histories: the more primitive endochondral bones of the cranial base originated as part of the postcranial endoskeleton, whereas the facial and neural bones originally evolved as a superficial exoskeletal armour (Moore and Lavelle 1974:96).

As a result it should be expected that the face and cranial base are influenced by different developmental factors and follow different ontogenetic trajectories. In particular, because the endochondral cranial base bones form earlier, and because their morphology is under greater genetic control based on the initial patterning of mesenchymal precursors, it could be expected that the cranial base exerts a greater integrative influence on the face than vice versa; because it develops later, the facial skeletal morphology must match the shape of the pre-existing base to which it must attach, and because the intramembranous bones' final form is dependent on the

morphology of complex functional modules involving multiple tissues under a greater influence of environmental factors, the morphology of facial bones is not strictly under genetic control in the same way as the cranial base, but results from a complex interplay between multiple ontogenetic factors.

Cranial Base Angle

Hominin evolution is characterized by trends toward increasing encephalization and associated size reduction and ventral retraction of the face; due to its role as an integrator between the two, it stands to reason that the human cranial base should exhibit a unique morphology among primates and mammals generally. Huxley (1867) discussed the role of midsagital cranial base structures in overall cranial integration early on, noting that variation in prognathism and brachycephalic/dolichocephalic morphologies relate to the relative rotation of the cranium around the "basicranial axis" (the orientation of the basiocciput and basisphenoid in the midsagital plane). He was the first researcher to record *cranial base angle* (as *basi-ethmoid angle*), the midsagital angle between the horizontal anterior (prechordal) and vertical/oblique posterior (postchordal) portions of the cranial base (Lieberman et al. 2000a), noting that the relatively high degree of flexion distinguished the human condition from that of "lower Mammalia" (Huxley 1867:67). Since then, at least 17 different measurements have been used to quantify this angle (Lieberman et al. 2000a), which vary considerably. Nonetheless, it is well-established that humans exhibit a markedly greater degree of ventral flexion in the midsagital cranial base than other animals.

Several hypotheses have been proposed to account for this phenomenon, but probably the best accepted is the "Spatial Packing" hypothesis (Biegert 1963; Ross and Ravosa 1993; Lieberman and McCarthy 1999; Lieberman et al. 2000a; 2008; Lieberman 2011; McCarthy 2001).

Because the chondrocranium serves as the platform which supports the brain, brain size/volume is limited by the absolute area allotted by it. As encephalization increased across hominin evolution, morphological changes to the basicranium were required in order to maintain functional integration. The spatial packing hypothesis states that flexion of the midsagital cranial base angle occurs to maximize the brain volume which can be supported by a cranial base of restricted dimensions – as brain size, and especially neocortical volume, increases, the cranial base flexes around a central "hinge" in the vicinity of the *sella*, and the brain and vault "roll up" posteriorly around the base of the skull, increasing the volume available above it (Biegert 1963).

The spatial packing hypothesis has been repeatedly supported by studies of CBA across primates and mammals. Ross and Ravosa (1993) found that CBA was significantly negatively correlated with the index of relative encephalization (IRE) across most primate taxa. Subsequently Spoor (1997) found that the same correlation in Pliocene hominins. Other researchers have demonstrated this relationship experimentally in non-human animals: Lieberman et al. (2008) investigated the relationship between CBA and brain size in mice, using genetic strains with known mutations that resulted in increased or decreased chondrocranial bone growth (resulting in relatively longer or shorter cranial bases, respectively) or in increased neural growth, resulting in larger but morphologically normal brains. Their results supported the spatial packing model: relative to basicranial length, larger brains correlate with greater flexion in the CBA.

While it is accepted that basicranial flexion serves to accommodate differences in brain volume and facial size/projection relative to basicranial length, it is clear that there are other confounding factors at play; in general the relationship between brain size and basicranial length only accounts for ~65% of variation in CBA (Lieberman 2011). This is unsurprising since the cranial base is a complicated three-dimensional structure and reducing it to a single angular

measurement is a gross oversimplification. Anteroposterior growth and changes in angulation in the cranial base both occur in the synchondroses, which act both as growth plates and as hinges, accommodating flexion either passively, in response to mechanical forces induced by differential growth rates in integrated structures (i.e. the brain and face), or actively, by differential rates of appositional bone growth between the superior and inferior portions of the synchondroses (Lieberman 2011). Additionally, flexion does not represent a simple angular change since three different synchondroses accommodate shape changes in the midline – the spheno-occipital (SOS), mid-sphenoidal (MSS), and spheno-ethmoidal (SES) (Lieberman et al. 2000a). Because so many different measurements for CBA exist, the actual measurement can vary within the same individual, and evolutionary patterns depend on which landmarks are used to define the prechordal (anterior) and postchordal (posterior) planes. For example, Spoor (1997) found that the relationship between CBA and brain size in modern humans conforms to the general primate trend while *Homo erectus* exhibits a greater degree of flexion than predicted for its brain size, while in contrast Ross and Henneberg (1995), using a different measure of CBA (excluding the cribriform plate), found that *Homo erectus* conforms to the general primate trend while CBA in modern humans is *less* flexed than expected based on brain size. Furthermore, Jeffery and colleagues (Jeffery and Spoor 2004; Jeffery 2005) have shown that during embryonic development, when the brain is expanding disproportionately to the rest of the head, the cranial base actually retroflexes (extends); this is accounted for by the cranial base's integrative role with the face.

While increasing ventral flexion in CBA increases the volume above the cranial base, this also necessarily implies that the volume below it will be proportionally reduced. Because the anterior cranial fossa constitutes the roof of the orbits, the orientation of the eyes and face is integrated with the anterior portion of the cranial base; and for reasons that are still unknown, in

anthropoids the neutral horizontal axis (NHA) of the orbits is always almost perfectly perpendicular to the posterior maxillary (PM) plane, the vertical line which denotes the posterior boundary of the face (Lieberman 2011). As a result, the orbits and ethmomaxillary complex maintain a strict orientational relationship, and as CBA flexion increases, the entire face rotates ventrally towards the posterior portion of the cranial base as an integrated "facial block", which reduces the length of the nasopharynx and oropharynx, and tucks the face underneath the anterior cranial fossa, resulting in a reduction in overall facial projection (McCarthy and Lieberman 2001). A counterpart to the spatial packing hypothesis, this phenomenon has been informally referred to as the "facial packing" hypothesis (Lieberman et al. 2008). Thus CBA reflects the integrative compromise between the brain's and face's bids for valuable cranial real estate.

Lateral Cranial Base Integration

Many studies have pointed out the limitations of reducing the complex nature of the cranial base to a single two-dimensional angle (e.g. Jeffery and Spoor 2004); as a result, more recent studies have focused on patterns of integration between lateral basicranial structures and the face and brain. The spatial packing hypothesis asserts that flexion of the CBA occurs to accommodate a greater brain volume above, but variation in mediolateral (i.e. breadth) dimensions of the cranial base could also result in a greater surface area to support the brain, without necessitating changes in basicranial length or flexion. Lieberman et al. (2000b) found CBA, basicranial length, and basicranial breadth to be mutually independent, and only the latter was found to have a significant correlation with brain and face size. Importantly, the authors found that face shape covaries with basicranial breadth because the absolute breadth of the cranial base limits the maximum breadth of the face, and due to this spatial constraint, narrow faces also tend to be anteroposteriorly longer.

Using 2D lateral radiographs, Bastir and Rosas (2006) found higher levels of covariation between the morphology of the face and lateral cranial base (middle cranial fossa) structures than between the face and the midline cranial base (CBA). These results were subsequently repeated by Gkantidis and Halazonetis (2011), who also found that while there was a higher degree of covariation between the midline cranial base and the face in children, covariation between the lateral cranial base and face became stronger in adulthood. This suggests that midline and lateral cranial base structures are characterized by developmental modularity.

It is likely that developmental modularity in the cranial base is related to the development of different brain structures, and because human evolution in characterized by increasing encephalization and neural reorganization, this has implications for interpretations about evolutionary modularity in the cranial base. The maximum breadth of the cranial base is measured across the middle cranial fossa (MCF), which supports, and consequently is highly integrated with, the temporal lobes of the brain. Bastir et al. (2008) found that in modern humans, the MCF exhibits a greater anterior projection relative to medial basicranial features (optic chiasma and foramen rotundum) than it does in chimpanzees and fossil hominins. Presumably, this morphology reflects evolutionary shape changes in the temporal lobes associated with linguistic and speech capabilities. But from the perspective of craniofacial integration, this has important implications because the PM plane of the face is defined based on the anteriormost point on the MCF; thus changing the anterior projection of the MCF changes the orientation of the PM plane, and as a result, the face as a whole (Bastir et al. 2008).

Other factors influence the orientation of the MCF as well. The posterior margin of the petrous pyramids marks the boundary between the MCF and posterior cranial fossa (PCF); this structure has been shown to rotate towards a more coronal orientation in primates with larger brains

(Spoor 1997; Lieberman 2011). It is believed that petrous rotation serves to accommodate a greater cerebellar volume by increasing the area of the PCF relative to the length of the midline cranial base (Spoor 1997), which has implications for the morphology of the MCF as well, and as a result potentially a cascading integrative influence on the face. However, during the period of greatest cerebellar expansion during prenatal growth, the petrous pyramids actually rotate towards a more sagittal orientation, and the overall relationship between petrous rotation and brain size is not fully understood (Lieberman 2011).

Bastir and Rosas (2009) investigated the relationship between these midline and lateral basicranial structures to determine their degree of modularity. Because, according to some measures, CBA remains stable across hominin taxa while brain volume increases (Ross and Henneberg 1995), the authors inferred that there must be other factors at play. Their results suggest that lateral basicranial morphology is relatively independent of midline basicranial topography, and that the cranial base morphology has been subjected to mosaic evolution. The midline base architecture, deriving from more primitive mesodermal precursors and serving as a foundation for the whole skull, remains relatively conserved, while the lateral base architecture, as it fuses with the intramembranous bones of the vault, is allowed more epigenetic flexibility to expand outwards through drift to accommodate the expanding brain. CBA has decreased under the general influence of increasing encephalization, while the lateral cranial base (i.e. MCF) has served as an integrative mediator between neural reorganization and facial morphology.

Climate

Nasal Cavity and Natural Selection:

Facial morphology differs from that of the cranial base and the vault in that it comprises

many independent functional modules which directly interact with the external environment, and consequently it has to integrate the influences of diverse environmental selective pressures on different modules. Among the functional modules of the face the nasal cavity should be expected to be particular sensitive to climatic pressures, since its function is to directly mediate the interaction between the internal body (lungs) and the external environment (inspired air). The nasal cavity serves as the passageway for air entering the lungs, and must permit a sufficient rate of airflow to supply the body's oxygen requirements at various levels of activity; but due to the sensitive nature of the lungs, rather than a simple tube the nasal cavity also plays the role of regulating the temperature and humidity of the air passing through it (Noback et al. 2011). Therefore the morphology of the nasal cavity can be understood to a great extent in terms of a trade-off between two competing functions: minimizing airflow resistance to promote efficient respiration on the one hand; and maximizing epithelial contact to promote heat and moisture exchange on the other. In contrast to the roles of other facial modules (e.g. vision, mastication, olfaction, communication) respiratory functions are more directly implicated in the day-to-day and minute-to-minute wellbeing of the animal and complications to this function are not as easily alleviated by behavioural modifications or cultural interventions.

On this basis, it might be expected that nasal morphology in humans from cold, dry climates should emphasize airflow resistance and epithelial contact, while that of humans from hot, humid climates should emphasize more efficient airflow, or even heat-dumping features. The shape of the external nose has long been known to vary among populations, and the nasal index has been thought to reflect an adaptation to climate (Franciscus and Long 1991); however, most of the physiological functions of the nasal airway occur within the internal nasal cavity (Lieberman 2011). Noback et al. (2011) performed a geometric morphometric landmark analysis of the internal

nasal cavity, and found that its morphology covaries with both average temperature and humidity. Supporting previous assumptions about the shape of the nasal aperture, they found that populations from cold, dry climates have relatively taller, narrower nasal cavities which are anteroposteriorly longer at the upper limits (within the ethmoid), while those from warm, humid climates have shorter, wider nasal cavities. This variation supposedly reflects a change in the volume/surface area ratio within the airway, maximizing turbulence and epithelial contact in colder, more physiologically demanding environments. Furthermore, they found that temperature and humidity had different and possibly conflicting effects on nasal cavity morphology: cold climates emphasize features that increase turbulence and residence time within the nasal capsule, primarily to warm air on inspiration; dry climates emphasize features of the nasopharynx (posterior to the choanae) which served to conserve moisture on expiration; they also found that cold temperatures had a more significant correlation with nasal morphology than dry climates.

The relationship between nasal cavity morphology and climate is not completely straightforward, however. Bastir et al. (2011) used a similar set of landmarks to investigate sexual dimorphism in the human airway, and found that males have relatively and absolutely larger cranial airways than females. This is presumably associated with sex-specific differences in body composition and energetics – males tend to be larger and more muscular than females, and therefore require disproportionately more oxygen relative to body size. In particular, the authors found that male nasal apertures, internal airways, and choanae tend to be taller than in females. Interestingly, while Bastir et al. (2011) suggest that this reflects a relative increase in airway volume in males, Noback et al. (2011) observed a similar phenomenon in cold-climate populations, which they suggested reflects an adaptation to reduce volume/surface area ratio and enhance air conditioning. In actuality, because nasal morphology likely reflects a compromise between these

roles, both interpretations are likely correct – a larger male airway volume is accommodated by greater height relative to breadth, increasing volume without decreasing the surface area/volume ratio, so that a greater volume of oxygen can be inspired without negatively impacting the efficiency of conditioning it.

Cranial Base and Climate:

While facial modules should individually be expected to be under unique selective pressures, some studies have shown variation in overall cranial shape between populations and/or climatic groups. Beals et al. (1983) found relationships between temperature (especially winter temperature) and both cranial index (i.e. brachycephalic/dolichocephalic morphologies), and relative brain size, in modern human populations as well as Pleistocene hominins. Subsequently, Beals et al. (1984) replicated these results, finding a latitudinal gradient in brain size among modern human populations. Importantly, these authors found that the increase in brain size in cold climate populations is driven primarily by an increase in cranial breadth relative to other dimensions. The results of Nowaczewska et al.'s study (2011) further support these findings: the authors found that the breadth of the basicranium specifically (bi-auricular breath) was more highly and more significantly correlated with mean annual temperature than four other measures of cranial length, breadth, and height (including maximum cranial breadth).

These authors interpret this variation in cranial shape as an adaptation to cold climates. An absolute increase in brain volume with a latitudinal gradient is consistent with Bergmann's Rule (Bernstein 2010). And increasing the breadth of the cranium relative to other dimensions decreases the cranial index, resulting in a more globular (i.e. spherical) cranium; this reduces the volume/surface area ratio of the head, and serves as a thermoregulatory adaptation by minimizing

heat loss through exposed surfaces, consistent with Allen's Rule (Bernstein 2010). As mentioned above, Lieberman et al. (2000b) found basicranial breadth to be significantly correlated with endocranial volume (ECV), while midline basicranial length and CBA were not. Additionally, Bastir and Rosas (2009) found evidence for mosaic evolution in the basicranium, with lateral and midline structures experiencing different evolutionary pressures at different times in human evolution. Combined, this evidence suggest that globularity in modern human crania may result from selective pressures (cold climates) acting on lateral portions of the cranial base, in combination with other factors influencing brain growth, to provide a relatively wider platform both to support a larger brain, and to drive overall changes in cranial vault shape.

Geometric Morphometrics

Introduction and Definitions:

Shape differences of the kind discussed above are the purview of the field of *morphometrics* (Zelditch et al 2012). Morphometrics can be considered a branch of mathematics, and refers to a suite of statistical tools typically used to quantify comparisons of shape and size in living things or their parts (Reyment 2010). The quantification of shape in the body proportions of humans and other living things has a deep history (consider Da Vinci's *Vitruvian Man*) which has been discussed by many authors (Slice 2005; Reyment 2010), but it has only been with the advent of computers that morphometricians have been able to fully take advantage of the statistical power of these techniques, and as a result the field has exploded in recent years. The following will briefly outline the principles of traditional and geometric morphometrics, and review the specific morphometric techniques employed in the studies mentioned above which will be employed in the course of this thesis.

Morphometrics is concerned with shape, which can be defined as "the geometric properties of an object that are invariant to location, scale, and orientation" (Slice 2005:3). The traditional morphometric approaches, often referred to as *traditional* or *multivariate morphometrics*, attempt to quantify shape through measurements of distances and/or angles, usually recorded using traditionally defined homologous landmarks as the endpoints for these line segments (Slice 2007; Zelditch et al. 2012). Multivariate statistical methods can be applied to these variables to develop a mathematical representation of the way in which sample organisms differ in proportion. However, these traditional approaches are insufficient to adequately represent the true geometry of the shape in question, since a limited number of linear measurements and angles fails to adequately represent the complete spatial relationships between the landmarks used to define them (Slice 2007). This problem can be partially resolved by increasing the number of variables, such as in Strauss and Bookstein's "box-truss" method (Zelditch et al 2012), which samples a crisscross network of linear measurements based on a more regular series of landmarks, as well as a series of angular measurements to quantify the geometric relationships between landmark points. However, as the number of variables increases, so does the number of angular measurements required to quantify their geometric relationships, to the point that these methods become unwieldy and impractical (Slice 2007). Moreover, because traditional approaches convert visibly apparent shapes into series of numerical variables, the output of multivariate statistical techniques tends to be numerical and esoteric, and there are no good methods of graphically (qualitatively) representing the shape changes these numbers represent.

Ultimately, the deficiency in traditional morphometrics stems from the fact that the variables used to define shape, primarily linear distances, are not actually measurements of *shape*, but rather of *size* – they reflect differences in magnitude of some length, breadth, or height variable

between individuals (Zelditch et al. 2012). Shape is effectively an emergent property of the geometric relationships between a series of size variables, and can be gleaned mathematically from traditional morphometric variables, provided that a suitable data set has been recorded. This can be achieved by recording every distance and angle possible within a series of landmark points, but the number of variables would be too large to be practical; it is likely that a smaller subset of variables would adequately represent the shape variation in the sample, but it is impossible to know which variables are important without having already done the analysis on the entire series (Zelditch et al. 2012).

This problem is resolved by *geometric morphometrics*, which differ from traditional morphometrics in that they retain *all* of the geometric relationships between landmark points (Slice 2005:5). This is accomplished by recording the Cartesian coordinates of landmarks directly, in 2D or 3D, rather than recording linear or angular measurements between them; by including the landmarks directly, the geometric relationships (angles and distances) between every combination of points are retained within the data, in a much smaller and easier to manipulate data set.

Furthermore, because the landmark coordinates are retained, geometric morphometrics offers much more intuitive methods for visualization of shape comparisons (Zelditch et al. 2012). Differences in shape, such as changes across ontogeny, or differences in mean shape between populations, can be plotted as vectors emanating from a graphical representation of the landmark coordinates, indicating the direction and magnitude of displacement required to deform one shape into the other, sometimes referred to as "lollipop graphs", because of the visual similarity between the landmark/vector combination and a lollipop (Klingenberg 2011). The same displacements can be graphically represented (sometimes in the same image) using a deformed grid, which depicts the compression and expansion of space between homologous landmarks; however this is only

applicable to 2D analyses, since the deformations in a 3D grid would overlap and become unintelligible. The landmark points can also be connected by lines to create "wireframe" depictions of the overall shapes they represent, which can be superimposed to demonstrate differences in shape between two groups (Klingenberg 2011).

The ability to retain all the geometrical information available within a series of landmarks, combined with the ability to graphically represent the actual shape changes described by the numerical data, make geometric morphometrics a powerful tool for anthropologists and other biologists to study shape in an objective, quantitative manner while being able to describe and visualize it in a more intuitive, qualitative manner.

Procrustes

Before differences in shape within a sample can be quantified, a number of extraneous factors typically need to be removed from the data. These factors, including size, location, and orientation, are referred to as "nuisance parameters" (Slice 2005), and they confound shape analysis by altering the spatial relationships between homologous points in different data sets. Size may be a biologically meaningful factor, as size variation naturally exists within a population, and as a result geometric morphometric techniques usually isolate the size variable and retain it for analysis independent of shape (Slice 2005). However, the size component needs to be removed from the data in order to compare shape, because size (distance) measures will alter the spatial relationships of homologous landmarks between individuals, even if their geometric relationships are identical, i.e. the analyses will identify spatial variation as differences in shape when in actuality the shapes could be identical but only differ in scale.

Size, as well as location and orientation, may also confound the analysis of shape due to

the nature of coordinate data. Landmark coordinates are in actuality only a combination of linear distance measurements from some arbitrarily defined reference point (i.e. their position within a Cartesian grid; Slice 2005). As a result, while these distance measures accurately reflect the geometric relationships between landmark points in arbitrarily defined space for each individual within the sample, the location, scale, and orientation of the object in question may differ between individuals with regards to the arbitrarily defined reference grid of the data file in which the landmarks are recorded – i.e. the position of an object within the bitmap of an image file (photograph or radiograph, or a stack of images used to reconstruct a 3D object, as in computed tomography data), or the position of a 3D surface determination within 3D shape space.

As a result, before geometric morphometric analyses can be performed, the raw coordinate data must be manipulated by scaling the individual objects to a common size, translating the object to a common position in space, and rotating the object so homologous landmarks occupy generally the same position, in order that differences between the position of these landmarks can be considered to reflect morphologically meaningful variation. In practice, this is more complicated than it seems, as there is no simple definition of "size" in complex shapes, such as the human skull, and as a result there are several possible methods to scale the raw data, all with implications that will need to be taken into account when interpreting results.

One of the simplest methods to do this is to use two landmarks to define a line that represents an arbitrary dimension along which to align individual landmark sets, and to scale the data to a common line length; this is referred to as *two-point* or *baseline registration* (Slice 2005). However, the selection of points used to define the baseline may have implications for the results of the analysis, and furthermore this method is difficult to apply to 3D data (Slice 2005).

By far, the most common method for scaling and translation in geometric morphometrics is the *procrustes superimposition* (Slice 2005). Rather than defining size based on a singular distance variable, as in baseline registration, procrustes superimposition incorporates positional information from every data point to establish a singular size value; it does this by minimizing the sum of the squared distances between all homologous landmarks within a sample. The landmark configurations are thus scaled to a common value, referred to as the centroid size, around which all landmarks are allowed to vary, as opposed to in baseline registration, where variability in landmark position is assessed relative to the two invariant points used to establish the baseline.

If two landmark configurations are being compared, the sum of the squared distances between points can be minimized by using one configuration as the baseline and scaling the second configuration to it; this is known as *ordinary procrustes analysis* (OPA; Slice 2005). Because most analyses employ a sample size larger than two, it is typically more useful to compare individual specimens to the mean shape for the entire sample; however, the mean shape cannot be computed until after superimposition and scaling have taken place. As a solution to this is, procrustes analysis initially uses one individual in the sample to stand in for the mean shape. After all individuals are scaled and oriented to this reference individual, a new mean is computed, and all the individuals are again superimposed using that mean as a reference point. This iterative process is repeated until the change in mean shape from one iteration to the next becomes negligible (Slice 2005); this process is referred to as *generalized procrustes analysis* (GPA).

Procrustes superimposition is not without its flaws. In particular, because every landmark point is used to define centroid size, major variations in the location of individual points have the potential to distort the shape comparisons in the rest of the structure. This is known as the "Pinocchio effect" (Slice 2005): when the puppet lies, his head remains the same shape and size

and only his nose grows; but the displacements of landmarks identifying nose shape will increase the sum of the squared distances between *all* landmarks, and this will be reflected in the procrustes analysis as changes in overall head shape, when in actuality shape change was localized in one structure. Despite issues like this, GPA remains the preferred method of superimposition in geometric morphometrics (Slice 2005), and it will be employed herein.

Multivariate Statistics

After superimposition, there are many statistical techniques that can be employed to quantify shape variation within a sample; two multivariate methods in particular, *principal components analysis* and *partial least squares*, have been noted to be especially relevant and useful in anthropological morphometrics (Slice 2007), and will be discussed below:

Principal components analysis (PCA; also known as *relative warps*) converts variation in a sample into orthogonal linear combinations of the original variables (principal components), in order to reduce the number of dimensions in the original data, as well as to facilitate visualizations of the shape variation within the sample (Slice 2007; Hammer 2012). Because each principal component tries to account for as much variation as possible remaining in the sample, most of the variation tends to be accounted for in the first few principal components; the first two principal components can be plotted against one another on a graph to provide a good visual approximation of the similarities and differences in shape between individuals in the sample (Hammer 2012).

PCA has been employed in the analysis of craniofacial integration by several studies relevant to the goals of this thesis. Bastir and Rosas (2006) used PCA to observe overall shape differences between ancestral groups (Africa, Asian, and European) in their total sample of craniofacial landmark coordinates; in a similar study, Gkantidis and Halazonetis (2011) used PCA

to observe overall craniofacial shape differences between adults and children. This thesis will employ PCA to observe potential differences between sample populations, as well as between males and females.

Whereas PCA is useful for visualizing shape variation within a sample, a method called partial least squares (PLS, or *singular warp analysis;* Bookstein et al. 2003) can be used to explore craniofacial integration by analyzing covariation between two related sets of landmarks. PLS extracts linear combinations of variables (similar to PCA) from two sets of variables, and attempt to maximize the covariance between sets (Hammer 2012; Slice 2007). Correlation between landmark sets does not imply morphological similarity, rather it means that variation across the singular warps (similar to principal components) of shape variation in one set tends to be associated with a certain component of shape variation in another (Slice 2007). From an anthropometric perspective, coordinated shape changes between different craniofacial modules can be interpreted as integration.

Bastir and Rosas (2006) and Gkantidis and Halazonetis (2011) both use PLS to identify patterns of integration between the cranial base and the face, employing several landmark sets to account for the face, midline cranial base, and lateral cranial base as distinct cranial modules. Bookstein et al. (2003) used PLS to observe patterns of covariation between the midsagittal face, vault, and cranial base across a sample of modern and archaic *Homo*. Because previous studies have used this technique to observe patterns of integration, the same technique will be used in this thesis in order to achieve comparable results.

Chapter 3: Materials and Methods

Sample

Landmarks were recorded on anonymized CT scans of adult human crania from medical contexts. A total sample of 59 individuals of mixed sex (female N=32; male N=27) were included in the analysis. The scans were obtained from two sources: a total of 61 scans were obtained from Dr. Djurdja Bracanovic, Department of Radiology, at the University of Belgrade; and as a comparative sample, five scans were obtained from Dr. F. Gigi Osler, Department of Otolaryngology-Head and Neck Surgery, at St. Boniface Hospital in Winnipeg.

The Belgrade sample is assumed to be of homogenous Serbian ancestry. CT scans were taken with a slice thickness of 0.75mm. Seven of the 61 scans were excluded from the analysis for various reasons: four scans were cut off above the area of the foramen magnum, obscuring the measurement of the opisthion (see landmark selection, below); two were excluded because of broken noses, influencing the rhinion, nasale inferius, and potentially other landmarks; and one individual was excluded due to an apparent pathological condition or scan error that obscured the entire left petrous pyramid. The remaining 54 individuals were included in the study (female N=28; male N=26).

The Winnipeg sample (N=5; female N=4; male N=1) is of mixed European (Scandinavian, English, Ukrainian) and unknown ancestry. Scans were taken at a slice thickness of 1.25mm. All five individuals were included in the study.

Because the scans come from medical contexts, sex and age are known. Roughly equal numbers of males and females were included in order to alleviate the potential influence of sexual

dimorphism on average shape. Only adults (18+ years) were included in the sample, because differences in the ontogenetic timing of shape changes in different cranial modules would obscure interpretations of adult cranial integration. Mature adult status was independently assessed based on eruption of the third molars; many individuals in the Belgrade sample were missing teeth, and in all cases where M3s were not present, this was determined to be the result of tooth loss and advanced age based on resorption of the alveolar process. The Serbian sample is characterized by a high degree of tooth loss: only seven individuals exhibit complete dentition, and five have no maxillary teeth; most of the individuals missing teeth are characterized by some degree of alveolar resorption. This is problematic because the resorption of the alveolar process may obscure some landmarks, such as the subspinale and the palatine/pterygoid suture, and the degree to which this may affect the analysis is hard to determine due to variability in the degree of resorption in different individuals. Unfortunately, due to constraints in the sample size, it is not possible to exclude individuals with significant tooth loss, and the implications of this will be covered in the Discussion section.

Considerations on Landmark Selection

Craniometric landmarks were selected to represent the structure of four cranial "modules" or areas: *midline cranial base*, *lateral cranial base*, *face*, and *internal nasal cavity*. Each of these areas has been the subject of 2D and/or 3D landmark-based geometric morphometric analyses of cranial integration between areas and/or adaptation to cold, and the selection process for landmarks in each area will be discussed below.

In order to select landmarks appropriate to this investigation, it was necessary to first establish a set of criteria to guide the selection process. In the words of Bookstein, "... landmarks

delimit our explanations of effects upon form; their function is not to just be there but to encourage hints about the processes that put them there" (Bookstein 1991: 59). In other words, homologous craniometric points are structures that exist to fulfil some physiological function, and not just to serve as convenient shape markers for anthropometrists; in order to understand the meaning of overall shape differences between modules, it is therefore critical to understand the functions that these craniometric points serve within the functional matrices of which they are a part, as well as to select landmarks whose variation should be expected to be relevant to the question at hand, and not the result of other confounding factors.

First and foremost, because this thesis is building on previous studies of cranial integration, selected landmarks should be comparable to those used by other authors in similar studies, in order for the results to be able to support or refute their findings. The easiest way to accomplish this would be to use identical landmark sets; however, there are many confounding factors that make this impossible:

- Where several authors have investigated the same modules they rarely use identical sets between them, and it is not practical to combine all the landmark points used by all authors because the datasets would be unnecessarily large; in particular, when different authors use landmarks that are very close to one another, or different points on the same structure, the inclusion of these points would exaggerate the influence of these structures on overall shape change patterns.
- Some landmarks used by other authors cannot be used because of limitations in the CT scans, e.g. *prosthion* could not be measured in a large portion of the scans because the scan area was cut off superior to this point. Additionally, mandibular landmarks cannot be included because the scans do not include the mandible.

- Certain points employed in 2D lateral radiograph studies would not translate well into 3D landmarks – particularly abstract points defined by the overlap of superimposed structures (e.g. "Type 3" landmarks; see below).
- Where authors have not provided detailed definitions of their landmarks, or the definitions are worded ambiguously, it is difficult to reproduce their landmarks with any certainty.

Additionally, other authors' landmarks should be independently assessed for their suitability to the goals of this thesis, and should not be included simply on the basis that other authors have used them previously. Potential landmarks should be assessed based on their representativeness of the genetic, ontogenetic, and functional integrative relationships within and between cranial modules under investigation; and furthermore, these relationships should be made explicit. Oddly, none of the authors cited herein discuss the reasoning underlying their landmark selection process. Even within a single cranial module or landmark data set, different landmark structures stem from different embryonic origins and their adult morphologies are regulated by the interactions of different functional and developmental constraints. An understanding of the integrative relationships between skeletal and soft-tissue modules associated with craniometric landmarks is therefore critical to making interpretations about morphological variability observed based on these landmarks.

Bookstein (1991) defines three craniometric landmark types: Type 1 landmarks include the "discrete juxtaposition of tissues" (Bookstein 1991:62), e.g. the intersection point of two cranial sutures; Type 2 landmarks refer to "maxima of curvature" (Bookstein 1991:64), e.g. the tips of bony processes; and Type 3 landmarks are diverse and often abstract, including points based on the relationships between other points, intersection points of chords or planes, endpoints of diameters, etc., and in 3D morphometric analyses they may not even fall directly on the skeletal

surface. Whereas Types 1 and 2 landmarks represent biologically-meaningful skeletal elements, Type 3 landmark definitions can be more or less arbitrary, providing more information about the relationship between skeletal aspects based on which they are defined and less about their exact location in space. Since this thesis is investigating spatial relationships between skeletal elements, introducing Type 3 landmark data would be circular, potentially confounding the results. Furthermore, due to the arbitrary nature of Type 3 landmarks, they have been shown to be more prone to inter-and intra-observer placement error than other types, and are therefore less reliable in geometric morphometric analyses (Ross and Williams 2008). (as a side note, the classification of landmarks according to this scheme seems to be more ambiguous in practice than in theory, and many authors' identification of landmark types contradicts those of others' for the same landmarks, even those of Bookstein [1991])

Following from these considerations, selection of landmark sets employed herein was undertaken within these guidelines: landmarks should be biologically meaningful (i.e. Type 1 or Type 2), and their biological function should be relevant to those aspects of shape that are pertinent to this thesis. Also, wherever possible, individual landmarks, as well as the overall configuration or each landmark set, should be comparable to those published by previous authors. Rather than establish strict criteria, each potential landmark was assessed individually for suitability within these guidelines, since no two landmark structures result from identical genetic and ontological influences, and since selection of points that are comparable to other authors' was sometimes at odds with selecting biologically meaningful landmarks. A detailed description of the selection process for each landmark set follows:

Midline Cranial Base Landmarks

Landmarks of the midsagittal cranial base have been employed in several studies of facial and basicranial integration in two dimensions (Bastir and Rosas 2006; Gkantidis and Halazonetis 2011) and three dimensions (Bastir and Rosas 2009; Neubauer et al. 2009); see Table 1 for the complete list of landmarks used by these authors. It has been well-established that the midline cranial base functions as an integrator between the brain and face, as it varies in its degree of ventral flexion as well as overall length – the so-called "spatial" and "facial packing" hypotheses, mediating brain and face size relationships by altering basicranial length and angulation at the synchondroses.

Therefore, midline basicranial landmarks should primarily reflect total basicranial length in addition to the relative lengths and orientations of the embryologically distinct midline basicranial components – mesethmoid, presphenoid, postsphenoid, and basioccipital (Sperber 2009). Considerations for each potential landmark, listed in Table 3.1, are outlined below.

Foramen caecum: In general, cranial foramina should be considered biologically meaningful in the course of landmark selection, in the sense that they generally serve to transmit blood vessels or nerves, and therefore their relationship to overall cranial shape reflects their relationship with vital soft-tissue modules following strict integrative patterns. This point marks the anteriormost midline point on the ethmoid bone, as the foramen forms within the suture between the ethmoid and frontal (presumably Bastir and Rosas' [2006] *anterior cribriform* is analogous to this point). As such it delimits the anteriormost margin of both the total cranial base, as well as the pre-chordal portion (mesethmoid). Additionally, this point is used in traditional measures of CBA (CBA1 and CBA3; Lieberman and McCarthy 1999) to define the chord

Table 3.1: Midline cranial base landmarks employed by previous authors

Landmark	Publication	Description
Foramen Caecum	Bastir and Rosas (2009); Neubauer et al. (2009)	Foramen anterior to the crista gali
Anterior Cribriform	Bastir and Rosas (2006); Gkantidis and Halazonetis (2011)	(2D) Undefined
Anterior sphenoid spine/posterior mid-cribriform	Bastir and Rosas (2006, 2009); Neubauer et al. (2009); Gkantidis and Halazonetis (2011)	Undefined; likely refers to the junction between the cribriform plate and sphenoid at the ethmoidal spine
Posterior Sphenoid	Bastir and Rosas (2006, 2009); Gkantidis and Halazonetis (2011)	"Posterior end of the sphenoid plane" (2006), "at the level of the orbital canals" (2009); aka *sphenoidale*: most posterior, superior midline point of planum sphenoidium (Lieberman et al. 2000a)
Pituitary point	Bastir and Rosas (2009)	Traditional landmark defined as the "anterior edge of the groove for the optic chiasma, just in front of the pituitary fossa" (Zuckerman 1955 as cited in Lieberman et al. 2000a)
Sella		Traditional landmark used in some measures of CBA; the point at the centre of the space enclosed by the hypophyseal fossa
Base of the Dorsum Sellae	Bastir and Rosas (2006); Gkantidis and Halazonetis (2011)	(2D) Undefined
Dorsum sellae	Bastir and Rosas (2009); Neubauer et al. (2009)	Traditional landmark defined as the posteriormost point on the internal contour of the sella turcica
Clival point	Lieberman et al. (2000a)	"midline point on the basioccipital clivus inferior to the point at which the dorsum sellae curves posteriorly"; used to define CBA3 and CBA4
Endosphenobasion	Neubauer et al. (2009)	Anteriormost midline point on the dorsal aspect of the basioccipital (as defined by Jeffery and Spoor 2004)
Basion	Bastir and Rosas (2006; 2009); Gkantidis and Halazonetis (2011); Neubauer et al. (2009)	Traditional landmark defined as "midsagittal point on the anterior margin of the foramen magnum" (e.g. Lieberman et al. (2000a)
Opisthion	Bastir and Rosas (2009); Neubauer et al. (2009)	Traditional landmark defined as "the most posterior point in the foramen magnum" (e.g. Lieberman et al. (2000a)

representing orientation of the prechordal portion of the cranial base. This point can be considered as a Type 1 landmark, by Bookstein's definition as "centres or centroids of 'sufficiently small' inclusions" (Bookstein 1991:63), as well as a discrete juxtaposition of tissues (suture between

frontal and ethmoid). While the *foramen caecum* has commonly been used to define the plane of the anterior cranial base, in practice it was observed that the superoinferior positioning of the point could be influenced by the degree of continuation between the *crista gali* and the frontal crest, such that the exact position of the foramen may be more or less displaced from the horizontal orientation of the cribriform plate and *planum sphenoideum* in different individuals. Nonetheless, as a convenient and easily identifiable trait consistent with previous authors in 3D (Bastir and Rosas 2009; Neubauer et al. 2009) and presumably consistent with the poorly defined "anterior cribriform" point used by others in 2D (Bastir and Rosas 2006; Gkantidis and Halazonetis 2011).

Ethmoidal spine: All authors investigating midline cranial base architecture employ some point demarcating the boundary between the cribriform plate and the sphenoid. While all authors use different names for this point and none set out clear definitions of the point they use, most used descriptive terminology in naming the point (Bastir and Rosas 2009, "posterior midcribriform"; Gkantidis and Halazonetis 2011, "posterior cribriform"; Bastir and Rosas 2006, "posterior end of cribriform plate"), indicating that they are all likely using the same point: the posteriormost midline point on the endocranial surface of the cribriform plate. Neubauer et al (2009) employ a point labelled "anterior sphenoid spine", a term that seems to be used extremely rarely and almost exclusively by these authors. Based on their illustration in Figure 1, the point they are employing is one that would more commonly be referred to as the *ethmoidal spine* of the sphenoid; as this point marks the midline boundary between the ethmoid and sphenoid, it can be considered as identical to the "posterior cribriform" point used by the other authors.

As this point marks the juxtaposition of two tissues (ethmoid and sphenoid) in the plane of symmetry, this can be considered a Type 1 landmark (Bookstein 1991), and because the cribriform plate serves as the interface between the olfactory bulb (1st cranial nerve) and the nasal cavity

(White and Folkens 2005), this point is biologically meaningful in that it delimits the posterior extent of the ethmoid's integrative relationship with the brain. However, since the cribriform plate also serves as the roof of the nasal cavity (which is considered independently of the cranial base in this thesis), and animals with greater reliance on olfaction tend to have longer and differently-oriented cribriform plates, basicranial landmarks that delimit cribriform length may exhibit higher levels of covariation with aspects of nasal cavity morphology related to inspiration and olfaction than other basicranial structures. As a result, inclusion of this point may have a confounding effect on the overall patterns of covariation observed in this study. This is an unavoidable methodological limitation, since the cribriform plate contributes to both the cranial base and the nasal cavity directly, and both structures are directly integrated through it. Nonetheless, this point will be included in the analysis and the implications will assessed in the Discussion section.

Sphenoidale: Three of the four authors employing midline basicranial landmark sets cited herein employ a point to delimit the posterior end of the planum sphenoidium, otherwise known as *sphenoidale* (Lieberman et al. 2000a), although none actually use this term; it is variably described as "the posterior end of the sphenoid plane" (Bastor and Rosas 2006:816), and the most posterior point on the sphenoid "at the level of the orbital canals" (Bastir and Rosas 2009:61).

This point represents a Type 2 landmark, as the maximum of curvature between the planum sphenoideum and the *hypophyseal fossa* in the midsagittal plane (Bookstein 1991). In conjunction with the ethmoidal spine and the *foramen caecum*, the *sphenoidale* helps to establish the total length and general contour of the midline ACF, aka the anterior portion of the midsagittal cranial base, and as such it is critical to employ a point in this vicinity. Additionally, this point is commonly used in traditional measures of CBA (CBA2, CBA4; Lieberman and McCarthy 1999).

Pituitary Point: Only one study (Bastir and Rosas 2009) employs this landmark, defined as the "anterior edge of the groove for the optic chiasma, just in front of the pituitary fossa" (Zuckerman 1955, as cited in Lieberman et al. 2000a). The groove for the optic chiasma is situated on the anterior surface of the hypophyseal fossa immediately posterior/inferior to the posterior end of the planum spheniodeum, i.e. the sphenoidale, which means that these two points lie in relatively close proximity to one another. Because the groove for the optic chiasma is immediately posterior/inferior to the sphenoidale, the sphenoidale effectively falls on the margin of this groove, meaning that both points are effectively denoting the same structure. The position of the groove for the optic chiasma, in practice, appears to be quite variable, i.e. the end of the planum sphenoideum may lie quite anteriorly to the pituitary point, forming a sort of shelf, or the sphenoidale may lie directly superior to the pituitary point, continuous with the anterior wall of the hypophyseal fossa; but while the morphology of this groove is biologically meaningful in that it reflects the sphenoid's integrative relationship with the optic nerve (2^{nd} cranial nerve), it is not clear what this variation means, and in any case it is not relevant to this study. Including both landmarks would emphasize variation within this structure, whereas this thesis is only interested in variation in the spatial organization of these structures. For this reason this point is excluded from the analysis. Oddly, Bastir and Rosas (2009) used both pituitary point and sphenoidale in their analysis, the implications of which are unclear.

Dorsum Sellae: 2D and 3D analyses differ in the way in which they measure the position of the dorsum sellae: 2D analyses (Bastir and Rosas 2006; Gkantidis and Halazonetis 2011) measured the "base of the dorsum sellae", which based on their images appears the be the point at which the dorsum sellae emerges from the sphenoid body; in 3D, Bastir and Rosas (2009) and Neubauer et al. (2009) name the point simply "dorsum sellae", but leave it undefined, although

traditionally dorsum sellae is defined as the posteriormost point on the internal contour of the *sella turcica*, which is not inconsistent with their diagrams. This point represents a Type 2 landmark, as a maximum of curvature in the plane of symmetry, or potentially a Type 3 landmark, since "most posterior" should be defined with reference to the imaginary plane of Frankfurt horizontal; nevertheless, the dorsum sellae itself marks the anterosuperior end of the postchordal portion of the midline cranial base, and in the absence of any more reliable landmarks this traditional point will be employed here.

Endosphenobasion: This point, used by Neubauer et al. (2009) is defined elsewhere as the "anteriormost midline point on dorsal aspect of basioccipital" (Jeffery and Spoor 2004:81); however their use of this point is questionable in adults, since fusion of the spheno-occipital synchondrosis precludes identification of the anteriormost margin of the basioccipital. This point may be considered roughly analogous to the *clival point*, a landmark which is not used by any morphometric studies cited herein, but which is used to define the clival plane, on which two traditional measures of cranial base angle are based (CBA3, CBA4; Lieberman and McCarthy 1999). In practice, the clival point seems to be extremely variable, especially with regards to its anteroposterior/superoinferior position along the basioccipital clivus. The point itself is not biologically meaningful (with regards to the relative positioning of any vital functional modules in the midsagittal plane), so insofar as the clival plane and measures of CBA based upon it are not critical to this thesis, inclusion of this point would only serve to introduce a dimension of variability not relevant to the hypotheses, and therefore this point, along with endosphenobasion, will be excluded.

Basion: This traditional landmark, defined as the midsagittal point on the anterior margin of the foramen magnum (Lieberman 2000a), is used by all four studies on which the midline

basicranial landmark selection is based, and is used to delimit the posterior end of the postchordal midline basicranial plane in the four most common measures of cranial base angle (CBA1-4; Lieberman and McCarthy 1999). This point is identified as a Type 2 landmark (Bookstein 1991; although Jeffery 2004 identifies it as Type 3), and it is biologically meaningful in that it marks the posterior boundary of the midline parachordal cartilages. In keeping with common acceptance, this point is ideal for inclusion in this dataset.

Opisthion: This traditional landmark, defined as the most posterior point on the foramen magnum (Lieberman 2000a), is used by both 3D studies cited in this section (Bastir and Rosas 2009; Neubauer et al. 2009) but neither 2D study (Bastir and Rosas 2006; Gkantidis and Halazonetis 2011). Opisthion is not included in traditional measures of CBA because CBA only takes into account the angulation of the cranial base anterior to the foramen magnum. It could be argued, following the criteria laid out herein, that inclusion of both opisthion and basion, two points on the same structure, could serve to overemphasize the contribution of this structure to overall shape variation in the midline basicranium; however, the foramen magnum is not a simple structure and contributes to several functional systems (neural, vascular, musculoskeletal). More recent studies of cranial integration and CBA have emphasized that midline cranial base morphology is complex and cannot be reduced to a single angular measurement (e.g. Lieberman et al. 2008); because the boundary of the foramen magnum is formed by the chondrification of the occipital sclerotomes (Sperber 2009), its morphology reflects the embryogenetic patterning of cartilages in this area. Furthermore, because it orients the head atop the body, the plane of the foramen magnum, defined by opisthion and basion, can gives clues about changes in the orientations of other parts of the midline cranial base relative to one another and to overall cranial orientation.

In addition to these points, sella is commonly used in measures of CBA (CBA1, CBA3;

Lieberman and McCarthy 1999), as it represents the apparent “hinge” around which the pre- and postchordal portions flex. Sella is a Type 3 landmark, typically measured in 2D lateral radiographs and defined as the “center of sella turcica, independent of contours of clinoid processes” (Lieberman 2000a). Because this thesis does not employ traditional measures of CBA, and because other, more biologically-meaningful landmarks are available, it is not pertinent to include this point.

Six landmarks were selected to represent the midline cranial base; these are presented in Table 3.2 and Figure 3.1. It should be noted at this point that all landmarks mentioned in this section are endocranial; as a result it could be expected that this will overemphasize covariation with the brain, and under-emphasize covariation with facial structures. Selection for midline basicranial landmarks is confounded by the fact that the inferior aspects of the midline basicranium represent the superior aspects of the internal nasopharyngeal complex, and including the same inferior midline basircranial landmarks in both datasets would result in erroneously high levels of integration between these structures. These concerns can be alleviated based on previously established patterns of covariation between CBA (based on internal landmarks) and facial morphology (e.g. Lieberman et al. 2008), as well as previous studies demonstrating higher levels of covariation between facial structures with the lateral cranial base than with the midline cranial base, based exclusively on endocranial midline cranial base landmarks (Bastir and Rosas 2006; Gkantidis and Halazonetis 2011). Since the null hypothesis states that the nasal cavity does not exhibit higher levels of integration with the lateral then with the midline basicranium, this will not be a problem in the case that the null hypothesis is rejected – it will only serve to negate the degree of covariation, resulting in more conservative results.

Table 3.2: Final Midline Cranial Base Landmarks

#	Name	Description
1	Foramen Caecum	Posteriormost endocranial margin of the foramen between the Crista Gali and the frontal crest
2	Ethmoid spine	Endocranial midline point at the tip of the spine projecting from the sphenoid body into the cribriform plate
3	Sphenoidale	The most superior midline point at the posterior end of the planum sphenoideum
4	Dorsum sellae	Posteriormost midline point on the internal contour of the dorsum sellae
5	Basion	Anteriormost point on the foramen magnum
6	Opisthion	Posteriormost point on the foramen magnum

Figure 3. 7: Finalized midline cranial base landmarks

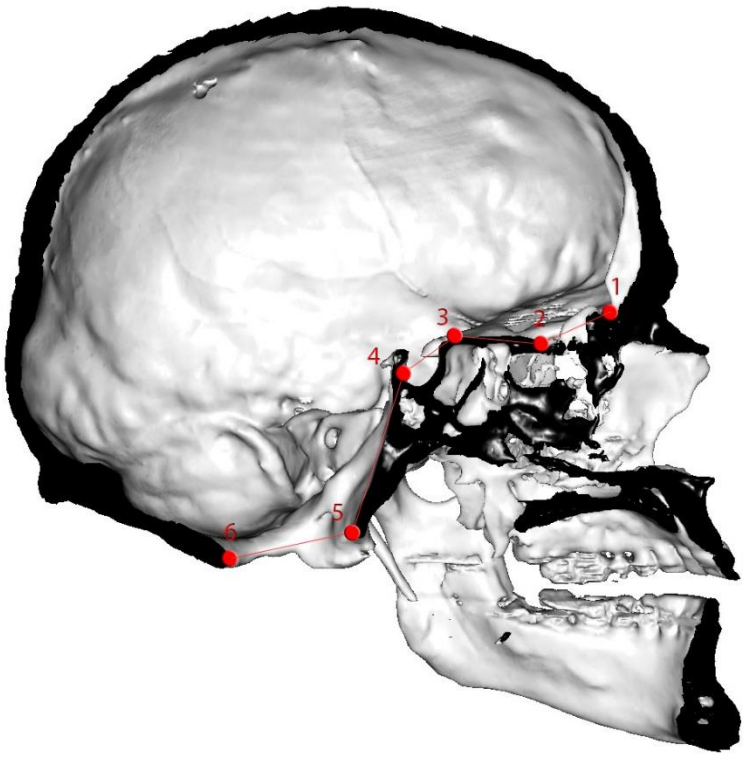

Lateral Cranial Base Landmarks

Lateral cranial base landmarks have been employed by Bastir and Rosas (2006) and Gkantidis and Halazonetis (2011) in 2D (lateral radiographs), and by Harvati and Weaver (2006), Bastir et al (2008), Bastir and Rosas (2009) and Neubauer et al. (2009) in 3D; additionally,

Nowaczewska et al. (2011) employ linear measurements of basicranial breadth based on lateral cranial base landmarks. The complete list of lateral cranial base landmarks is compiled in Table 3.3.

Table 3.3: Lateral Cranial Base Landmarks employed by previous authors

Landmark	Publication	Description
Sphenoparietal Junction (centre)	Bastir and Rosas (2006; 2009), Gkantidis and Halazonetis (2011)	(2D/3D) Limit between ACF and MCF; the centre of fusion between the frontal, great sphenoid wing, and parietal (defined in Bastir and Rosas 2009)
Anterior MCF point	Bastir and Rosas (2006), Bastir et al. (2008), Gkantidis and Halazonetis (2011)	(2D/3D) Anteriormost point on greater sphenoid wing (Bastir and Rosas (2006); Maximal 3D curvature of greater sphenoid wings (Bastir et al. 2008);
Inferiormost point on MCF	Bastir and Rosas (2006), Gkantidis and Halazonetis (2011)	(2D) Undefined
Petroso-parietal junction (centre)	Bastir and Rosas (2006; 2009), Gkantidis and Halazonetis (2011)	(2D/3D) Limit between MCF and PCF; Pyramidal base (defined in Bastir and Rosas 2009)
Anterior orbital roof	Bastir and Rosas (2006), Gkantidis and Halazonetis (2011)	(2D) Intersection between orbital roof and inner frontal table
Posterior orbital roof	Bastir and Rosas (2006), Gkantidis and Halazonetis (2011)	(2D) Intersection between greater and lesser sphenoid wing
Internal Acoustic Porus	Bastir et al. (2008), Bastir and Rosas (2009), Neubauer et al. (2009)	(3D) Supero-medial border (Bastir et al. 2008); Antero-lateral vertex (Bastir and Rosas 2009); undefined by Neubauer et al. (2009)
Petrosal Apex	Bastir et al. (2008), Bastir and Rosas (2009), Neubauer et al. (2009)	(3D) Most medial point (undefined by Neubauer et al. 2009)
Foramen Ovale	Bastir et al. (2008); Bastir and Rosas (2009), Neubauer et al. (2009)	(3D) Most medial point (undefined by Neubauer et al. 2009)
Foramen Rotundum	Bastir et al. (2008); Bastir and Rosas (2009), Neubauer et al. (2009)	(3D) Most medial point (undefined by Neubauer et al. 2009)
Orbital/optical Foramen/optic canal	Bastir et al. (2008), Bastir and Rosas (2009), Neubauer et al. (2009)	(3D) Antero-lateral vertex/border (undefined by Neubauer et al. 2009)
Anterior Clinoid process	Neubauer et al. (2009)	(3D) undefined
Jugular Foramen	Harvati and Weaver (2006), Neubauer et al. (2009)	(3D) ectocranial, most medial point and most lateral point (Harvati and Weaver 2006), undefined by Neubauer et a;. (2009; endocrainial)
Hypoglossal Canal	Neubauer et al. (2009)	(3D) undefined

Superior orbital fissure	Neubauer et al. (2009)	(3D) undefined
Maximum curvature point between transverse and petrous curve	Neubauer et al. (2009)	(3D) sliding landmark
Radiculare	Nowaczewska et al. (2011)	(chord) Used to determine biauricular breadth (basicranial breadth)
Porion	Lieberman et al (2000b)	Used to measure basicranial breadth (bi-porionic breadth)
Asterion	Harvati and Weaver (2006)	(3D)
Stylomastoid Foramen	Harvati and Weaver (2006)	(3D)

In contrast to the midline cranial base, in which landmarks were selected to represent anteroposterior length and angular orientation, lateral cranial base landmarks will be selected primarily to account for breadth dimensions. Bastir and Rosas (2006) and Gkantidis and Halazonetis (2011) found higher and more significant levels of covariation between the face and lateral cranial base than between the face and midline cranial base; however, these analyses were performed in 2D on lateral radiographs, which means that their results only relate to the anteroposterior and superoinferior relationships of landmarks. Therefore, in order to extend their analyses to 3D, lateral cranial base landmarks should emphasize the mediolateral relationships of landmarks.

Mediolateral cranial base landmark relationships are evolutionarily and ontogenetically relevant for several reasons. Some studies (e.g. Lieberman et al. 2008) have shown that breadth variables account for a significant amount of variation in CBA, since a greater basicranial breadth results in a greater surface area, requiring less flexion to support a given brain volume above it. Due to the inverse relationship observed between CBA and facial size, it follows that lateral cranial base structures should exhibit a similar integrative relationship with the face, which is indeed what Bastir and Rosas (2006) and Gkantidis and Halazonetis (2011) demonstrate. Furthermore, covariation between breadth variables and cold climates has been demonstrated in the cranial base

(Nowaczewska et al. 2011) as well as the nasal cavity (Noback et al. 2011), and overall facial morphology has also been shown to covary with climate (Harvati and Weaver 2006). To the extent that adaptation to climatic variation should be expected to underlie patterns of basicranio-facial integration, it is apparent that breadth variables should be expected to play a significant role.

Whereas the midline cranial base landmarks account for anteroposterior length and midsagittal angulation, in addition to mediolateral breadth the lateral cranial base landmarks should respect the angular orientation of the petrous pyramids in the transverse plane. Petrous rotation changes throughout ontogeny (Lieberman 2011) and reflects relative size differences in different parts of the growing brain; furthermore, petrous angulation reflects species differences across primate taxa, the angle having been shown to be significantly negatively correlated with brain size, and over the course of human evolution there is an evident trend towards decreasing petrous angulation (i.e. rotation towards a more coronal orientation) associated with neural reorganization and changes in the size of the cerebellum and brainstem (Spoor 1997; Lieberman et al. 2000a).

Because of this relationship between the relative proportions of brain structures and lateral basicranial morphology, the complete set of lateral basicranial landmarks should therefore respect not simply breadth, but the relative breadths of areas integrated with particular brain structures, i.e. the cranial fossae, as well as the spatial relationships between them, especially the boundary between the middle and posterior fossae, delimited by the angle of the petrous pyramid. Potential landmarks are assessed below based on these considerations.

Many authors employ landmarks that delineate points of maximal curvature of the cranial fossae, including the inferiormost and anteriormost points on the MCF (Bastir and Rosas 2006; Bastir et al. 2008; Gkantidis and Halazonetis 2011), and the sliding semi-landmark identified as

the point of maximal curvature between the transverse and petrous curve (Neubauer et al. 2009). While these serve to define the overall shape of the cranial fossae and temporal lobe and cerebellum, they are less straightforward to measure in 3D than in 2D. Furthermore, they do not represent homologous structures in different individuals, so while they reflect shape differences in the brain, they do not necessarily reflect spatial displacements of integrated skeletal/neural structures relative to one another, which represent differences in the kind of genetic/epigenetic processes relevant to this thesis. Similar Type 3 landmarks, such as the "anterior/posterior orbital rooves" (Bastir and Rosas 2006; Gkantidis and Halazonetis 2011) are identified based on the superimposition of structures in radiographs and are not identifiable in 3D. Neither kind of landmarks are suitable to this thesis.

Foramina for Cranial Nerves: Many foramina for cranial nerves have been employed in lateral cranial base geometric morphometric analyses, including the *optic foramen* (optic nerve/cranial nerve II), *superior orbital fissure* (oculomotor/III, trochlear/IV, ophthalmic/V1, and abducens/VI), *foramen rotundum* (maxillary nerve/V2), *foramen ovale* (mandibular nerve/V3), the *internal acoustic porus* (facial/VII and vestibulocochlear/VIII nerves), the *jugular foramen* (glossopharyngeal/IX, vagus/X, spinal accessory/XI nerves and of course the jugular vein), the *hypoglossasl canal* (hypoglossal nerve/XII), and the *stylomastoid foramen* (facial nerve/VII, through the facial canal)(Monkhouse 2006). As noted above, these foramina can be considered inherently biologically meaningful, in that they result from the fusion of chondrocranial precursors around the pre-existing cranial nerves (Sperber 2009), and as a result their position and orientation are dependent on the genetic patterning of brain structures and epigenetic interactions of the brain and chondrocranium.

These foramina tend not to be "sufficiently small" (Bookstein 1991:63) such that their

centres could be taken as Type 1 landmarks (especially in 3D), so in practice most researchers seem to record them as Type 2 landmarks based on a specifically defined point of maximal curvature on their margin. This becomes problematic for several reasons. First, different authors do not always use the same point on each foramen (e.g. most lateral vs. most medial point, etc.), and often they simply name the opening without describing where the point was measured (the most troublesome example is Neubauer et al.'s [2009] undefined "superior orbital fissure"). But more problematically, the points they define may be difficult to clearly determine in practice. Bastir and colleagues (Bastir and Rosas 2008; Bastir. et al 2009) record the "most medial point" on the foramen rotundum, but while the lateral margin of this foramen forms a distinct ridge, the medial margin is indistinct, forming the wall of a canal continuous with the sphenoid body. Likewise, Bastir et al. (2008) record the superomedial border of the internal acoustic porus, but due to the angle at which the foramen penetrates the petrous bone the medial margin remains continuous with the bone with no distinct demarcation; furthermore, Bastir and Rosas (2009) record the "antero-lateral vertex" of this foramen, but because of the anteromedial-posterolateral orientation of the posterior wall of the petrous pyramid into which this foramen opens, an "antero-lateral vertex" doesn't exist.

Nonetheless, these basicranial foramina are ideal for the purposes of this thesis in that they are biologically meaningful, and they take into account the genetically- and epigenetically-determined mediolateral positions of the medial portions of the cranial fossae, and additionally help to determine the medial boundaries between fossae (i.e. the optic foramen delimits the boundary between ACF and MCF, while the internal acoustic porus helps to define the orientation of the boundary between the MCF and PCF).

Most studies of lateral basicranial integration tend to focus on either endocranial (when

investigating neural/cranial fossa integration) or ectocranial (when measuring dry skulls where only ectocranial features are measurable) landmarks exclusively, but because this thesis is employing CT scans, it is possible to include both in the analysis. Because they are determined by brain morphology, the openings of these foramina on endo- and ectocranial surfaces should be expected to be consistent, especially in the sphenoid where the bone is thin, so the endo- and ectocranial positioning should be expected to equally reflect genetic and epigenetic integrative factors between the brain and cranial base; conversely, because the ectocranial base also serves as the attachment site for muscles related to head posture, mastication, speech, etc., there is much more potential for these surfaces to be influenced by activity patterns that might influence remodelling and obscure phylogenetic patterns of morphology, and therefore it could be argued that endocranial landmarks would better reflect patterns of genetic and epigenetic integration. Specific marginal points are determined based on the suitability in each case (See Table 3.4 for details).

Petrosal Apex: An endocranial Type 2 landmark, the most medial point on the petrous pyramid is used by all authors employing 3D endcranial landmarks cited herein (Bastir et al. 2008; Bastir and Rosas 2009; Neubauer et al. 2009). This point marks the medial end of boundary between the MCF and PCF, and is essential to defining the plane of petrosal angulation, and is therefore suitable for inclusion in the analysis.

Neubauer et al. (2009) employ another medial Type 2 Landmark, the anterior *clinoid process,* which serves as an attachment site for the tentorium cerebelli and thus results from genetic and epigenetic integrative processes between the brain and sphenoid. It lies in close proximity to the optic foramen, projecting posteriorly from its superolateral margin, and thus inclusion of both points may over-represent this area in the dataset.

The lateralmost basicranial landmarks are somewhat more problematic, since the lateral boundaries of the cranial fossae are delimited by the intramembranous bones of the neurocranium, and their morphology is not under the same strict genetic control as the endochondral basicranial precursors – rather, lateral expansion in the basicranial margins occurs through differential deposition and resorption in the outer and inner tables of the vault (Lieberman 2011). Several authors (Bastir and Rosas 2006; Bastir et al. 2009; Gkantidis and Halazonetis 2011) delimit the lateral boundary between the ACF and MCF as the centre of fusion between the parietal, frontal, and greater sphenoid wing. In theory, this discrete juxtaposition of tissues represents a Type 1 landmark which sufficiently defines the boundary between the ACF and MCF and also represents the point of maximal breadth of the ACF; however, in practice this point is difficult to identify reliably due to obliteration of sutures in elderly individuals. As well, due to the variability of suture morphology, especially in the pterion, it is not guaranteed that this landmark represents homologous points on different specimens, or even on different sides of the same specimen.

The lateral limit between the MCF and PCF is problematic for the same reasons but to a potentially greater degree. Several authors delimit this boundary at the petroso-parietal junction (Bastir and Rosas 2006, 2009; Gkantidis and Halazonetis 2011) where the base of the petrous pyramid meets the suture between the temporal and parietal. In practice, due to variation in the morphology of the sigmoid sulcus (i.e. the degree to which it is present, if at all, on the parietal) it is not apparent that this intersection should represent homologous points in different individuals. Furthermore, the way in which the superior margin of the posterior pyramid curves continuously into the margin of the transverse sulcus makes it difficult to define the point at which one ends and the other begins. Neubauer et al. (2009) mark the boundary based on a sliding semi-landmark defined as the point of maximum curvature between the transverse and petrosal curves, which

serve to best approximate the point where these structures diverge, but disregards the ontogenetic processes that result in their actual morphology. Harvati and Weaver (2009), though not explicitly as the boundary between these fossae, employ the ectocranial *asterion*, which is in the general vicinity of the pyramidal base, but it is not evident that it should serve as a suitable proxy. Therefore, in the absence of any better options, the sphenoparietal junction and the petrosoparietal junction will be used to mark the lateral boundaries between the ACF and MCF and the MCF and PCF, respectively, following the former authors; the implications of potential error will be established as part of the discussion on intraobserver error.

Finally, because of the importance of breadth variables in this landmark set, and because maximum basicranial breadth has been shown to be significantly correlated with cold climates (Beals et al. 1983; 1984; Nowaczewska et al. 2011) and with overall facial proportions (Lieberman et al. 2000b), this set should include a landmark that represents the point of maximum basicranial breadth. Nowaczewska et al. (2011) define maximum basicranial breadth as biauricular breadth, measured from radiculare to radiculare – *radiculare* defined as the point of maximum incurvature of the zygomatic process. This Type 3 landmark is inherently deficient as the curvature of the zygomatic is gentle and the point of maximum incurvature may be continuous over a relatively large area, and since the zygomatic serves as an attachment site for muscles related to mastication its morphology may be influenced by activity patterns throughout life. Lieberman et al. (2000b) define maximum basicranial breadth as bi-porionic breadth – *porion* defined as the most superior, lateral point on the external auditory meatus; in practice the EAM slopes somewhat gently and does not present a clear lateral margin. Within the vicinity of these points, a reliably identifiable homologous point on the EAM is the most superior point on the tympanic part surrounding the meatus. Employing this point alleviates problems of ambiguity that plague the previous two points,

and because the tympanic ring ossifies from cartilages of the first branchial arch, and forms the support for the tympanic membrane (eardrum) (Lupu et al. 2010), this point can be considered homologous across individuals; therefore this point will be included as a representation of maximum basicranial breadth. Sixteen landmarks were selected to represent the lateral cranial base; these are listed in Table 3.4 and presented in Figure 3.2.

Table 3.4: Final Lateral Cranial Base Landmarks

#	Name	Description
1,2	Optic foramen	Bilateral point at which the superior margin of the optic foramen originates from the sphenoid body
3,4	Foramen rotundum	Bilateral point on the lateralmost endocranial margin of the foramen rotundum
5,6	Foramen spinosum	Bilateral point on the endocranial margin of the foramen spinosum where the meningeal groove emerges
7,8	Petrosal apex	Bilateral point at the medial tip of the petrous pyramid where it projects towards the spehoid body/dorsum sellae
9,10	Internal acoustic porus	Posteriormost bilateral point on the margin of the opening
11,12	Sphenoparietal junction	Because the sutures were obscured, this was measured as the bilateral endocranial point at the lateral origin of the crest that forms the boudary between the ACF and MCF
13,14	Petrosoparietal junction	Because the sutures were obscured, this was measured as the bilateral endocranial point at the lateral origin of the crest that forms the boudary between the MCF and PCF
15,16	External Auditory Meatus	Bilateral ectocranial point on the EAM at the superiormost point on the tympanic part

Facial Landmarks

Bastir and Rosas (2006) and Gkantidis and Halazonetis (2011) used 2D lateral facial landmarks to explore patterns of facial/basicranial integration, and Harvati and Weaver (2009) and Butaric et al. (2010) employed facial landmarks to investigate relationships between facial structures and climate. The complete list of facial landmarks employed by all authors is found in Table 3.5.

Figure 3. 8: Finalized lateral cranial base landmarks.

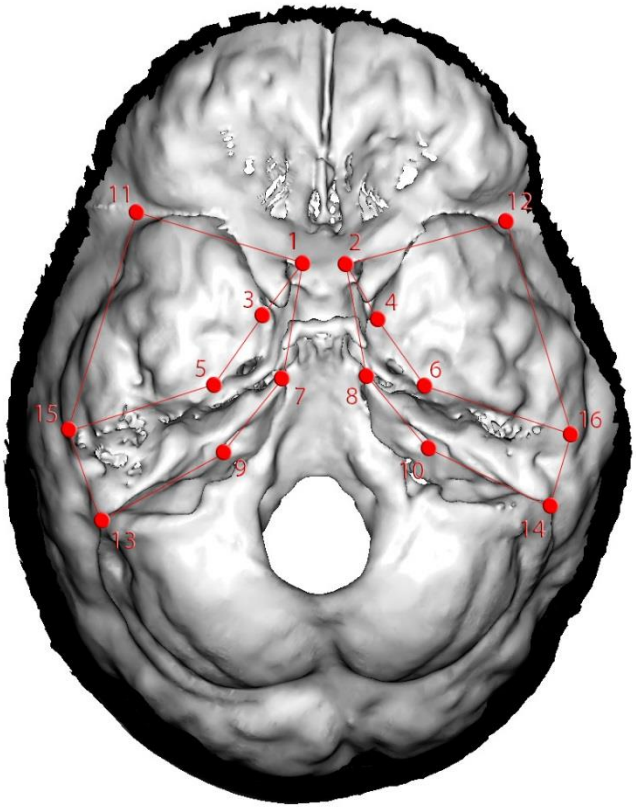

This facial landmark set will differ significantly from other authors in that these analyses will consider facial and internal nasal cavity landmarks as two distinct sets, to disentangle the integrative relationships between each and the cranial base, on the basis of previous claims of the relative morphological independence of the nasal cavity from the rest of the face (Bastir and Rosas 2013). While many studies use landmarks of the nasal aperture in their facial data sets, these points will need to be excluded from the facial dataset *a priori* due to the necessity of including them in the nasal cavity landmark set.

Table 3.5: Facial landmarks employed by previous authors

Landmark	**Publication**	**Description**
Glabella (unpaired)	Bastir and Rosas (2006); Gkantidis and Halazonetis (2011); Harvati and Weaver (2006); Butaric et al. (2010)	Traditional Landmark – most anteriorly-projecting midline point on the supercilliary arch
Sellion (unpaired)	Butaric et al. (2010)	Midsagittal point at the deepest point of the concavity associated with the nasal root, wherever it falls
Nasion (unpaired)	Bastir and Rosas (2006); Gkantidis and Halazonetis (2011); Harvati and Weaver (2006)	Traditional Landmark – intersection of internasal and frontonasal sutures
Rhinion (unpaired)	Bastir and Rosas (2006); Gkantidis and Halazonetis (2011)	Traditional Landmark – inferiormost point on the internasal suture, on the superior margin of the nasal aperture
Anterior nasal spine (ANS; unpaired)	Bastir and Rosas (2006); Gkantidis and Halazonetis (2011)	Traditional Landmark – anteriormost midline point on the tip of the spine inferior to the nasal aperture
A-point (*subspinale*; unpaired)	Bastir and Rosas (2006); Gkantidis and Halazonetis (2011)	Traditional Landmark – the point of greatest incurvature inferior to the anterior nasal spine
Prosthion (unpaired)	Bastir and Rosas (2006); Gkantidis and Halazonetis (2011); Harvati and Weaver (2006); Butaric et al. (2010)	Traditional Landmark – anteroinferiormost midline point on the intermaxillary suture (aka supradentale, G&H 2011)
Posterior nasal spine (PNS; Staphylion; unpaired)	Bastir and Rosas (2006); Gkantidis and Halazonetis (2011); Butaric et al. (2010)	Traditional Landmark – posteriormost midline point on the median palatine suture
Frontomalare temporale (paired)	Harvati and Weaver (2006)	Traditional Landmark – lateralmost point on the frontozygomatic suture
Dacryon (paired)	Butaric et al. (2010)	"Apex of the lacrymal fossa"
Ectoconchion (paired)	Butaric et al. (2010)	"Anterior border of the lateral side of the orbit"
Infraorbital foramen (paired)	Harvati and Weaver (2006)	Authors do not define this point (centre, margin, etc.)
Zygomaticotemporal suture	Harvati and Weaver (2006)	Suture between temporal and zygomatic bone on the superior aspect of the zygomatic process
Malar root at alveolus (paired)	Harvati and Weaver (2006)	undefined
- **(**paired**)**	Harvati and Weaver (2006)	Suture between palatine pyramidal process and pterygoid plate
Posterior Maxillary Alveolar Border (paired)	Bastir and Rosas (2006); Gkantidis and Halazonetis (2011)	(2D lateral radiograph)

Apart from that, facial landmarks should represent overall facial morphologies, i.e. the

relative proportions of height and breadth, or brachyfacial vs. dolichofacial morphologies. Because the CT scans available to me were taken in the context of nasal- or sinus-related medical procedures, the mandible is excluded from the scan region; therefore mandibular landmarks will not be included in the dataset.

Unlike the cranial base which was divided into lateral and midline sets, the face will be considered as a single unit, and therefore it will include both midline (unpaired) and lateral (paired) landmarks. Many midline facial landmarks are well-established and common traditional landmark points, and therefore it will be possible to achieve a high degree of consistency with other studies in the respect.

The superior midline boundary of the face is usually represented at the brow ridge by the *glabella* (Bastir and Rosas 2006; Gkantidis and Halazonetis 2011; Harvati and Weaver 2006; Butaric et al. 2010). This is a ubiquitous landmark in facial studies, but it is not unproblematic. Defined as the point of maximum anterior curvature of the supraorbital torus in the midline in Frankfurt Horizontal, it is an abstract Type 3 landmark, inherently defined based on the relationship between basicranial (porion) and facial (orbitale) structures (White and Folkens 2005). Furthermore, the supraorbital torus is a superstructure which is commonly understood to be moderately sexually dimorphic in humans, and its morphology may therefore be significantly confounded by factors unrelated to genetic or epigenetic integration.

Inferior to the glabella, the *nasion* represents a reliable midline Type 1 landmark (the intersection of the internasal and frontonasal sutures; Bastir and Rosas 2006; Harvati and Weaver 2009; Gkantidis and Halazonetis 2011). Nasion has been used in measures relating to the nasal airways (e.g. to determine nasal height, used to quantify the nasal index; Franciscus and Long

1991); however, as an ectocranial landmark it does not directly reflect the dimensions of the internal nasal cavity, and therefore serves better as a facial landmark. Butaric et al. (2010) record *sellion* instead of nasion, defined as the point of maximum incurvature associated with the nasal root, wherever it lies; nasion should be preferred for its biological relevance and greater measurement reliability.

Whereas landmarks on the margin of the nasal aperture will be included in the nasal cavity landmark set, a point inferior to the nasal aperture should be included in the facial set to quantify the inferior margin of the face. All authors cited herein (Bastir and Rosas 2006; Gkantidis and Halazonetis 2011; Harvati and Weaver 2006; Butaric et al. 2010) employ the *prosthion* (i.e. *supradentale*) in their analyses. Defined as the anteroinferiormost point on the intermaxillary suture, this Type 1 landmark suitably quantifies the anteroinferior extent of the cranial face; however, due to limitations in the sample scans prosthion cannot be reliably measured in a large number of individuals (a large proportion of scans are cut off superior to this point, and many individuals are missing teeth resulting in resorption of the alveolar process).

In order to approximate the prosthion and represent the morphology of the lower face, *subspinale* (i.e. *A-point*) can be used (Bastir and Rosas 2006; Gkantidis and Halazonetis 2011). This is defined as the point of maximum incurvature between the anterior nasal spine and the prosthion, and represents a Type 2 landmark (unless the definition is taken as “most posterior midline point between the ANS and prosthion”, implicating a reference to Frankfurt Horizontal, which would make it a Type 3 landmark); as such is it deficient compared to prosthion, but under the circumstances it is the best landmark available to delimit the anteroinferior boundary of the face in the midline.

Lateral (paired) facial landmarks should take into account biorbital, midfacial and alveolar breadth. Butaric et al. (2010) employ the *ectoconchion*, defined as the "anterior border of the lateral side of the orbit" at the level of its central horizontal axis, to account for upper facial breadth. This is an arbitrarily-defined Type 3 landmark with no biological significance, and not necessarily any geometric significance either (i.e. it may or may not reflect maximum biorbital breadth). Harvati and Weaver (2009) record *frontomalare temporale*, the lateralmost point on the frontozygomatic suture, a Type 1 landmark which is homologous among individuals and reliably identifiable, and which provides an indication of upper facial/biorbital breadth, as well as approximating the lateral boundaries of the supraorbital torus. Therefore, frontomalare temporale represents a more suitable landmark to account for this dimension.

Butaric et al. (2010) also record the medial position of the orbit at *dacryon*, a Type 1 landmark at the intersection of the frontal, lacrimal, and maxilla. While this landmark is biologically meaningful and reliably identifiable, other authors have used this point to define the morphology of the internal nasal cavity (see below for discussion). Regardless, while this point would provide resolution concerning orbital dimensions and interorbital breadth, this thesis is not concerned with specific facial structures but only overall patterns of facial shape (i.e. brachyfacial vs. dolichofacial), and therefore inclusion of this point would be superfluous.

The *zygomaticotemporal suture* (Harvati and Weaver 2009), recorded at its most superior point, accounts for maximum facial breadth in the midface, represents a homologous Type 1 (or 2) landmark which can be reliably identified. The most superior point is the ideal point to record, as the inferior portion of the zygomatic arch serves as the origin for the masseter, and therefore could be expected to be under a greater influence of mechanical remodelling. It also represents the point at which the bones of the lateral face (zygomatic) are integrated with the bones of the

cranial base (temporal), although this process of integration is mediated by the zygomatic process of the temporal (of intramembranous origin, in contrast to the basal parts of the temporal bone).

Because midfacial midline landmarks will be included in the nasal cavity landmark set and excluded from the facial set, the *infraorbital foramen* (Harvati and Weaver 2009) can be recorded to give an approximation of midfacial projection relative to other facial structures. Additionally, because the foramen allows the passage of a branch of the fifth cranial nerve (White and Folkens 2005), which exits the cranial base through the foramen rotundum, inclusion of this point may help to reveal the role played by vital neural structures in patterns of integration between the cranial base, brain, and face.

Harvati and Weaver (2009) record the *malar root*, i.e. the root of the malar process of the maxilla, where it originates on the alveolar process. This probably presents a Type 2 landmark, but due to the continuous nature of this area the "root" may be more or less distinct in different individuals, and Bookstein (1991) specifically addresses the problems of measuring Type 2 landmarks in "saddle-shaped" structures such as this. A more significant problem, however, results from the high degree of tooth loss observed in the Serbian sample. A high proportion of individuals exhibit some degree of remodeling of the alveolar process associated with tooth loss. It is notable that the skull on which the authors demonstrate their landmark points (Harvati and Weaver 2009:Fig. 2) is missing teeth; however, the alveoli appear to be present, and because they used dry crania it is not clear whether or not tooth loss occurred in life, and if they took this into account in their crania selection process. At any rate, due to the high potential for measurement error, this point will be excluded from the analysis.

The breadth of the dental/alveolar complex can be accounted for at the posterior end of the

alveolar process. Analyses using 2D lateral radiographs (Bastir and Rosas 2006; Gkantidis and Halazonetis 2011) record the "posterior maxillary alveolar border", which is not sufficiently defined to be located in three dimensions (and anyway, being in 2D, the authors use this point to determine anteroposterior length of the lower face only, and not breadth). Harvati and Weaver (2009) record the better-defined "suture between the palatine pyramidal process and pterygoid plate", but considering this suture is continuous along the medial, inferior, and lateral articulation between these structures, the definition remains somewhat ambiguous (in the authors' fig.2, this landmark is located unhelpfully by arrows pointing to the hidden pterygoid region on a cranium in the anterior aspect). In order to best represent the posteroinferior margin of the face, this point will be recorded as the posteriormost point on the suture between the pterygoid process and the alveolar process, in between the pterygoid plates. While it is not clear that this landmark reflects a homologous point with regards to the morphology of the dental arcade, as the mediolateral relationship observed between the last molar and the pterygoid plates seems to vary, it should represent a homologous point with regards to the pterygoid plates, which are integrated with the naso-oro-pharyngeal complex as well as the cranial base, and for this reason this point should not be as susceptible to the problem of alveolar resorption related to tooth loss as other landmarks on the posterior alveolar process.

Thirteen landmarks were selected to represent the face; these are listed in Table 3.6 and presented in Figure 3.3.

Table 3.6: Final facial landmarks.

#	Name	Description
1	Glabella	Anteriormost midline point on the supraorbital torus
2	Nasion	Intersection between the internasal and frontonasal sutures
3	Subspinale	Point of maximum incurvature on the intermaxillary suture inferior to the ANS
4,5	Frontomalare temporale	Lateralmost bilateral point on the frontotemporal suture
6,7	Inferior orbital foramen	Superiormost point on the ectocranial margin of the foramen
8,9	Zygomaticotemporal suture	Superiormost bilateral point on the suture between the zygmatic and temporal
10,11	Zygomaticomaxillary suture	Inferiormost bilateral point on the suture between the zygmomatic and maxilla
12,13	Maxillopterygoid suture	Bilateral point between the alveolus of the maxilla and the pterygoid process, at the point where the medial and lateral plates converge

Figure 3. 9: Finalized facial landmarks

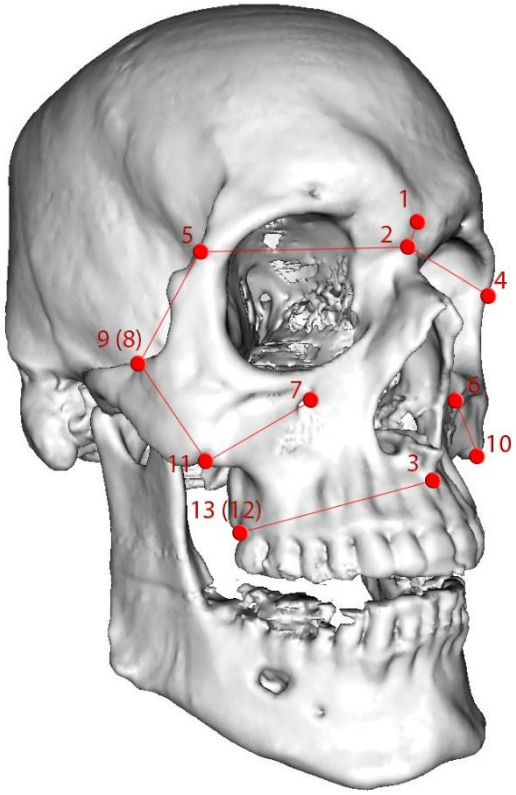

Nasal Cavity Landmarks

Landmarks of the internal nasal cavity have been employed to investigate the relationship between airway morphology and climate (Noback et al. 2011), sexual dimorphism (Bastir et al. 2011), and integration between the airways and outer face (Bastir and Rosas 2013); the complete list of potential landmarks can be found in Table 3.7. There is a high degree of consistency among the landmark sets of all these authors, so it should be relatively straightforward to select nasal landmarks following their example; however, in all cases these authors measured their landmarks on 3D surface scans of dry crania, and were therefore limited to externally observable landmarks, whereas the CT scans employed herein present no such limitation. This will be taken into consideration when assessing these authors' landmarks.

Because the dimensions of the internal nasal cavity have been shown to covary with climate (Noback et al. 2011) landmark selection should reflect the overall shape of the nasal cavity in three dimensions. Furthermore, because the internal anatomy of the nasal cavity reflects a trade-off between two vital physiological functions, i.e. increasing airflow turbulence for air conditioning, while at the same time allowing the passage of a sufficient volume of oxygen to maintain a given level of activity, landmarks should represent the anatomy of these vital internal structures – the turbinates and the morphology of the nasal aperture and choanae (Bastir et al. 2011).

Table 3.7: Nasal Landmarks employed by previous authors

Landmark	Publication	Description
Anterior Ethmoid Foramen (paired)	Noback et al. (2011); Bastir et al. (2011); Bastir and Rosas (2013)	Anterior Margin
Posterior Ethmoid Foramen (paired)	Noback et al. (2011); Bastir et al. (2011)	Posterior margin
Dacryon/Lacrymal (paired)	Bastir et al. (2011); Bastir and Rosas (2013)	B&R (2013) only list "lacrymal" with no description; presumably they are referring to dacryon
Rhinion (unpaired)	Noback et al. (2011); Bastir et al. (2011); Bastir and Rosas (2013)	Midline point at inferior free end of internasal suture
Nasale inferius/Nasomaxillary junction (paired)	Noback et al. (2011); Bastir et al. (2011); Bastir and Rosas (2013)	Nasomaxillary suture At piriform aperture
Alare (paired)	Noback et al. (2011); Bastir et al. (2011); Bastir and Rosas (2013)	Lateralmost margin of nasal aperture
Inferior Nasal Border (paired)	(Noback et al. 2011)	Inferiormost margin of nasal aperture
Anterior nasal spine (ANS; unpaired)	Noback et al. (2011); Bastir et al. (2011); Bastir and Rosas (2013)	Tip of median bony process of maxilla
Poserior nasal spine (PNS; staphylion; unpaired)	Noback et al. (2011); Bastir et al. (2011); Bastir and Rosas (2013)	Posterior tip of midsagittal bony palate
Inferolateral choanal corner (paired)	Noback et al. (2011); Bastir et al. (2011); Bastir and Rosas (2013)	Most lateral intranasal point at the palate (B&R 2013)
Choana roof (paired)	Noback et al. (2011); Bastir et al. (2011); Bastir and Rosas (2013)	Superiormost point on the choana
Hormion (unpaired)	Noback et al. (2011); Bastir et al. (2011); Bastir and Rosas (2013)	Posteriormost midline point on vomer
Posterosuperior end of medial pterygoid plate (paired)	Noback et al. (2011)	as per name
Pharyngeal tubercle	Noback et al. (2011); Bastir et al. (2011); Bastir and Rosas (2013)	Variably defined as most inferior midpoint (N et al 2011) and maximal projection (B&R 2013)
Inferior turbinate insertion	Bastir et al. (2011)	Posterior origin of the inferior turbinate
Middle turbinate insertion	Bastir and Rosas (2013)	Most posterior point on the middle turbinate at the choana level
Optic canal	Bastir and Rosas (2013)	most inferior, medial point

Landmarks of the Nasal Aperture: The nasal aperture represents the anterior boundary of the internal nasal cavity, and its outline can be delineated with a number of reliably identifiable landmarks – most of which have been consistently applied by the three papers on which the selection process outlined herein is based (Noback et al. 2011; Bastir et al. 2011; Bastir and Rosas 2013). The superiormost midline point on the nasal aperture is marked by the *rhinion* (all authors), a Type 1 landmark defined as the intersection of the internasal suture with the margin of the nasal aperture. Inferior to this point, the lateral dimensions of the aperture are marked by the (paired) Type 1 *nasale inferius* (all authors), the intersection of the nasomaxillary suture at the aperture margin.

All authors record the maximum breadth dimensions at the *alare*, the lateralmost point on the nasal aperture; while it's been established that breadth in the nasal cavity appears to be evolutionarily and energetically relevant, alare is not uncomplicated because the lateral margins of the nasal aperture may remain somewhat parallel at the widest point, making its superoinferior position ambiguous, and creating the potential for measurement error. For this reason, in place of alare the point on the margin of the nasal aperture at the level at which the inferior turbinate originates will be included. While this point will not represent the absolute maximum breadth of the nasal aperture, it lies immediately superior to this point and therefore should serve as a sufficient proxy; additionally, because the turbinates serve a vital anatomical function, their superoinferior and mediolateral positioning arguably reflects more biologically-meaningful variability than the absolute maximum breadth of the nasal opening; and furthermore, because the point is less ambiguous than alare, there is less concern about measurement error (there is variability in the proximity of the turbinate origin to the nasal margin – sometimes these structures intersect, while in other individuals they do not; the first case represents a Type1 landmark, while

the second could be best defined as Type 3. Nonetheless this point is preferred for the reasons outlined above).

All authors mark the inferior midline margin of the nasal aperture at the Type 1 *anterior nasal spine (ANS)*, "the tip of the median bony process of the maxilla" (Noback et al. 2011:602). In practice, the spine is often bifurcated and asymmetrical, and therefore the landmark should be recorded not at the absolute anteriormost point, but rather that anteriormost point on the intermaxillary suture. Noback et al. (2011) record a paired point not employed by Bastir and colleagues at the inferiormost bilateral margins of the nasal aperture. This point should serve to more accurately reflect the dimensions of the nasal aperture, since inferiormost points lie somewhat below the ANS, and reflect the true dimensions of the nasal openings, while the ANS lies within the nasal septum. However, this Type 2 landmark suffers from the same complication as the alare, in that the inferior margins may be more or less continuous horizontally and therefore the mediolateral position of this point may be ambiguous. Classically, nasal index has been known to vary with population and climate, and the variation has been suggested to be primarily influenced by variations in nasal height (Franciscus and Long 1991), measured as the chord from nasion to the midline point that intersects the line between the inferiormost points on the nasal margin. It is unclear the degree to which the ANS covaries with the inferior nasal margin, and therefore these points may be required to adequately represent the absolute anterior depth of the nasal cavity. The reliability of these points will be assessed in the discussion of intraobserver error.

Landmarks of the choanae/nasopharynx: Posteriorly, landmarks should reflect the height, breadth, and orientation of the choanae as well as the orientation of the nasophangyeal complex. The absolute height and orientation of the choanal area can be quantified in the midline based on two Type 1 landmarks: the *posterior nasal spine* (the tip of the median bony process at the

interpalatine suture; all authors) and the *hormion* (the posteriormost midline point on the vomer, where it articulates with the sphenoid; all authors).

The inferior breadth is measured at the inferolateral choanal corner (all authors), which can be described as Type 2 (the maximum of curvature between the horizontal and vertical portions of the palatine), and due to the horizontal nature of the palate the plane between the lateral choanal corner and the PNS represents the inferior boundary of the choanae. The inferolateral choanal corner is characterized by the presence of the lesser palatine foramen, which allows the passage of the lesser palatine nerves (White and Folkens 2005); problematically, this foramen sometimes presents as a notch, resulting in a deepening of the lateral corner of the choanae. In such cases, the point can be measured on the inferior margin of the notch, which is typically characterized by distinct bony processes which fail to completely enclose the foramen, in order to avoid recording non-homologous points.

Since the hormion does not reflect the actual height of the nasal airways, all authors record the maximum height of the posterior airways at the *choana roof*, the superiormost point on the constriction of the posterior nares. As previously mentioned, Bookstein (1991) discusses the trouble of reliably identifying Type 2 landmarks on saddle-shaped surfaces such as this, but in practice this point seems to be relatively straightforward to identify in CT scans, as the body of the sphenoid forms a gentle ridge continuous with the ridge formed by the alae of the vomer, the extremal point of which can be easily identified in sagittal slices. Noback et al. (2011) note that this point exhibited a relatively high degree of intraobservor measurement error, but that the amount of error observed was related to the experience of the observor.

Because the choanae are teardrop-shaped and somewhat pointed superiorly, it should not

be necessary to delimit the maximal superior breadth of the posterior nares; rather the bilateral choanal rooves will give an indication of overall mediolateral displacement of the choanae as a unit. However, Bastir and colleagues variably identify points along the lateral choanal border to delimit overall choanal shape as well as breadth superior to the palate: Bastir et al. (2011) record the posteriormost origin of the *inferior turbinate*, while Bastir and Rosas (2013) identify the analogous point in the *middle turbinate*. It is unclear why the same authors employed different points to measure this dimension, but insofar as only one paired point should be sufficient for this purpose, the inferior turbinate is arguable more suitable, for several reasons: 1) since the inferior turbinate is a distinct bone, while the middle turbinate is part of the ethmoid, its articulation with the palatine serves as a reliably-identifiable, homologous, Type1 landmark, in stark contrast to the origin of the middle turbinate; 2) because the anterior position of the inferior turbinate has been included in this landmark set, this would be complemented by the posterior origin – the combination of these points represents the biologically-meaningful plane that separates the inferior from the middle meatus of the internal nasal airway, reflecting not only length and breadth, but also the morphology of the internal airways.

While they do not record breadth at the level of the choanae superior to the palate, in contrast to the other authors Noback et al. (2011) record breadth in the nasopharynx at the *posterosuperior end of the medial pterygoid plate*. This Type 2 landmark is located at the extremal point of the bulge at the root of the medial pterygoid plate, and presumably accounts for integration, especially with regards to mediolateral displacement relationships, between the chondrocranial sphenoid body and the intramembranous bones of the nasal airways. Choanal breadth at the turbinates may be more relevant than this point, because the choanae play a more significant role in air conditioning than the nasopharynx, serving as a point of constriction (i.e. a

Venturi throat) to increase turbulence on expiration (analogous to the role of the anterior nares on inspiration); because the majority of air conditioning occurs in the area of the turbinates, between the choanae and nasal aperture (Lieberman 2011), anatomy in this area should be under a greater selective pressure from climatic variables, while the nasopharynx should experience a greater integrative influence of musculature associated with mastication.

Nonetheless, dimensions and orientation of the nasopharynx need to be quantified, and the angulation and length of this area relative to the area of the turbinates plays roles in respiration, air conditioning, and speech (Lieberman 2011). All authors account for variation in the area at the *pharyngeal tubercle*, the site of the origin of several pharyngeal constrictors (Gray 2005); while muscle attachment sites are not ideal, in the case of the nasopharynx the anatomical structure is composed of soft tissue only, and therefore this point provides the best available skeletal proxy. The tubercle itself is a variably shaped bulge on the basioccipital, and the exact measurement is variably defined by the authors: Noback et al. (2011) record the "most inferior midpoint" (Type 3, i.e. most inferior with reference to Frankfurt horizontal), while Bastir and Rosas (2013) record the point of maximal projection (Type 2). The definition of Bastir and Rosas (2013) is preferred, not only as a Type 2 landmark, but also because due to the oblique orientation of the basiocciput, the "most inferior midpoint" may or may not correspond to the most maximal projection, resulting in a greater potential for measurement error and/or lack of homology between individuals.

Landmarks of the upper airway: All three papers cited in this section employ 3D surface scans of dry crania, and therefore are limited to externally observable landmarks; because direct observations of the superior portions of the nasal airway are precluded by structures of the external face, all three therefore employ externally-observable facial landmarks as proxies for the internal dimensions of the superior nasal cavity. These points include the *ethmoid foramina* (anterior and

posterior), *dacryon* (discussed above as a potential facial landmark), and the *optic foramen* (recorded at its opening inside the orbit, as opposed to in the lateral basicranial landmark sets, where it was recorded at its endocranial margin). All four of these points lie within the medial wall of the orbit. Based on their analyses using these landmarks, these authors have suggested that the internal nasal cavity is relatively and absolutely taller in males than in females (Bastir et al. 2011), and that it is relatively taller, wider, and longer in cold-climate populations, especially in the superior portions (Noback et al. 2011); however, it is troubling that none of these authors discuss the suitability of landmarks they are using to define the maximum height, and length and breadth of the superior nasal airways.

The ethmoid foramina are located in the suture between the frontal and the lateral plates of the ethmoid, and allow the passage of nerves from the brain via canals which open endocranially as foramina of the same name, situated along the suture between the frontal and the cribriform plate. But while the cribriform plate constitutes the roof of the nasal airway, the lateral plates of the ethmoid are spatially separated from the lateral walls of the ethmoidal airway by the lateral masses, and the authors do not support the implication that ethmoidal breadth at the ethmoid foramina correlates in any way with ethmoidal airway breadth between the lateral masses.

Similar, since no midline points are used by any authors, the maximal height and length of the upper nasal cavity area is based on the use of landmarks of the medial orbital wall. The dacryon marks the anterosuperiormost point used for this purpose (Bastir et al. 2011; Bastir and Rosas 2013) and the optic canal marks the posterosuperiormost point (Bastir and Rosas 2013; Noback et al. 2011 rely solely on the ethmoid foramina for these dimensions). The dacryon is separated from the narrow internal airways of the ethmoid by the lateral masses, suffering the same problem as the ethmoid foramina, and likewise there is no immediately obvious correlation between its

anteroposterior position and the most anterior extent of the interior airway at its most superior point. The optic foramina are more problematic: these foramina are situated laterally on the sphenoid body, and beyond the posteriormost extent of the ethmoidal airways – and therefore it is unclear why they should be expected to accurately reflect any dimensions of the nasal airway. Rather, their position should be expected to reflect integration with highly conserved structures like the chondrocranial presphenoid and with brain and orbit morphology, and are wholly unsuitably for describing nasal airway dimensions.

The actual airways within the ethmoid reach their most superior point as very narrow passages immediately lateral to the nasal septum. Because this thesis employs CT scans as opposed to 3D surface scans, these internal nasal structures are accessible, so landmarks that directly represent the structures in question should be sought, i.e. the bilateral points that represent the anterosuperiormost and posterosuperiormost points within the ethmoidal airways. Practically, it was impossible to identify landmarks that could be measured with any reliability in these regions (see Intraobserver Error Tests, below). The ethmoidal airways are labyrinthine, extremely variable in shape, and often asymmetrical; the anterior boundary was easier to assess than the posterior one, but the walls of the airway are often continuous with no clear demarcation between the horizontal cribriform plate and the nasal bones, and conversely the anterior region of the ethmoid may or may not open into the foramen caecum; the posterior boundary was more problematic, due to the tendency of the ethmoidal airways to flare laterally posteriorly, and to remain continuously open into the sphenoid sinus, presenting no clear posterior boundary to the ethmoidal airways.

Because the cribriform plate represents the roof of the nasal cavity, the solution to these problems may be to record its dimensions to account for superior nasal cavity morphology. While the endocranial ethmoid foramina might be good candidates for this purpose, they are very small

and the bone of the cribriform plate is very thin, and as a result these foramina are rarely identifiable at the resolution used in these scans. It is potentially more practical to simply record the anterior and posterior corners of the cribriform plate itself: the posterior ethmoid foramina are located at the posterolateral corners of the cribriform plate anyway, and the corners are easy to identify due to the relief between the cribriform plate and the frontal and sphenoid; additionally, the posterior end of the cribriform plate sufficiently demarcates the posterosuperior extent of the nasal airway, where it opens into the sphenoid sinus. Conversely, the anterior endocranial ethmoid foramina are not actually located at the anteriormost extreme of the cribriform plate, so recording the anteriormost points on the plate itself should better reflect the true length of the roof of the ethmoid airways (anecdotally, the anteriormost points on the cribriform plate tend to fall very close to the points recorded at the anterosuperiormost margins of the ethmoidal airways, which, while it was difficult to identify these points with consistency, suggests the cribriform plate may serve as a more reliably measurable proxy).

Both the antero- and posterosuperiormost points of the internal ethmoid airway and the anterior and posterior corners of the cribriform plate were recorded, but the latter were chosen to represent the upper airway and the former discarded, based on their intraobserver measurement reliability (see below). The (ectocranial) ethmoid foramina were recorded, but were used only to test the implicit assumption by previous authors that they serve as a suitable proxy for the ethmoidal airways.

Twenty one landmarks were chosen to represent the internal nasal cavity; these are listed in Table 3.8 and presented in Figure 3.4.

Table 3.8: Final Nasal Cavity Landmarks

#	Name	Description
1	Rhinion	Midline point where the internasal suture meets the nasal aperture
2,3	Nasale inferius	Bilateral point where the nasomaxillary suture meets the nasal aperture
4,5	Anterior turbinate origin	Bilateral point on the margin of the nasal aperture at the level of the inferior turbinates
6,7	Inferior nasal margin	Inferolateralmost bilateral point on the margin of the nasal aperture
8	Anterior nasal spine	Anterosuperiormost midline point on the intermaxillary suture; the tip of the bony spine on the inferior margin of the nasal aperture
9	Posterior nasal spine	Posteriormost midline point on the interpalatine suture
10,11	Inferior choana corner	Inferiolateralmost point on the margin of the posterior nares
12,13	Posterior turbinate origin	Bilateral point on the posterior nares at the level of the inferior turbinates
14,15	Choana roof	Superiormost bilateral point on the external nares; the centre of the saddle-shaped structure that forms the roof of the choana
16	Hormion	Posteriormost midline point on the vomer, where it articulates with the sphenoid
17	Pharyngeal tubercle	Point of maximal projection in the midline
18,19	Anterior cribriform	Anterolateral corners of the cribriform plate
20,21	Posterior cribriform	Posterolateral corners of the cribriform plate

Figure 3. 10: Finalized nasal cavity landmarks. a. Nasal aperture; b. choanae/nasopharynx; c. upper airways/cribriform; d. overview of nasal cavity landmarrks in the lateral aspect.

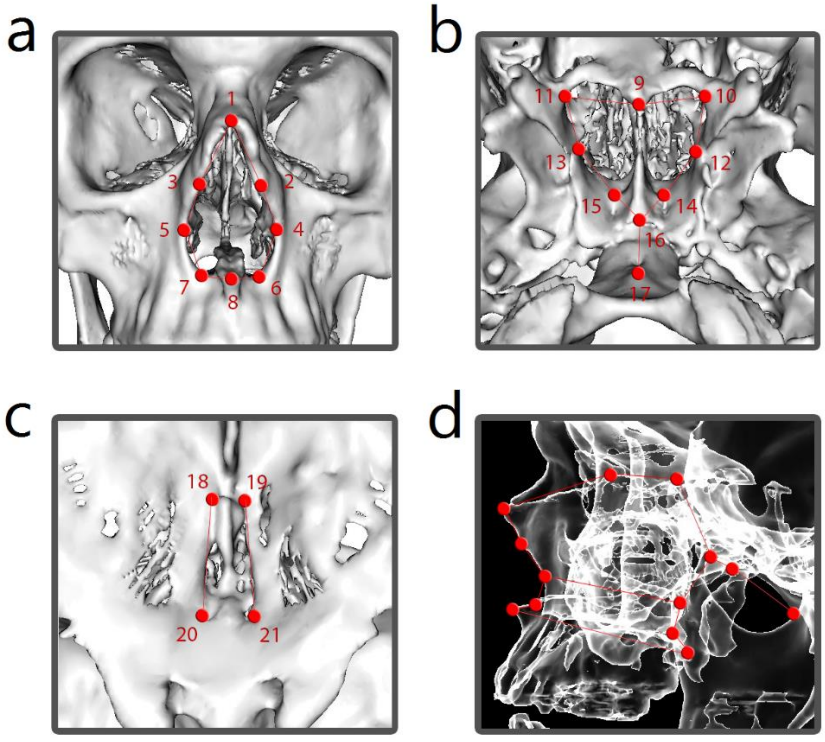

Statistics

Data Acquisition

Landmark coordinates were recorded using Mimics Innovation Suite (Materialise). 3D surfaces of cranial structures were reconstructed from CT scans, using Mimics' preset for bone (grey value threshold of 226) and most landmarks were applied directly to these surfaces. Some landmarks, such as those of the internal nasal cavity, were recorded on 2D slices, as opposed to on the surface reconstructions, because their internal location was obscured. Landmark data was exported as Cartesian (x,y,z) coordinates to a text (.txt) file.

Multivariate Analysis

Multivariate statistical analyses were performed in MorphoJ, v.1.06c (Klingenberg 2011). A series of principal components analyses was performed on the covariance matrices of each of the procrustes-transformed landmark sets representing the four cranial modules in question (midline cranial base, lateral cranial base, face, and internal nasal cavity), in order to observe group-specific variation and sex differences in each module.

A series of two-block partial least squares (singular warps) analyses was conducted on the procrustes-transformed landmark coordinates of the four cranial modules in question. A total of six PLS analyses were performed, in order to investigate all possible integrative relationships between combinations of these modules. Two-block PLS using the procrustes-transformed data for each block independently is preferred over within-configuration PLS, using a common procrustes superimposition of a single dataset representing two modules, because this includes information regarding the orientation and positioning of modules relative to one another; this

would exaggerate the degree of covariation between facial and basicranial modules, because of the orientational relationships between these structures, as mediated by cranial base angle (see above). Two-block PLS removes information regarding the relative sizes and orientations of blocks, and therefore assesses covariation in shape alone. Because the variables in question are explicitly shape-related (relative basicranial breadth; relative height, breadth, and length of the nasal cavity) covariation in size and orientation would obscure the shape relationships this thesis is seeking to observe.

In order to assess the suitability of the ethmoid foramina as a proxy for the internal ethmoid airways, two more PLS analyses were performed. A two-block PLS analysis was performed using the four ethmoid foramina and the four corners of the cribriform plate, in order to assess the degree of covariation between the relative breadths and lengths of these structures. Additionally, a within-configuration PLS analysis was conducted for the same eight points as a single block; in this case, the within-configuration analysis is informative since the orientation and size of these structures relative to one another is relevant to the question at hand. (It should be noted that the reasoning here is potentially circular, since the representativeness of the ethmoid foramina as a proxy for ethmoidal airway dimensions is being assessed based on a separate set of points which have been selected as a better proxy, with no independent test for *their* suitability as a proxy for the same thing. Nonetheless, because the cribriform plate itself comprises the roof of the ethmoidal airways, while the ethmoid foramina are spatially separated from it by the lateral masses, and based on the assumption that previous authors would have used some other landmark if they were not limited to externally-observable landmarks, it will be accepted *a priori* that these points are the more suitable proxy, and any discrepancies between the two will be discussed; at any rate, due to the irregular nature of the actual airway within the ethmoid, this may simply be a practical limitation

of landmark-based studies).

Error Tests

An assessment of intraobserver error was initially attempted following Noback et al. (2011): four individuals were selected at random and landmarks were recorded three times on different occasions (minimum one-week interval). Error was assessed by measuring Euclidean distances between the repeated measurements for each individual, and comparing these with the Euclidean distances between the remaining 55 individuals. Distances were recorded on the procrustes-transformed data for each module independently, because orientational variation between modules might exaggerate distances between some points more than others. Noback et al. (2011) determined their measurement error to be negligible, because the distribution of repeat distances did not overlap with the distribution of distances between individuals. In this analysis, I was unable to achieve such a separation (Fig.3.5), which was deemed to be the result of a shortcoming of the methodology and not the result of unacceptably high measurement error: because procrustes superimposition minimizes the sum of squared distances between landmark points, it could be expected that landmarks in morphologically-conserved areas would be scaled to within the degree of acceptable measurement error – the scaling and superimposition of points in different individuals to within very small distances has no real bearing on whether or not repeated measurements were recorded consistently.

As a result a new methodology was developed which compares the Euclidean distances between repeated measurements for the same individual with the distances between homologous landmarks between different individuals, for each landmark independently. The distances between repeat landmark measurements for each individual are compared with the distances between the

four remeasured individuals at the same landmark, instead of the distances between the other 55 individuals in the sample. This approach recognizes that different landmarks should express different levels of variability within a population, and therefore different levels of measurement error may be acceptable for different landmarks; it also allowed me to assess measurement error independently for each landmark to determine whether or not any landmarks should be excluded from the analysis.

Figure 3.5: Initial error test. Histograms representing the Euclidean distances between homologous landmarks in the entire sample (blue bars) and between repeat landmark measurements for four individuals (coloured bars, amplified by a factor of 10 for visibility)

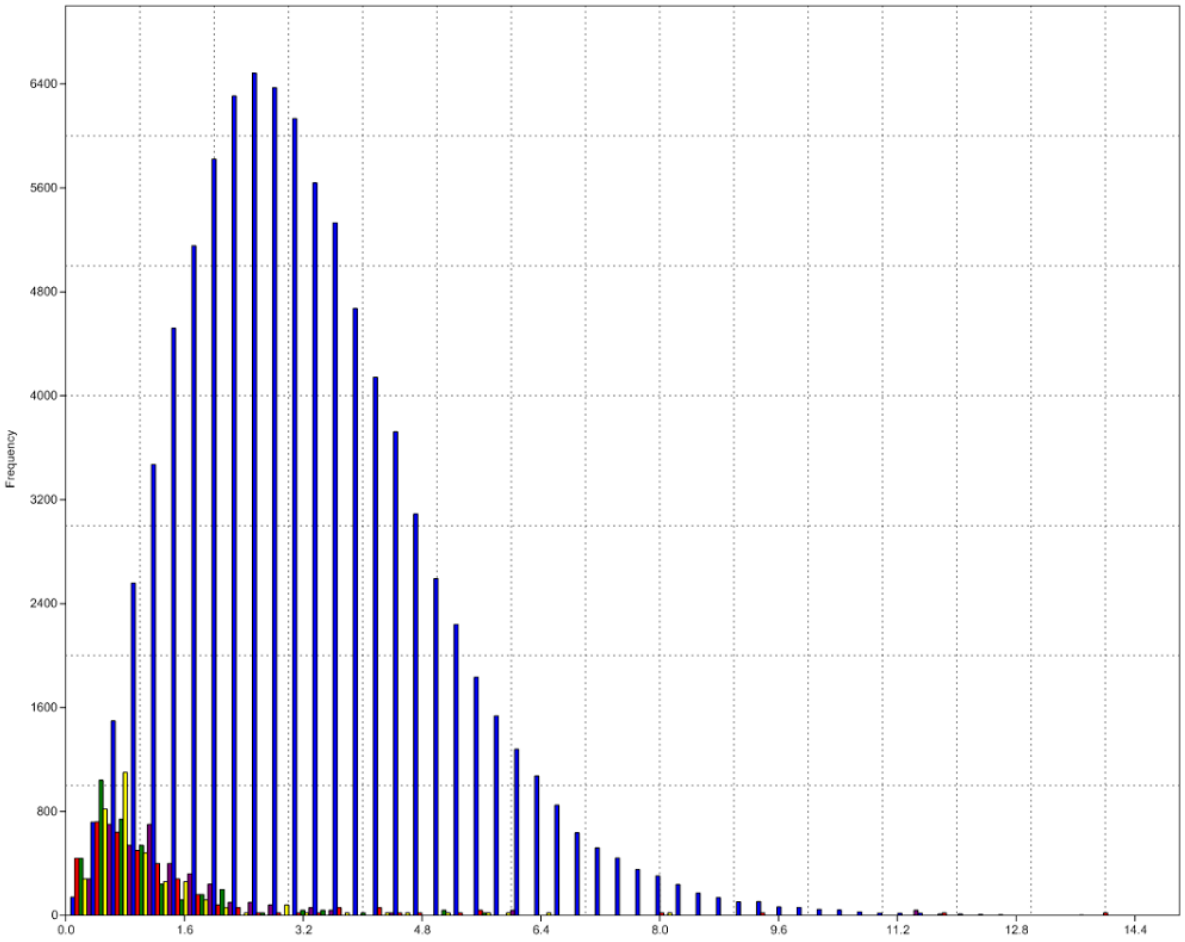

Figure 3.6 presents the Euclidean distances between repeat measurements

superimposed over boxplots representing the distribution of distances between the same points in the four remeasured individuals. Overall, the distances between repeat measurements tend to fall outside of or near the low end of the range of distribution of distances between individuals. The most obvious exception is the posterosuperiormost point in the ethmoidal airway (PA), and to a lesser extent the anterosuperiormost point in the ethmoidal airway (AA), which show a very low reliability in repeat measurements; therefore these points are excluded from the analysis.

All other distance measurements that overlap significantly with the between-individual distributions are represented by two distances for one or two individuals. Because the data points on the graph represent distances between points, where two distances are large and one is small, this means that two landmark measurements were consistent (one small distance between them) while one was aberrant (two greater distances between it and the other two points). In order to assess the degree to which the aberrant measurements were the result of inexperience in placing landmarks, all landmarks were recorded three more times for each of four individuals at minimum 24 hour intervals. The rejected landmarks, the anterosuperiormost and posterosuperiormost points in the ethmoidal airways, have been excluded and replaced by the anterior and posterior corners of the cribriform plate. Additionally, it was found that one individual used in the initial error test was erroneously included in the analysis despite having a broken nose; this individual was replaced with another randomly selected individual.

The results of the second error test are presented in Figure 3.7. Overall, there is much less overlap between the distances between repeat measurements and the between-individual distance distributions, which supports the assessment that experience gained in the course of landmark placement resulted in more consistency in landmark placement, and for this reason landmarks were re-recorded for the entire sample for the final analysis. Regarding the landmarks of the cribriform

plate, these landmarks are much more reliable than the landmarks of the internal ethmoidal airways, and therefore the former will be used in the final analysis and the latter excluded.

Figure 3.6: First measurement error test: median and 25-75% quartiles (boxplots) and min/max distribution (whiskers) for Euclidean distances between individuals; points represent the Euclidean distances between three repeat measurements, colour-coded by individual

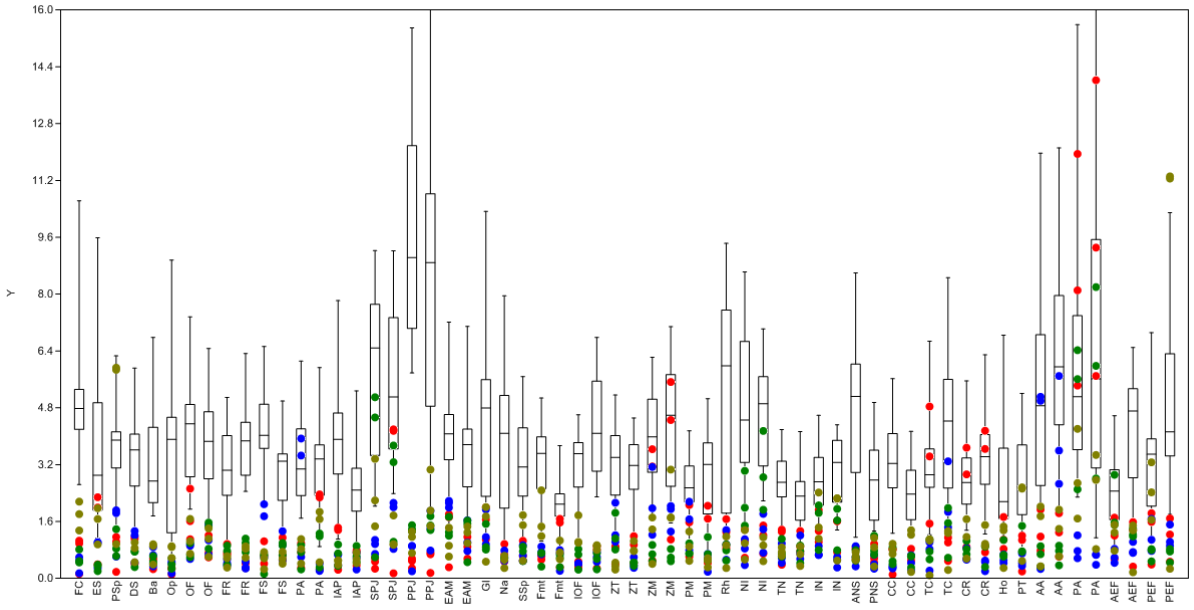

Several repeat distances overlap with the between-individual distributions, although there are fewer than in the first analysis. In some cases, such as foramen caecum (FC) and nasale inferius (NI), the aberrant distances are represented by only one individual; this suggests that while certain landmarks may be consistent and reliably identifiable in most individuals, a small number of individuals may have unusual morphologies that complicate landmark placement; furthermore, since all four individuals are outliers with regards to at least one landmark, this suggests that the problem is not with any one individual or any one landmark in particular, but rather is the result of the complex nature of inter-individual cranial variability – every landmark has the potential to be morphologically unusual in some individuals, and every individual has the potential to be

morphologically unusual at some landmark. Additionally, some bilateral landmarks show discrepancies in repeat consistency between left and right sides, e.g.: petrosal apex (PA), frontomalare temporale (Fmt). I interpret this to mean that, because the landmark placement can be demonstrated to be consistently repeatable on one side, the discrepancy is not the result of the fallibility of the landmark itself but of ambiguous individual landmark morphology due to individual variability. The takeaway is that, while there may be the potential for ambiguity in measurement placement in any individual at any landmark, this is the unfortunate but unavoidable reality of cranial variability.

Figure 3.7: Second measurement error test: median and 25-75% quartiles (boxplots) and min/max distribution (whiskers) for Euclidean distances between individuals; points represent the Euclidean distances between three repeat measurements, colour coded by individual.

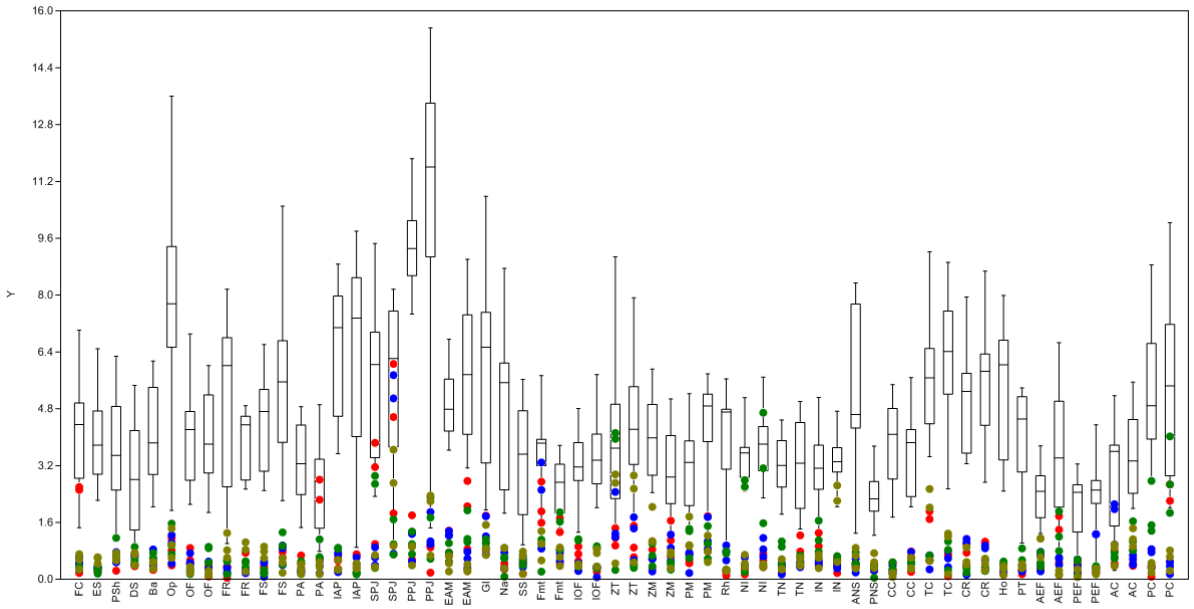

Chapter 4: Results

Principal Components Analysis

The results of the four principal components analyses are presented in Figures 4.1-4.4. Scatterplots of the first two principal components show no obvious population- or sex-specific signals for any of the four modules (midline cranial base, lateral cranial base, face, and nasal cavity).

95% confidence ellipses for the Belgrade and Winnipeg populations overlap substantially in all four modules (Figs. 4.1a-4.4a). The Winnipeg ellipses do tend to be elongated and extend beyond the range of the Belgrade ellipses, but this is probably an effect of the small sample size of the Winnipeg population (N=5). Since the Winnipeg sample is of primarily of mixed European ancestry, it is not surprising that there would be no significant differences in cranial morphology from the Belgrade sample.

Figure 4.1: Principal components analysis of midline cranial base landmarks. (a) PC1 and PC2 with 95% confidence ellipses for the Belgrade (black) and Winnipeg (grey) samples. (b) PC1 and PC2 with 95% confidence ellipses for male (black) and female (grey) samples.

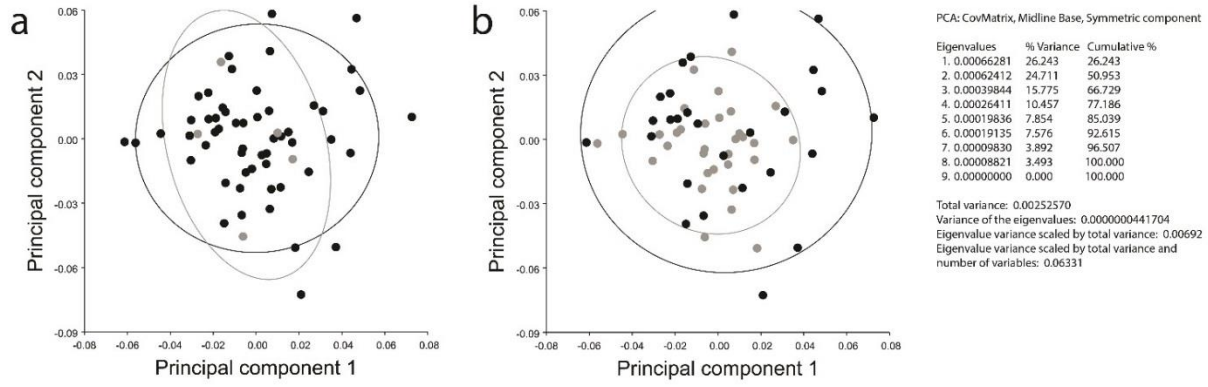

Similarly, the 95% confidence ellipses for male and female samples overlap almost entirely in all four modules Figs.4.1b-4.4b). The female sample falls entirely within the male range of variability for the midline cranial base (Fig.4.1b), which may suggest male midline cranial base architecture is more variable or less conserved than female, but it does not reveal and trends

regarding shape differences. While the ranges overlap substantially regarding male and female nasal cavity morphology, the 95% ellipses lie somewhat orthogonal to one another (Fig.4.4b), which might relate to sex-specific differences in male and female nasal morphology observed by other authors (Bastir et al. 2011), but it could also be due to the small sample size.

Figure 4.2: Principal components analysis of lateral cranial base landmarks. (a) PC1 and PC2 with 95% confidence ellipses for the Belgrade (black) and Winnipeg (grey) samples. (b) PC1 and PC2 with 95% confidence ellipses for male (black) and female (grey) samples.

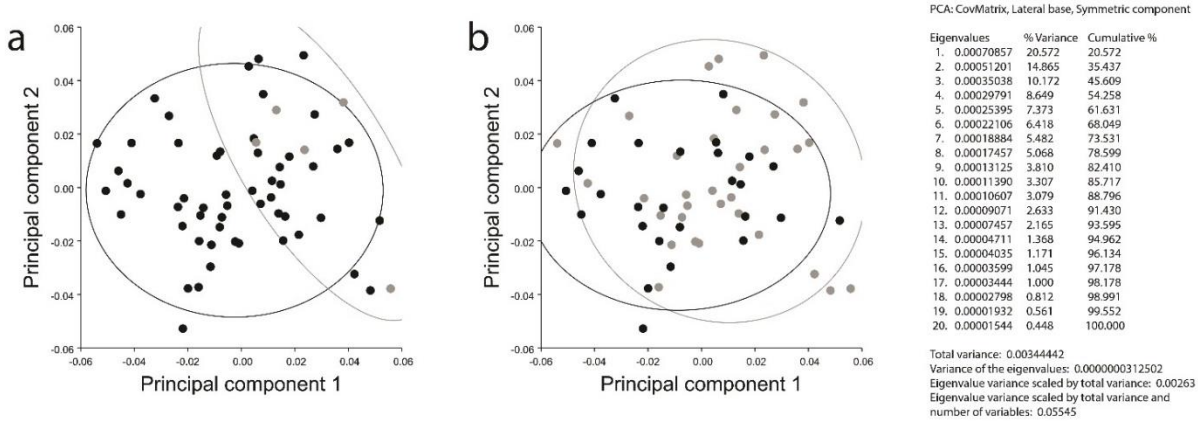

PCA: CovMatrix, Lateral base, Symmetric component

Eigenvalues		% Variance	Cumulative %
1.	0.00070857	20.572	20.572
2.	0.00051201	14.865	35.437
3.	0.00035038	10.172	45.609
4.	0.00029791	8.649	54.258
5.	0.00025395	7.373	61.631
6.	0.00022106	6.418	68.049
7.	0.00018884	5.482	73.531
8.	0.00017457	5.068	78.599
9.	0.00013125	3.810	82.410
10.	0.00011390	3.307	85.717
11.	0.00010607	3.079	88.796
12.	0.00009071	2.633	91.430
13.	0.00007457	2.165	93.595
14.	0.00004711	1.368	94.962
15.	0.00004035	1.171	96.134
16.	0.00003599	1.045	97.178
17.	0.00003444	1.000	98.178
18.	0.00002798	0.812	98.991
19.	0.00001932	0.561	99.552
20.	0.00001544	0.448	100.000

Total variance: 0.00344442
Variance of the eigenvalues: 0.0000000312502
Eigenvalue variance scaled by total variance: 0.00263
Eigenvalue variance scaled by total variance and number of variables: 0.05545

Figure 4.3: Principal components analysis of facial landmarks. (a) PC1 and PC2 with 95% confidence ellipses for the Belgrade (black) and Winnipeg (grey) samples. (b) PC1 and PC2 with 95% confidence ellipses for male (black) and female (grey) samples.

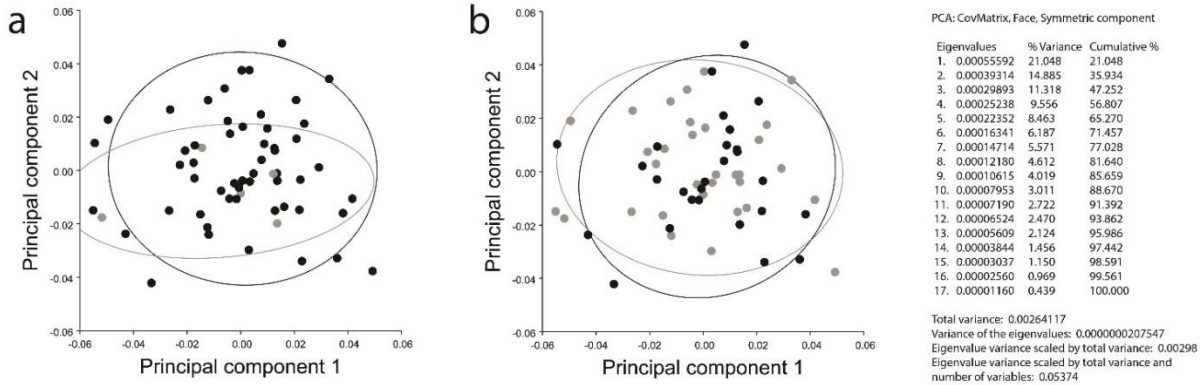

PCA: CovMatrix, Face, Symmetric component

Eigenvalues		% Variance	Cumulative %
1.	0.00055592	21.048	21.048
2.	0.00039314	14.885	35.934
3.	0.00029893	11.318	47.252
4.	0.00025238	9.556	56.807
5.	0.00022352	8.463	65.270
6.	0.00016341	6.187	71.457
7.	0.00014714	5.571	77.028
8.	0.00012180	4.612	81.640
9.	0.00010615	4.019	85.659
10.	0.00007953	3.011	88.670
11.	0.00007190	2.722	91.392
12.	0.00006524	2.470	93.862
13.	0.00005609	2.124	95.986
14.	0.00003844	1.456	97.442
15.	0.00003037	1.150	98.591
16.	0.00002560	0.969	99.561
17.	0.00001160	0.439	100.000

Total variance: 0.00264117
Variance of the eigenvalues: 0.0000000207547
Eigenvalue variance scaled by total variance: 0.00298
Eigenvalue variance scaled by total variance and number of variables: 0.05374

Figure 4.4: Principal components analysis of nasal cavity landmarks. (a) PC1 and PC2 with 95% confidence ellipses for the Belgrade (black) and Winnipeg (grey) samples. (b) PC1 and PC2 with 95% confidence ellipses for male (black) and female (grey) samples.

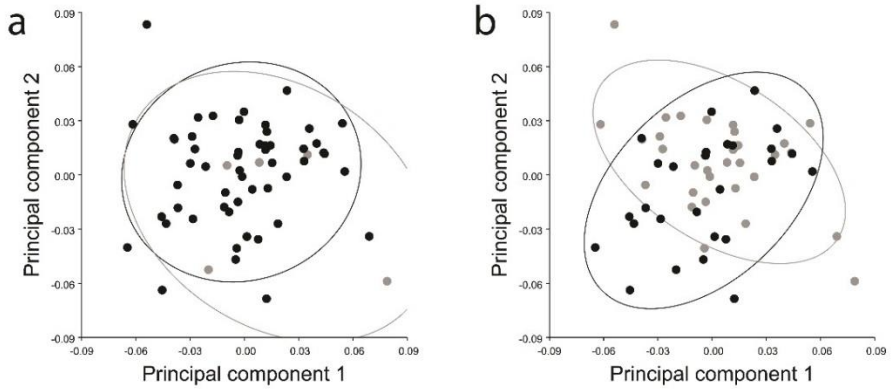

PCA: CovMatrix, Nasal Cavity, Symmetric component

Eigenvalues		% Variance	Cumulative %
1.	0.00100974	20.311	20.311
2.	0.00084953	17.088	37.399
3.	0.00056317	11.328	48.727
4.	0.00035371	7.115	55.841
5.	0.00029080	5.849	61.691
6.	0.00025650	5.159	66.850
7.	0.00023111	4.649	71.499
8.	0.00019918	4.006	75.505
9.	0.00017820	3.585	79.090
10.	0.00015294	3.076	82.166
11.	0.00014590	2.935	85.101
12.	0.00011580	2.329	87.430
13.	0.00009906	1.992	89.422
14.	0.00007340	1.476	90.899
15.	0.00006844	1.377	92.276
16.	0.00006253	1.258	93.533
17.	0.00004842	0.974	94.507
18.	0.00004092	0.823	95.330
19.	0.00003863	0.777	96.107
20.	0.00003190	0.642	96.749
21.	0.00002821	0.567	97.317
22.	0.00002611	0.525	97.842
23.	0.00002189	0.440	98.282
24.	0.00001862	0.375	98.657
25.	0.00001664	0.335	98.991
26.	0.00001443	0.290	99.282
27.	0.00001205	0.242	99.524
28.	0.00001083	0.218	99.742
29.	0.00000730	0.147	99.889
30.	0.00000553	0.111	100.000

Total variance: 0.00497150
Variance of the eigenvalues: 0.0000000575476
Eigenvalue variance scaled by total variance: 0.00233
Eigenvalue variance scaled by total variance and number of variables: 0.07226

Table 4.1: PLS correlations and statistical significance

Modules	**Correlations Coefficient (RV)**	**Significance (p)**
Midline base/lateral base	0.2884	<0.0001
Midline base/face	0.1957	0.0019
Midline base/nasal cavity	0.2571	<0.0001
Lateral base/face	0.2790	0.0001
Lateral base/nasal cavity	0.2454	0.0009
Face/nasal cavity	0.3123	<0.0001

Partial Least Squares

The results of the partial least squares analyses are presented in Table 4.1. Statistically significant correlations were observed for the first singular warp in all six combinations of modules. The strongest overall correlation was between the face and the nasal cavity (RV=0.3123, P<0.0001), while the weakest was between the face and the midline cranial base (RV=0.1957, P=0.0019). Overall, the first singular warps (PLS1) in all analyses are very strong, and appear to represent covariation along the dimension of dolicho/brachycephalic morphologies: variation in

midline basicranial length and flexion; rotation of the petrous pyramids and depth of the MCF in the lateral cranial base; short/wide vs. tall/narrow faces; and the height of the ethmoidal airways and area of the choanae in the nasal cavity.

Figure 4.5: PLS, midline base vs. lateral base. (a) Projection of individuals along the first singular warp (PLS1) of the midline and lateral cranial base. Average shapes (grey) and positive shape deformations (black; scale factor 0.1) of (b) the midline cranial base (lateral aspect), and (c) the lateral cranial base (superior and lateral aspects).

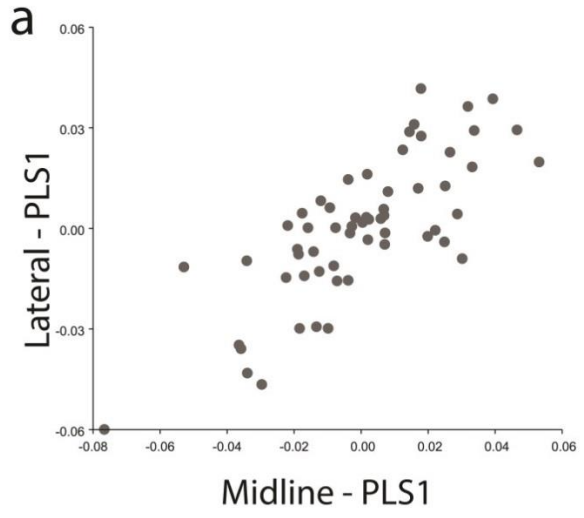

PLS: MidlineCranial base/lateral cranial base

Overall strength of association between blocks:
RV coefficient: 0.2884

Permutation test against the null hypothesis of independence
Number of randomization rounds: 10000
P-value: <.0001

Singular values and pairwise correlations of PLS scores between blocks:

	Singular value	P-value (perm.)	% total covar.	Correlation	P-value (perm.)
PLS1	0.00040186	0.0001	47.288	0.77320	<.0001
PLS2	0.00030030	<.0001	26.406	0.64300	0.0024
PLS3	0.00021038	0.0001	12.960	0.59223	0.0131
PLS4	0.00014849	0.0083	6.456	0.49523	0.1263
PLS5	0.00010504	0.0973	3.231	0.42457	0.2991
PLS6	0.00007724	0.2451	1.747	0.39059	0.2822
PLS7	0.00006516	0.0816	1.243	0.41567	0.0598
PLS8	0.00004778	0.0970	0.669	0.43025	0.0038
PLS9	0.00000019	0.4338	0.000	0.41821	0.0283

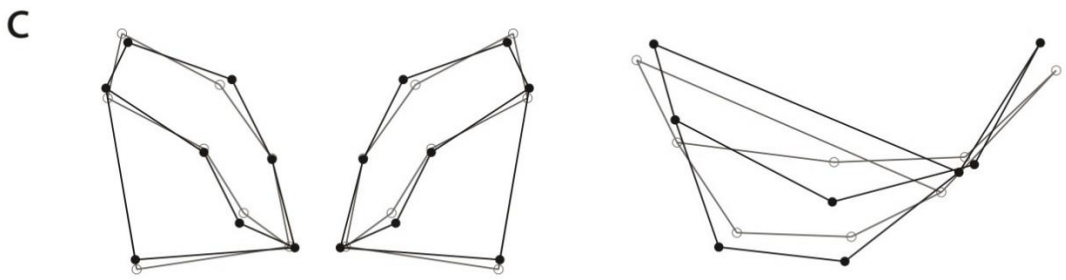

PLS – Midline/Lateral Cranial Base

The singular warps for the midline and lateral cranial base are presented in Figure 4.5. The

first singular warp (PLS1) is characterized by a strong correlation (RV=0.7732) and accounts for 47% of the total covariation (plotted in Fig.4.5a). Variation along this axis is expressed by the degree of flexion and overall length of the midline cranial base, and by the degree of petrous rotation and depth of the MCF in the lateral cranial base. Overall, longer, extended midline cranial bases correlate with coronally rotated petrous pyramids and shallower MCFs.

Figure 4.6: PLS, midline base vs. face. (a) Projection of individuals along the first singular warp (PLS1) of the midline cranial base and face. Average shapes (grey) and positive shape deformations (black; scale factor 0.1) of (b) the midline cranial base (lateral aspect), and (c) the face (anterior and superior aspects)

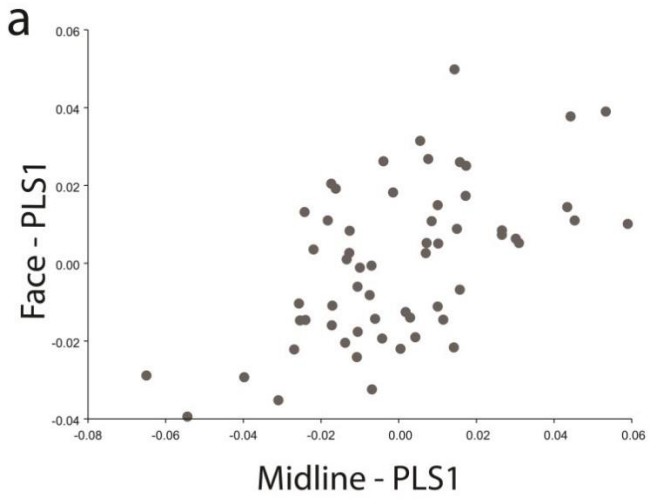

PLS: Midline cranial base/Face

Overall strength of association between blocks:
RV coefficient: 0.1957

Permutation test against the null hypothesis of independence
Number of randomization rounds: 10000
P-value: 0.0019

Singular values and pairwise correlations of PLS scores between blocks:

	Singular value	P-value (perm.)	% total covar.	Correlation	P-value (perm.)
PLS1	0.00027841	0.0353	42.262	0.57580	0.1190
PLS2	0.00022134	0.0070	26.712	0.49223	0.2956
PLS3	0.00015878	0.0259	13.746	0.49000	0.1678
PLS4	0.00010959	0.1813	6.548	0.46390	0.1688
PLS5	0.00008724	0.1646	4.149	0.41588	0.2171
PLS6	0.00007289	0.0661	2.897	0.41030	0.1004
PLS7	0.00006384	0.0054	2.222	0.39334	0.0432
PLS8	0.00005181	0.0010	1.464	0.37800	0.0055
PLS9	0.00000014	0.6348	0.000	0.35371	0.0572

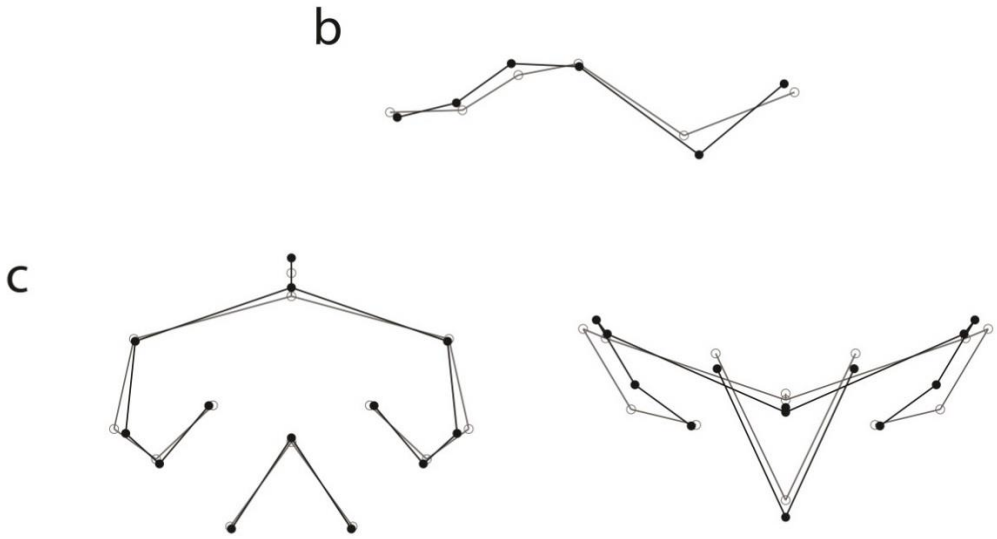

PLS – Midline Cranial Base/Face

The singular warps for the midline cranial base and face are presented in Figure 4.6. PLS1 is characterized by a moderate to strong correlation (RV=0.5758) and accounts for 42% of the total covariation (Fig.4.6a). Along this axis, facial variation reflects dolicho- vs. brachyfacial morphologies (tall and narrow vs. short and wide), and, as evident in the superior aspect (Fig.4.6c), dolichofacial morphologies are associated with an anterior rotation of the lateral parts of the face relative to midline structures (glabella/nasion, dental arcade). Overall, dolichofacial morphologies correlate with increased basicranial flexion while brachyfacial morphologies correlate with increased extension and overall length of the midline cranial base; however, these modules have the weakest overall integrative relationship of any observed in this study (RV=0.1957).

PLS – Midline Cranial Base/Nasal Cavity

The singular warps for the midline cranial base and nasal cavity are presented in Figure 4.7. PLS1 exhibits a strong correlation (RV=0.6696) and accounts for 43.365% of the total covariation. Nasal cavity variation along this axis seems to be driven primarily by the position of the cribriform plate (especially the posterior part) and the nasopharynx (the choanal rooves, hormion, and pharyngeal tubercle). Notably, these structures can be interpreted to be part of the cranial base, since they are parts of the ethmoid and sphenoid and derive from the chondrocranium, whereas all the other nasal cavity landmarks lie on intramembranous bone. Therefore, the integrative relationship between the nasal cavity and midline cranial base seems to be the result of constraints imposed by midline cranial base flexion and length on the superior and posterior parts of the nasal cavity.

Figure 4.7: PLS, midline base vs. nasal cavity. (a) Projection of individuals along the first singular warp (PLS1) of the midline cranial base and nasal cavity. Average shapes (grey) and positive shape deformations (black; scale factor 0.1) of (b) the midline cranial base (lateral aspect), and (c) the nasal cavity (lateral and anterior aspects).

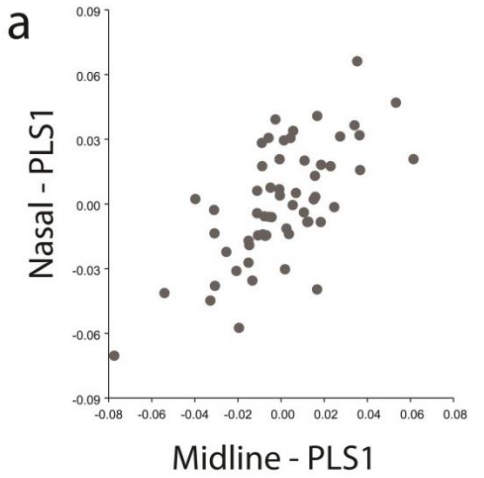

PLS: midline cranial base/Nasal cavity

Overall strength of association between blocks:
RV coefficient: 0.2571

Permutation test against the null hypothesis of independence
Number of randomization rounds: 10000
P-value: <.0001

Singular values and pairwise correlations of PLS scores between blocks:

	Singular value	P-value (perm.)	% total covar.	Correlation	P-value (perm.)
PLS1	0.00043707	0.0023	43.365	0.66960	0.0009
PLS2	0.00037019	<.0001	31.109	0.61245	0.0097
PLS3	0.00022116	0.0130	11.103	0.56373	0.0450
PLS4	0.00016293	0.0472	6.026	0.51977	0.1216
PLS5	0.00014619	0.0026	4.852	0.49354	0.1446
PLS6	0.00008418	0.5945	1.608	0.48631	0.0823
PLS7	0.00007224	0.2775	1.185	0.38419	0.4471
PLS8	0.00005754	0.1743	0.752	0.41286	0.1078
PLS9	0.00000028	0.1808	0.000	0.48265	0.0245

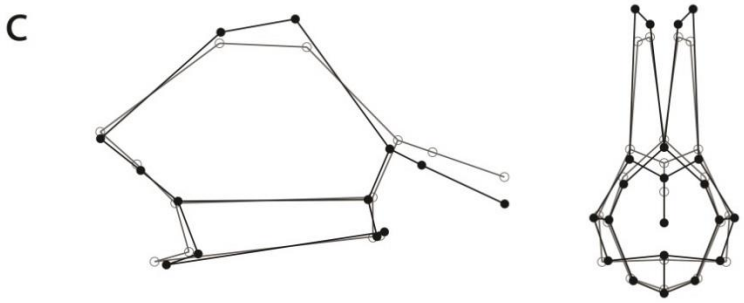

PLS – Lateral cranial base/face

The singular warps for the lateral cranial base and the face are presented in Figure 4.8. PLS1 is characterized by a strong correlation (RV=0.69955) and accounts for 55% of the total covariation. Along this axis, variation in both structures is generally the same as that observed in their relationships with the midline cranial base: shallower, more coronally-oriented petrous bones correlate with short and wide faces. In the superior aspects (Fig. 4.8b,c), it is evident that as the

petrous pyramids and MCF rotate coronally relative to the midline cranial base, they are accompanied by an anterior rotation of the lateral parts of the face relative to midline structures.

Figure 4.8: PLS, lateral base vs. face. (a) Projection of individuals along the first singular warp (PLS1) of the lateral cranial base and face. Average shapes (grey) and positive shape deformations (black; scale factor 0.1) of (b) the lateral cranial base (superior and lateral aspects), and (c) the face (anterior and superior aspects).

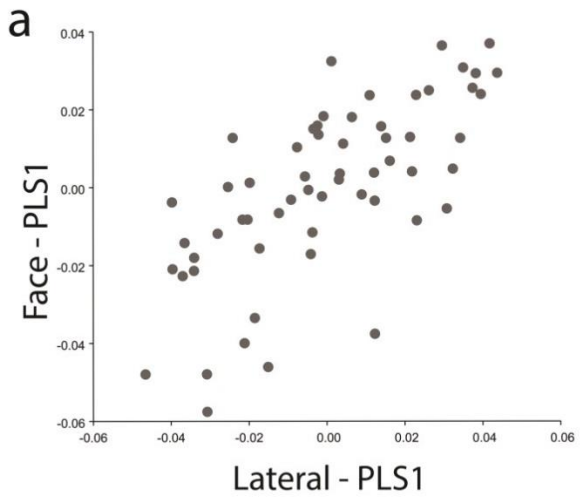

PLS: Lateral cranial base/Face

Overall strength of association between blocks:
RV coefficient: 0.2790

Permutation test against the null hypothesis of independence
Number of randomization rounds: 10000
P-value: 0.0001

Singular values and pairwise correlations of PLS scores between blocks:

	Singular value	P-value (perm.)	% total covar.	Correlation	P-value (perm.)
PLS1	0.00038408	0.0001	54.838	0.69955	0.0023
PLS2	0.00017957	0.4074	11.987	0.67221	0.0073
PLS3	0.00016828	0.0430	10.527	0.56749	0.2082
PLS4	0.00015380	0.0035	8.793	0.56581	0.1330
PLS5	0.00011466	0.0868	4.887	0.51961	0.2558
PLS6	0.00009048	0.3186	3.043	0.46209	0.4926
PLS7	0.00006903	0.7803	1.771	0.42254	0.6057
PLS8	0.00005401	0.9450	1.084	0.43186	0.3777
PLS9	0.00004922	0.7889	0.901	0.32304	0.8979
PLS10	0.00004602	0.3711	0.787	0.42911	0.1275
PLS11	0.00003517	0.6925	0.460	0.39627	0.1417
PLS12	0.00003027	0.5115	0.341	0.35821	0.1784
PLS13	0.00002628	0.2754	0.257	0.30386	0.2819

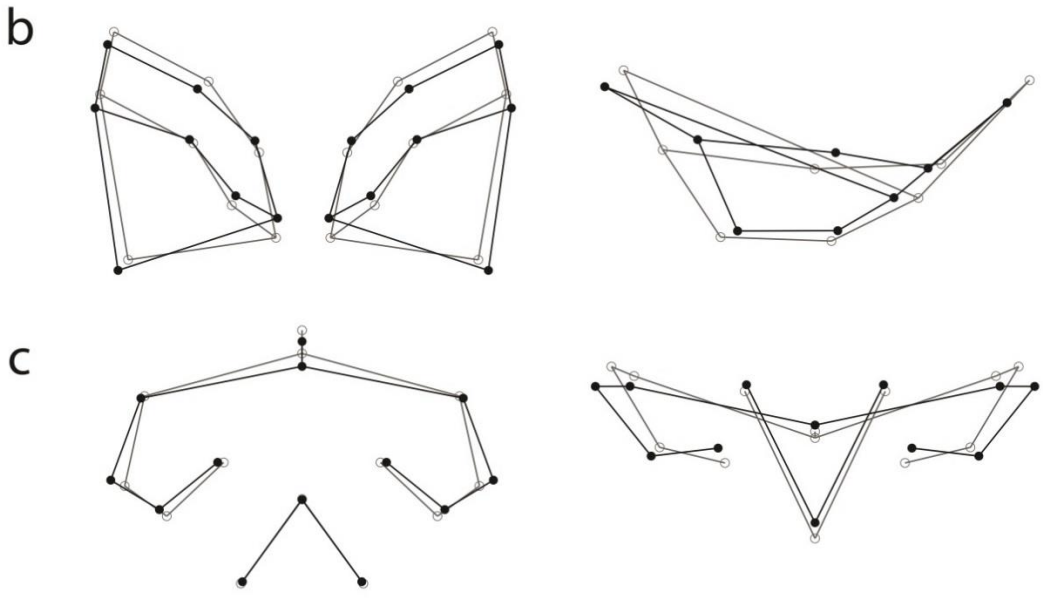

PLS – Lateral Cranial Base/Nasal Cavity

The singular warps for the lateral cranial base and nasal cavity are presented in Figure 4.9. PLS1 exhibits a moderate to strong correlation (RV=0.61803) and accounts for 40% of the total

covariation. Variation in petrous rotation and MCF depth along this axis is correlated primarily with the superoinferior position and breadth of the cribriform plate, as well as with the size of the choanae and, to a lesser degree, the nasal aperture (i.e. cold climate vs. warm climate morphologies observed by Noback et al. 2011). Overall, coronally-rotated and shallow petrous pyramids correlate with shorter internal nasal cavities that are broader with larger openings.

While the correlation is relatively strong for the first singular warp (RV=0.618), PLS1 accounts for the lowest percentage of total variation out of all of the first singular warps in all six analyses (40%), and it is not significant at the .95 level (p=0.08). While it only represents a small percent of the total variation (13%), in this analysis PLS3 exhibits a stronger correlation than PLS1 (RV=0.69575) and statistically significant (p=0.0026). This may reflect a dimension of variability unique to the relationship between the lateral cranial base and face (Figure 4.10).

PLS – Face/Nasal Cavity

The singular warps for the midline cranial base and nasal cavity are presented in Figure 4.11. PLS1 exhibits a strong correlation (RV=0.67315) and accounts for 42% of the total covariation. Variation along this axis is yet again similar to that observed in the previous relationships: faces that are shorter, broader, and which are characterized by anterior rotation of the lateral regions relative to the midline, are correlated with nasal cavities that are shorter and broader, and which are characterized by larger openings at the nasal aperture and choanae. Additionally, these two modules expressed the strongest integrative relationship of all those observed in the study (RV=0.3123).

Figure 4.9: PLS, lateral base vs. nasal cavity. (a) Projection of individuals along the first singular warp (PLS1) of the lateral cranial base and nasal cavity. Average shapes (grey) and positive shape deformations (black; scale factor 0.1) of (b) the lateral cranial base (superior and lateral aspects), and (c) the nasal cavity (lateral and anterior aspects).

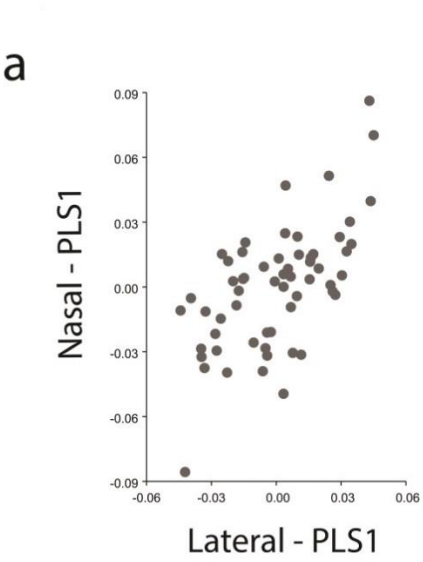

PLS: Lateral cranial base/Nasal Cavity

Overall strength of association between blocks:
RV coefficient: 0.2454

Permutation test against the null hypothesis of independence
Number of randomization rounds: 10000
P-value: 0.0009

Singular values and pairwise correlations of PLS scores between blocks:

	Singular value	P-value (perm.)	% total covar.	Correlation	P-value (perm.)
PLS1	0.00041510	0.0128	39.843	0.61803	0.0770
PLS2	0.00033080	0.0013	25.303	0.59316	0.1011
PLS3	0.00023348	0.0248	12.605	0.69575	0.0017
PLS4	0.00015900	0.5527	5.846	0.46085	0.8343
PLS5	0.00014512	0.2304	4.870	0.58926	0.1241
PLS6	0.00010841	0.8610	2.718	0.51576	0.4417
PLS7	0.00009370	0.8677	2.030	0.49144	0.5065
PLS8	0.00008382	0.7724	1.625	0.48823	0.4200
PLS9	0.00006942	0.9131	1.114	0.49654	0.2491
PLS10	0.00006520	0.6349	0.983	0.48770	0.2012
PLS11	0.00005958	0.3621	0.821	0.44866	0.3361
PLS12	0.00005477	0.1276	0.694	0.30518	0.9784
PLS13	0.00004777	0.0949	0.528	0.41461	0.3717
PLS14	0.00003529	0.6533	0.288	0.55309	0.0017
PLS15	0.00003426	0.1416	0.271	0.40282	0.2582
PLS16	0.00002705	0.3718	0.169	0.29330	0.8342
PLS17	0.00002223	0.4263	0.114	0.27234	0.8144
PLS18	0.00001838	0.3857	0.078	0.38122	0.0623
PLS19	0.00001504	0.2892	0.052	0.26618	0.4078
PLS20	0.00001448	0.0130	0.048	0.26832	0.1082

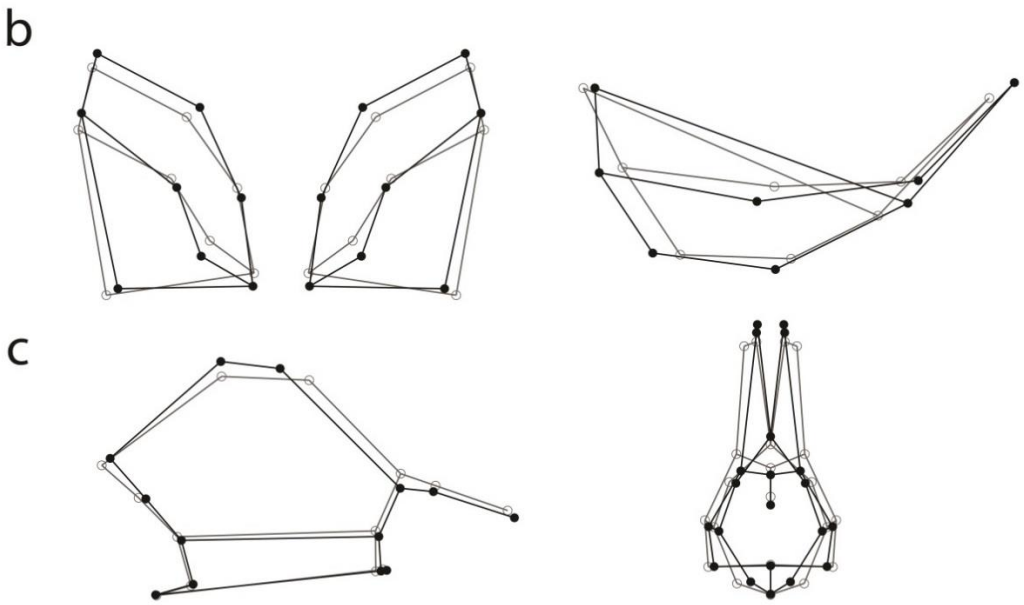

Similarly to the relationship between the lateral base and nasal cavity, PLS3 exhibits a stronger and more significant correlation than PLS1 (RV=0.7184, p=0.0004). Shape changes in the nasal cavity along this dimension are similar to those in PLS3 lat/nas: in both cases, this dimension reflects differences in the area of the choanal openings, as well as a skewing relationship

between the upper and lower portions of the internal nasal cavity in the lateral aspect (Fig.4.10). This might suggest a dimension of shape variability in the nasal cavity, outside of the general brachy/dolicohcephalic dimension, which is having a small but detectable integrative influence on the rest of the cranium.

Figure 4.10: PLS3, lateral base vs. nasal cavity. Average shapes (grey) and positive shape deformations (black; scale factor 0.1) of (a) the lateral cranial base (superior and lateral aspects), and (b) the nasal cavity (lateral and anterior aspects) along PLS3.

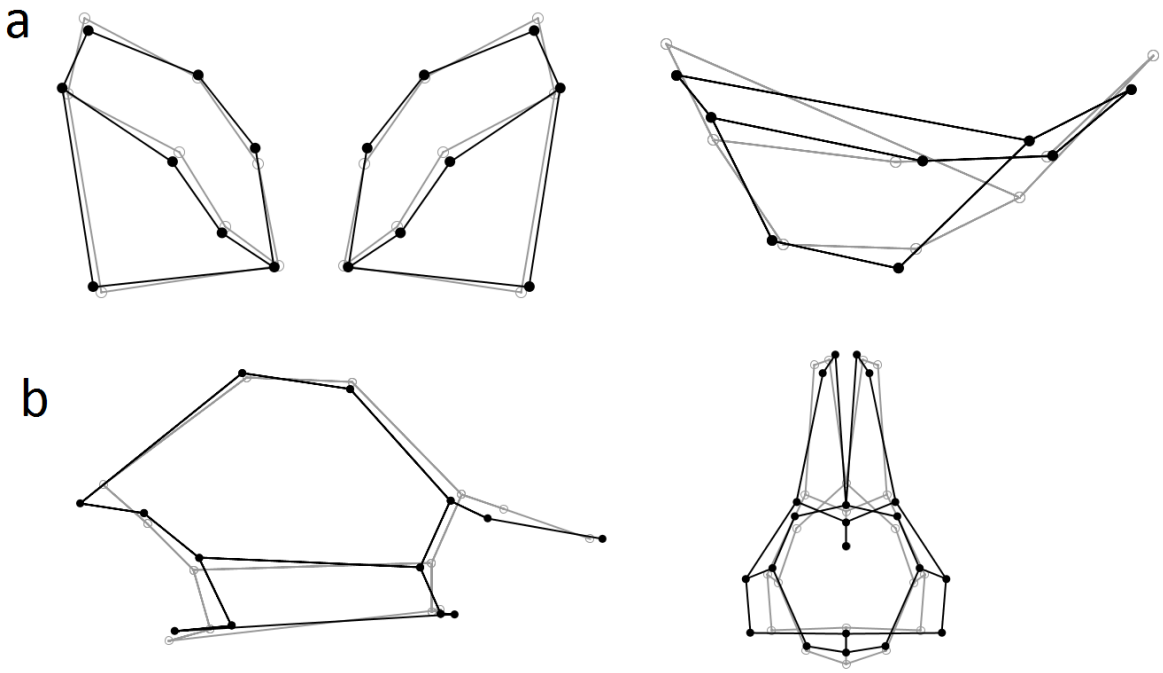

Figure 4.11: PLS, Face vs. nasal cavity. (a) Projection of individuals along the first singular warp (PLS1) of the face and nasal cavity. Average shapes (grey) and positive shape deformations (black; scale factor 0.1) of (b) the face (anterior and superior aspects), and (c) the nasal cavity (lateral and anterior aspects.)

a

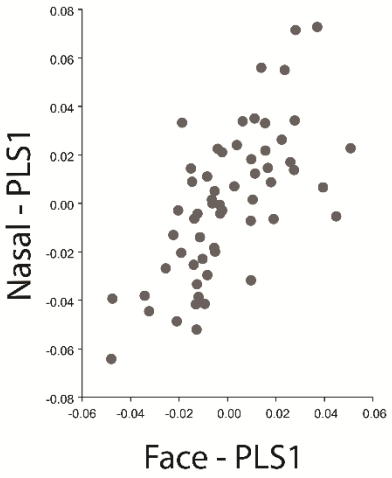

PLS: Face/Nasal cavity

Overall strength of association between blocks:
RV coefficient: 0.3123

Permutation test against the null hypothesis of independence
Number of randomization rounds: 10000
P-value: <.0001

Singular values and pairwise correlations of PLS scores between blocks:

	Singular value	P-value (perm.)	% total covar.	Correlation	P-value (perm.)
PLS1	0.00042837	0.0004	42.120	0.67315	0.0069
PLS2	0.00033572	<.0001	25.870	0.66822	0.0047
PLS3	0.00020523	0.0264	9.667	0.71840	0.0001
PLS4	0.00017137	0.0147	6.741	0.54986	0.2596
PLS5	0.00014221	0.0194	4.642	0.68551	0.0010
PLS6	0.00012558	0.0062	3.620	0.55360	0.1411
PLS7	0.00010254	0.0258	2.413	0.53602	0.1547
PLS8	0.00008205	0.1687	1.545	0.46120	0.4849
PLS9	0.00006446	0.5654	0.954	0.46199	0.3601
PLS10	0.00005727	0.4010	0.753	0.46911	0.2155
PLS11	0.00004992	0.3275	0.572	0.50889	0.0353
PLS12	0.00004113	0.4632	0.388	0.50714	0.0170
PLS13	0.00003405	0.5340	0.266	0.35490	0.5434
PLS14	0.00003015	0.2831	0.209	0.45362	0.0309
PLS15	0.00002301	0.5150	0.122	0.45824	0.0084
PLS16	0.00002021	0.1925	0.094	0.35481	0.0959

b

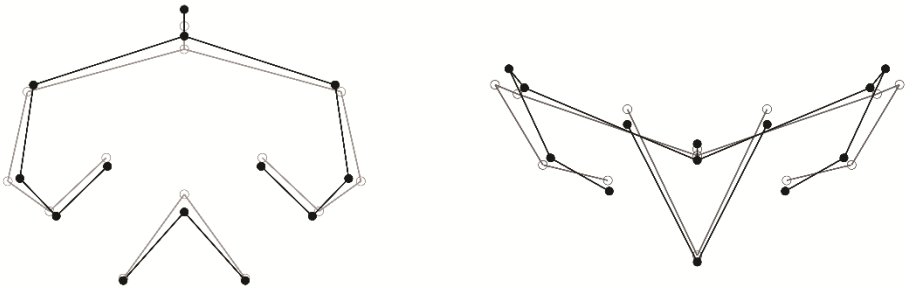

c

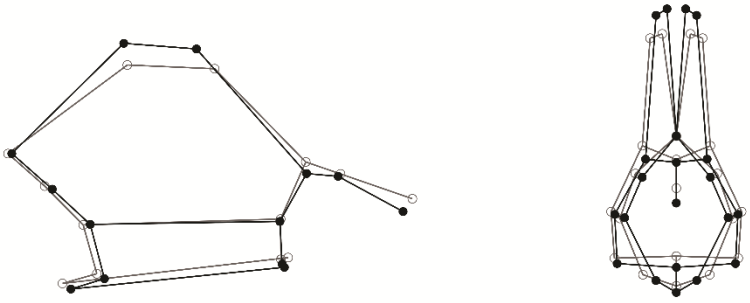

Figure 4.12: Two-block PLS, upper airways. (a) Projection of individuals along the first singular warp (PLS1) of the upper airways. Average shapes (grey) and positive shape deformations (black; scale factor 0.1) of (b) the ethmoid foramina, and (c) the cribriform plate (superior aspect, anterior is down).

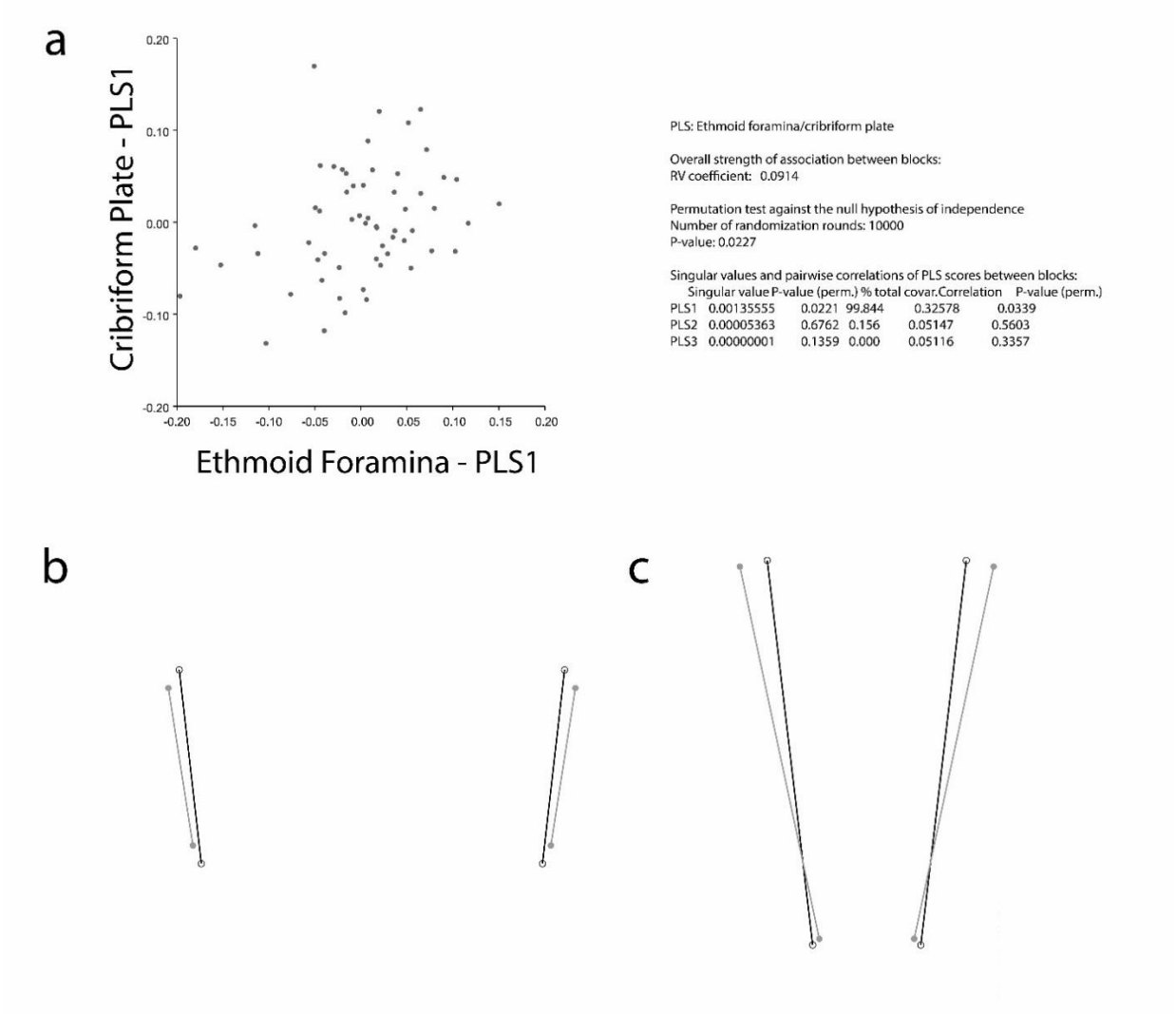

PLS – Upper Airways

The results of the two-block PLS for the ethmoid foramina and cribriform plate are presented in Figure 4.12. The wireframe graphs (Fig.4.12b,c) suggest an inverse relationship between the anteroposterior length between the ethmoid foramina and the length of the cribriform plate – longer cribriform plates correlate with smaller distances between ethmoid foramina; however, the correlation observed between these two modules is negligible (RV=0.0914).

Figure 4.13: *Within-configuration PLS, upper airways. (a) Projection of individuals along the first singular warp (PLS1) of the upper airways. (b) Average shapes (grey) and positive shape deformations (black; scale factor 0.1) of the ethmoid foramina (lateral lines), and the cribriform plate (medial lines; superior aspect, anterior is down).*

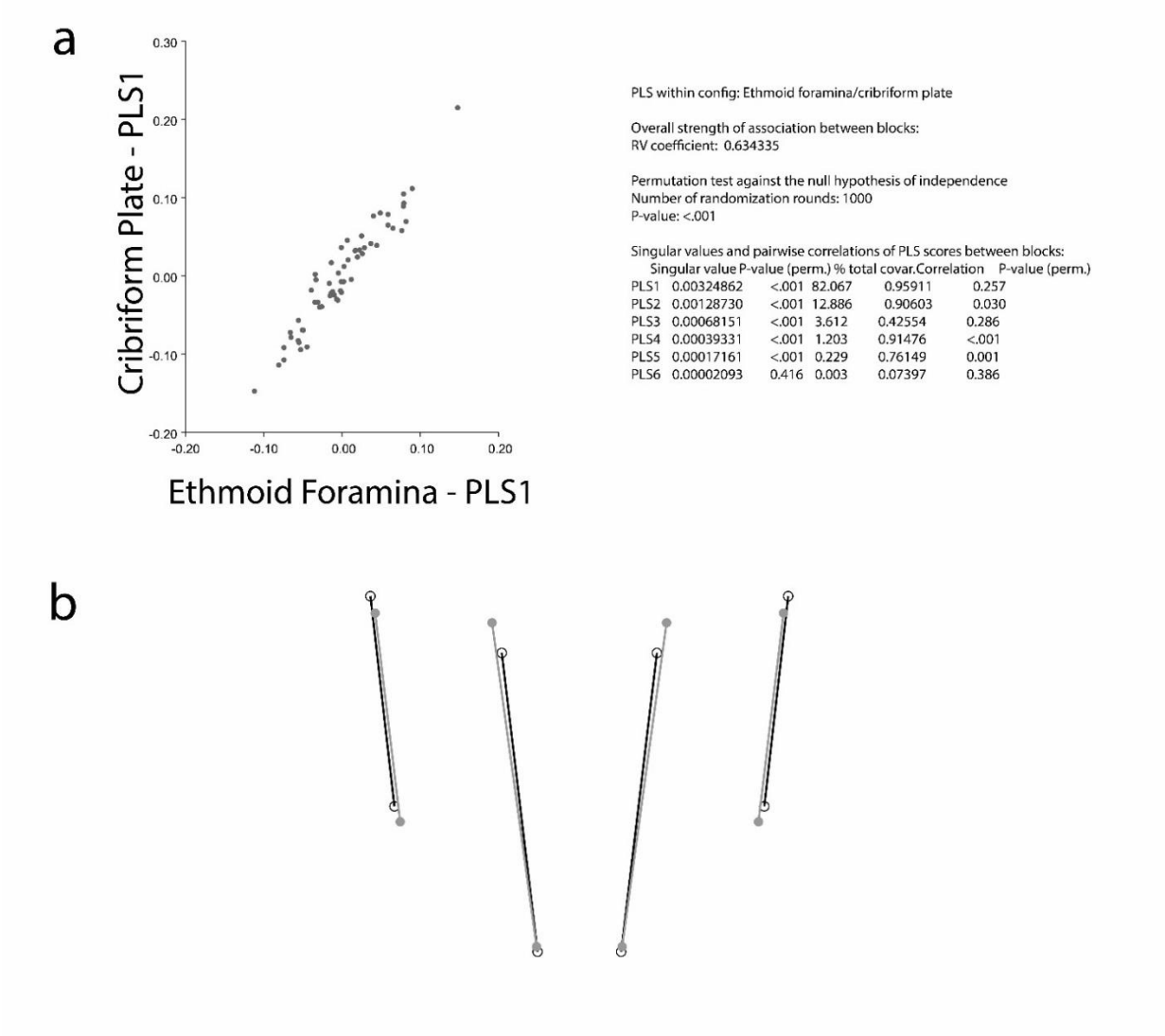

The two-block PLS removes size and orientation information, but in this case size-free shape data does not necessarily reveal the true shape relationship in question. The within-block PLS (Fig.4.13) preserves the relative size and orientation of the blocks, which overestimates the degree of morphological covariation (RV= 0.6343). Regardless, when size and orientation are included in the analysis, a slightly different picture of covariation emerges (Fig.4.13b). Along the first singular warp, which accounts for 95.911% of the variation, apparently inverse relationships

are observed, to some degree, between: 1) the anteroposterior distance between the ethmoid foramina and the length of the cribriform plate; 2) the mediolateral distance between ethmoid foramina and the breadth of the cribriform plate; and 3) the anteroposterior position of each block relative to one another.

Chapter 5: Discussion

Craniofacial Integration

One of the main goals of this thesis is to explore the nuances of the previously-established relationships between the basicranium and the face (Bastir and Rosas 2006; Gkantidis and Halazonetis 2011). Following from earlier work which established the integrative role of cranial base angulation in brain/face interactions (e.g. Ross and Ravosa 1993; Ross and Henneberg 1995; Lieberman and McCarthy 1999; McCarthy 2001; Lieberman et al. 2000ab, 2008), more recent research has focused on the role of lateral parts of the cranial base in craniofacial integration (e.g Spoor 1999; Bastir et al. 2008; Bastir and Rosas 2006, 2009; Gkantidis and Halazonetis 2011). The results of my PLS analysis largely conform to the results of these previous studies and allow for interpretations of lateral cranial base/face integration at a greater resolution.

Whereas Bastir and Rosas (2006) and Gkantidis and Halazonetis (2011) found a stronger integrative relationship between the lateral cranial base and the face than between the midline cranial base and face in 2D lateral radiographs, I tested the hypothesis that the same patterns can be demonstrated in 3D; the results of the PLS analyses support this hypothesis. A stronger correlation was found between the lateral cranial base and face (RV=0.2790) than between the midline cranial base and the face (RV=0.1957). The main component of these integrative shape changes (PLS1) appears to be related to rotational displacement of lateral parts of the cranium relative to the midline; this finding reflects a dimension that is not observable in the previous 2D studies, and it allows for a new perspective on this integrative relationship.

In the lateral cranial base, the primary component of shape change relates to the rotation of

the petrous pyramids and the MCF, a dimension of variability that has been observed across primate evolution and human ontogeny (Spoor 1997; Lieberman 2011). The first singular warp (Fig.4.8) shows that anterior rotation of the lateral margins of the MCF relative to the midline is correlated with an anterior rotation of the lateral parts of the face (the orbits and cheekbones) relative to the midline (the nasal bridge and dental arcade). This phenomenon also supports previous suggestions that cranial base breadth limits facial breadth, and that narrow faces tend to be relatively taller and anteroposteriorly longer (Lieberman et al. 2000b).

The results of all six PLS analyses are internally consistent. In each analysis, the first singular warp represents the same dimension of shape change for each module: angulation and length in the midline base; petrous rotation and MCF depth in the lateral base; tall/narrow vs. short/wide faces; and height, breadth, and opening dimensions in the nasal cavity. It can therefore be interpreted that each of the local relationships between modules explored in this thesis collectively represent a single global pattern of craniofacial integration, which can be distilled to dolichocephalic vs. brachicephalic morphologies. Brachycephalic individuals have extended (retroflexed) and long midline cranial bases, relatively coronally (anteriorly) rotated petrous pyramids, and associated anterior rotation in the lateral parts of the face; the outward and forward rotation of the lateral parts of the cranium result in wider cranial bases and faces, and the extension of the cranial base is associated with shallower MCFs and shorter faces, while the nasal cavity morphology is proportional to the face and cranium overall – short, broad faces and crania have short, broad nasal cavities.

This consistency suggests the principal integrative relationships between craniofacial modules observed herein are mediated by a common global mechanism rather than independently

by local mechanisms, and it is likely that brain development plays a major role in these patterns. The most significant component of shape change observed in the lateral cranial base, the anterior rotation of the MCF and petrous pyramids, conforms to previously established patterns of evolutionary integration between the brain and MCF in primates (Bastir et al. 2008), which are understood to reflect size and shape changes in the temporal lobes and cerebellum. Integration between the brain and cranial base subsequently has a cascading effect on the morphology of the developing face: Parsons et al. (2011) found a covariation between brain and face shape experimentally in mouse embryos; after controlling for environment, genetic variation, and allometry, the authors suggest this covariation potentially results from the integrative influence of growth factors in the developing head, but more likely from direct physical integration between growing modules. Because the facial skeleton develops later than both the brain and the chondrocranium, it is likely that variation in brain morphology, in combination with chondrocranial morphology, plays a major role in patterns of overall face shape. While these results conform to this assertion, it is beyond the scope of this paper to speculate on causation.

The Role of the Nasal Cavity

Given that covariation between climate and both nasal cavity morphology and cranial base breadth has been observed independently in cold-climate populations, this paper sought to investigate the integrative relationship between the nasal cavity and the lateral cranial base. The results do not support the hypothesis that these two modules express a higher degree of integration that other modules. The PLS analysis of lateral base/nasal covariation found only a relatively moderate correlation (RV=0.2454) between these two modules. While this value is similar to the others observed, it is the second lowest out of the six relationships tested – the only weaker

relationship observed was between the face and midline base (RV=0.1957).

Interestingly, the strongest two relationships observed were between the face and nasal cavity (RV=0.3123) and between the midline and lateral cranial base (RV=0.2884). These results are not surprising since these relatiopnships represent two ontogenetically distinct regions (the viscerocranium and chondrocranium, respectively). However, they do somewhat contradict previous studies that suggest a degree of modular independence between the midline and lateral cranial base (Bastir and Rosas 2009), and of the nasal cavity within the face as a whole (Bastir and Rosas 2013).

The results of this study do not indicate that facial/basicranial integration is strongly influenced by nasal cavity morphology. The strength of the correlation between the face and nasal cavity seems to suggest that nasal cavity morphology is highly dependent on the shape of the head it finds itself in: tall faces have tall nasal cavities, broad faces have broad nasal cavities. Relationships between the lateral cranial base and nasal cavity are mediated by the lateral base's relationship with the face, reflecting the same common global pattern of cranial integration described above. The midline and lateral base are developmentally integrated, and flexion and length of the midline base correlates with petrous rotation and MCF depth, following the pattern that has been well established, possibly influenced by expansion of the developing brain atop the size constraints imposed by the cranial base (Lieberman 2011); likewise, the nasal cavity is centrally integrated in the entire facial complex, possibly reflecting their common embryogenetic origins and/or complex patterns of integration within the face as a whole.

Selection in Cold Climates

While these results allow for a tidy interpretation of overall patterns of cranial integration, the question of the influence of natural selection remains elusive. While a modest correlation was observed between the lateral cranial base and the nasal cavity (RV=0.2454), the morphological relationship between them is opposite to that which should be predicted based on previous studies: selection for cold climates should hypothetically favour brachycephalic (wide cranial base) morphologies (Beals et al. 1983, 1984) as well as tall and narrow nasal airways (Noback et al. 2011); however, these results suggest that wider cranial bases correlate with relatively wider and shorter nasal airways (Fig. 4.9). Therefore, the hypothetically optimal cold-climate morphology of wide base and tall and narrow airway is at odds with the global pattern of integration outlined above. There are several possible explanations for this apparent paradox.

Most obviously, this may reflect the lack of a cold-climate population in the sample. The second hypothesis assumes that integrated cold-adapted morphologies in the cranial base and nasal cavity would be the result of general patterns of cranial integration common to all populations (i.e. dolicho/brachycephaly). However, while general brachycephalic morphology might be selected for in cold climates (Beals et al. 1983, 1984), it is possible that nasal morphology is influenced independently by some novel mechanism localized to the nasal cavity, which would represent a unique adaptive morphology in cold-climate populations.

Conversely, it may reflect the fact that the studies on selection in cold climates did not sample identical cold-climate populations. To observe relationships between climate and cranial shape, Beals et al. (1983,1984) employed large databases with as many as 362 global populations; Noback et al. (2011) only included ten populations, two of which were from cold climates (Greenland and Siberia), and only sampled ten individuals per population. Because Noback et al.

(2011) only recorded nasal morphology, and not basicranial breadth, it is impossible to say that the tall/narrow cold climate nasal morphologies they observed actually contradict the patterns of integration observed in this study, because it is not known whether they are actually associated with dolicho- or brachycephalic morphologies, and therefore the assumed contradiction may not be such.

With both of these considerations in mind, a closer examination of the results may hint at a unique mechanism characterizing integration between the nasal cavity and other parts of the skull. The PLS analyses both of the nasal cavity and face, and the nasal cavity and lateral cranial base, were characterized by a higher correlation coefficient on PLS3 than on PLS1 (RV=0.71840 vs. 0.67315 and 0.69575 vs. 0.61803, respectively), which were more statistically significant. While, in both cases, PLS3 only represents a small proportion of the total variation within the sample, this might suggest a mechanism influencing nasal cavity morphology, apart from the general integrative trends associated with dolicho/brachicephaly, which results in unique integrative relationships between the nasal cavity and the face and cranial base respectively. This could represent the integrative relationship between the lateral cranial base and the nasal cavity associated with climatic adaptation, sought in the second hypothesis; due to the homogeneity of the sample and the lack of a cold climate population, there may not be enough variation along this dimension within the sample to leave a strong signature.

However, this is probably not the case, as the shape variation in the nasal cavity in both analyses is primarily related to the angulation of the nasopharynx and the area of the choanae (Figure 4.10), both of which are related to adaption to hot and humid climates – while the nose and internal nasal cavity are implicated more strongly in air conditioning on inspiration, the

nasopharynx and internal nares play a bigger role in moisture and heat retention on expiration (Noback et al. 2011; Holton et al. 2013). Therefore, it is unlikely that this dimension of shape variability reflects adaptation to cold climates. Nevertheless, it does hint at a unique integrative mechanism which characterizes the relationships between the nasal cavity and the rest of the skull, and suggests that it may be fruitful to continue exploring these relationships.

Finally, this discrepancy might be the result of differences in landmarks employed. Both Noback et al. (2011) and Bastir et al. (2011) used the anterior and posterior ethmoid foramina as a proxy for upper airway morphology, because their sample consisted of digitized surface scans of dry skulls, and they were therefore limited to ectocranially observable landmarks; because CT scans have no such limitation, upper airway morphology was recorded based on the dimensions of the cribriform plate, which represents the actual roof of the airways and therefore better reflects the upper airway dimensions.

Methodological Considerations

Landmark selection methodology has comprised a large part of this thesis, and the problem of the suitability of selected landmarks to authors' research questions deserves significant attention. In order to investigate the suitability of the ethmoid formina as a proxy for upper airway dimensions, I conducted a two-block PLS analysis of the anterior and posterior ethmoid foramina and the anterior and posterior corners of the cribriform plate (Fig.4.11). (It is assumed *a priori* that the dimensions of the cribriform plate better reflect the actual dimensions of the internal airway, since they actually comprise part of the roof or the airway, while the ethmoid foramina are somewhat spatially displaced by the lateral masses). If the ethmoid foramina represented a suitable proxy for the internal nasal airways, a strong correlation between these structures should be

expected; this is not the case. Only a very weak correlation (RV=0.0914) was observed between these structures, and the shape correlations do not seem to be very informative (Fig.4.11b,c): differences in relative length between anterior and posterior ethmoid foramina do not appear to be correlated with changes in length in the cribriform plate. The correlation coefficient is low enough that these relationships are negligible.

It should be noted that, because procrustes is performed on these blocks separately, this analysis cannot yield valid results of the length/breadth relationships of these blocks are not isometric: if the shapes only differ in length, but not breadth, procrustes will scale the blocks to a common centroid size, obscuring the relationships of both dimensions.

Therefore, a second, within-configuration PLS was conducted to better investigate this relationship. While the within-config PLS was not appropriate for observing patterns of integration in the primary analysis, it is in this case because it retains size and orientation information between modules, and the suitability of these landmarks as a proxy is dependent on their relative size and orientational relationships. The within-config PLS (Fig.4.12) shows a relatively strong correlation between these modules (RV=0.6343), which is to be expected, since the size and orientation information exaggerate the strength of the relationship. Significantly, however, the correlation reflects an inverse morphological relationship between the two modules in the first PLS, in all dimensions (Fig.4.12b): a relatively greater breadth of the cribriform plate correlates with a medial displacement of both anterior and posterior ethmoid foramina; relatively longer cribriform plates correlate with very slightly shorter anteroposterior distances between the ethmoid foramina (although very little difference in anteroposterior distance is observed between ethmoid foramina in the first PLS); and a relative posterior displacement of the cribriform plate as a whole correlates

with an anterior displacement of the ethmoid foramina. These results indicate that the ethmoid foramina may not be acceptable proxy for the length, breadth, or relative position of the upper airways.

The implications of this on the results are unclear. The primary components of shape variation observed herein are essentially the same as those published by authors employing ethmoid foramina in their datasets: in all analyses, nasal cavities with larger, wider, and shorter nasal openings and choanae also had shorter and broader upper airways, conforming to the patterns observed in relations to climatic adaptation (Noback et al. 2011) and sexual dimorphism (Bastir et al 2011), suggesting the influence is negligible. It may be that in the broader context of the face, the inverse shape correlation observed between these landmarks is overshadowed by greater common positional and shape differences relative to other facial structures, e.g. the superoinferior position of both modules within the face, relative to the lower nasal airways, may be much greater than the superoinferior discrepancy between the two, such that the net difference remains relatively true to the biological reality.

Nonetheless, these results highlight the importance of clarity and transparency with regards to the publication of craniometric landmarks in geometric morphometric analyses. A common theme in landmark-based studies identified in this thesis is a complete lack of any discussion of landmark selection methodology. As discussed in the Methods section, this poses significant problems for replicability of results, as in cases where non-traditional landmarks are not clearly described or are described incorrectly. More importantly, in cases such as the ethmoid foramina, where landmarks are employed without evidence that they actually represent the shape variation in question, they may cast doubt on the results altogether.

Chapter 6: Conclusions

This thesis sought to test two primary hypotheses: 1) patterns of integration between the face and cranial base observed in 2D can be replicated in 3D; and 2) the lateral cranial base and nasal cavity are characterized by a higher degree of covariation with one another than they do with other cranial modules.

The first hypothesis is supported by the results: a greater correlation coefficient was observed between the lateral cranial base and face than between the midline cranial base and face in landmark-based geometric morphometric analyses. These results also provide a greater resolution than previous 2D analyses: all analyses suggest that the most significant integrative relationships between cranial modules reflect dolicho/brachycephalic morphologies. These integrative relationships likely reflect developmental interactions between genetically-patterned brain and chondrocranial morphology and physical integration with the face: the brain and chondrocranium develop early in ontogeny, influencing facial morphology through cascading integrative effects in the lateral cranial base.

The second hypothesis is not supported: the nasal cavity and lateral cranial base do not exhibit a stronger integrative relationship with one another than they do with other cranial modules. However, the results do hint at a potential distinct relationship between nasal cavity morphology and that of the face and cranial base, outside of the general dolicho/brachycephalic pattern. Because this analysis is limited by a small sample size and homogeneity of population, it is possible that this reflects a different mechanism of nasal cavity integration underlying population-specific differences in nasal morphology related to climatic adaptation. This will be the purview of future research.

This thesis also highlights the problem of landmark selection methodology. The continuous nature of cranial variation is seemingly at odds with developing a consistent and repeatable landmark selection methodology applicable to all geometric morphometric analyses, and it is likely that morphometricians will need to develop unique landmark sets to suit different craniometric goals. In particular, the use of the ethmoidal foramina as a proxy for the internal dimensions of the upper airways (Noback et al. 2011; Bastir et al. 2011) cannot be recommended based on the results of this thesis. Therefore it is critical to include clear descriptions/definitions of landmarks, and to assess landmarks individually for their suitability to specific research questions, in order for the results to be valid, and to allow for replicability by other authors.

References

Bastir M & Rosas A. 2006. Correlated variation between the lateral basicranium and the face: A geometric morphometric study in different human groups. *Archives of Oral Biology 51*: 814-824.

Bastir M & Rosas A. 2009. Mosaic evolution in the basicranium of *Homo* and its relation to modular development. *Evolutionary Biology 36*: 57-70.

Bastir M & Rosas A. 2013. Cranial airways and the integration between the inner and outer facial skeleton in humans. *American Journal of Physical Anthropology 152*:287-293.

Bastir M, Rosas A, Lieberman DE & O'Higgins P. 2008. Middle cranial fossa anatomy and the origin of modern humans. *The Anatomical Record 291*: 130-140.

Bastir M, Rosas A, Stringer C, Cuétara JM, Kruszynski R, et al. 2010. Effects of brain and face size on basicranial form in human and primate evolution. *Journal of Human Evolution 58:*424-431.

Bastir M, Godoy P & Rosas A. 2011. Common features of sexual dimorphism in the cranial airways of different human populations. *American Journal of Physical Anthropology 146*:414-422.

Beals KL, Smith CL & Dood SM. 1983. Climate and the evolution of brachycephalization. *American Journal of Physical Anthropology 62:*425-437.

Beals KL, Smith CL, Dodd SM, Angel JL, Armstrong E et al. 1984. Brain size, cranial morphology, climate, and time machines. *Current Anthropology 25*(3):301-330.

Bernstein RM. 2010. The big and small of it: How body size evolves. *Yearbook of Physical Anthropology 53*:46-62.

Biegert J. 1963. The evaluation of characteristics of the skull, hands and feet for primate taxonomy. Pp. 116-145 in *Classification and Human Evolution* (SL Washburn, ed.). Chicago: Aldine Publishing Company.

Bookstein FL, Gunz P, Mitteræcker P, Prossinger H, Schæfer K & Seidler H. 2003. Cranial integration in Homo: singular warps analysis of the midsagittal plane in ontogeny and evolution. *Journal of Human Evolution 44:*167-187.

Bookstein FL. 1991. *Morphometric Tools for Landmark Data: Geometry and Biology*. Cambridge University Press.

Boughner JC, Wat S, Diewert VM, Young NM, Browder LW & Hallgrímssion B. 2008. Short-faced mice and developmental interactions between the brain and the face. *Journal of Human Anatomy 213:*646-662.

Butaric LN, McCarthy RC & Broadfield DC. 2010. A Preliminary computed tomography study of the human maxillary sinus and nasal cavity. *American Journal of Physical Anthropology 143*:426-436.

Franciscus RG & Long JC. 1991. Variation in human nasal height and breadth. *American Journal of Physical Anthropology 85*:419-427.

Franciscus RG. 2003. Internal nasal floor configuration in Homo with special reference to the evolution of Neandertal facial form. *Journal of Human Evolution 44:*701–729.

Gkantidis N & Halazonetis DJ. 2011. Morphological integration between the cranial base and the face in children and adults. *Journal of Anatomy 218*: 426-438.

Gray H. 2005. *Gray's Anatomy: The Anatomical Basis of Clinical Practice* (Standring S, Ellis H & Berkovitz BKB, Eds.). New York: Elsevier Churchill Livingstone.

Hammer, Ø. 2012. PAST: PAleontological Statistics 2.16, Reference Manual. Natural History Museum, University of Oslo.

Harvati K & Weaver TD. 2006. Human cranial anatomy and the differential preservation of population history and climate signatures. *The Anatomical Record Part A 288A*: 1225-1233.

Holton NE & Franciscus RG. 2008. The paradox of a wide nasal aperture in cold-adapted Neandertals: A causal assessment. *Journal of Human Evolution 55:*942–951.

Huxley, TH. 1867. On two widely contrasted forms of the human cranium. *Journal of Anatomy and Physiology, 1*(1), 60–77.

Jeffery N. 2005. Cranial base angulation and growth of the human fetal pharynx. *The Anatomical Record Part A 284A:*491-499.

Jeffery N & Spoor F. 2004. Ossification and midline shape changes of the human fetal cranial base. *American Journal of Physical Anthropology* 123:78-90.

Klingenberg CP. 2011. MorphoJ: an integrated software package for geometric morphometrics. *Molecular Ecology Resources 11:*353-357.

Lieberman DE. 2011. *The Evolution of the Human Head*. The Belknap Press of the University of Harvard Press.

Lieberman DE & McCarthy RC. 1999. The ontogeny of cranial base angulation in humans and chimpanzees and its implications for reconstructing pharyngeal dimensions. *Journal of Human Evolution 36*:487-517.

Lieberman DE, Hallgrímsson B, Liu W, Parsons TE & Jamniczky HA. 2008. Spatial packing, cranial base angulation, and craniofacial shape variation in the mammalian skull: Testing a new model using mice. *Journal of Anatomy 212*:720-735.

Lieberman DE, Ross CF & Ravosa MJ. 2000a. The Primate cranial base: ontogeny, function, an integration. *Yearbook of Physical Anthropology* 43:117-169.

Lieberman DE, Pearson OM & Mowbray KM. 2000b. Basicranial influence on overall cranial shape. *Journal of Human Evolution 38*:291-315.

Lupu G, Popescu D, Panus V & Popescu G. 2010. Ontogenetic landmarks of the organ of hearing in fetal age determination. *Romanian Journal of Legal Medicine 2*:129-132.

McCarthy RC. 2001. Anthropoid cranial base architecture and scaling relationships. *Journal of Human Evolution 40*:41-66.

McCarthy RC & Lieberman DE. 2001. Posterior maxillary (PM) plane and anterior cranial architecture in primates. *The Anatomical Record 246*:247-260.

Mitterœcker P & Bookstein F. 2008. The evolutionary role of modularity and integration in the hominoid cranium. *Evolution 62*:943-958.

Monkhouse S. 2006. *Cranial Nerves: Functional Anatomy*. Cambridge University Press.

Moore WJ & Lavelle CLB. 1974. *Growth of the Facial Skeleton in the Hominoidea*. London: Academic Press.

Moss ML. 1968. A Theoretical analysis of the functional matrix. *Acta Biotheoretica 18*(1):195-202.

Moss ML. 1997a. The functional matrix revisited 1: The role of mechanotransduction. *American Journal of Orthodontics and Dentofacial Orthopedics 122*(1):8-11.

Moss ML. 1997b. The functional matrix revisited 2: The role of an interosseus connected cellular network. *American Journal of Orthodontics and Dentofacial Orthopedics 122*(2):221-226.

Moss ML. 1997c. The functional matrix revisited 3: The genomic thesis. *American Journal of Orthodontics and Dentofacial Orthopedics 122*(3):338-342.

Moss ML. 1997d. The functional matrix revisited 4: The epigenetic antithesis and the resolving synthesis. *American Journal of Orthodontics and Dentofacial Orthopedics 122*(4):410-417.

Moss ML, Bromberg BE, Song IC & Eisenman G. 1968. The Passive role of nasal septal cartilage in mid-facial growth. *Plastic and Reconstructive Surgery* 41(6):536-542.

Moss ML & Salentijn L. 1969. The primary role of functional matrices in facial growth. *American Journal of Orthodontics 55*(6):566-577.

Neubauer S, Gunz P & Hublin J-J. 2009. The patterns of endocranial ontogenetic shape changes in humans. *Journal of Anatomy 215*: 240-255.

Noback ML, Harvati K & Spoor F. 2011. Climate-related variation of the human nasal cavity. *American Journal of Physical Anthropology 145*: 599-614.

Nowaczewska W, Dabrowski P & Kuzminski L. 2011. Morphological adaptation to climate in modern *Homo sapiens* crania: The importance of basicranial breadth. *Collegium Anthropologicum 35*: 625-636.

Reyment RA. 2010. Morphometrics: An historical essay. Pp.9-24 in *Morphometrics for Nonmorphometricians* (AMT Elewa, ed.). New York: Springer.

Rosas A, Bastir M, Martínez-Maza C, García-Tabernero A & Lalueza-Fox C. 2008. Inquiries into Neanderthal craniofacial development and evolution: "accretion" versus "organismic" models. Pp. 37-70 in *Neanderthals Revisited: New Approaches and Perspectives* (K. Harvati and T. Harrison, eds.). Springer.

Ross A & Williams S. 2008. Testing repeatability and error of coordinate landmark data acquired from crania. *Journal of Forensic Science 53*(4):782-785.

Ross CF & Ravosa MJ. 1993. Basicranial Flexion, Relative Brain Size, and Facial Kyphosis in Nonhuman Primates. *American Journal of Physical Anthropology 91*:305-324.

Ross CF & Henneberg M. 1995. Basicranial flexion, relative brain size, and facial kyphosis in *Homo sapiens* and some fossil hominids. *American Journal of Physical Anthropology 98*:575-593.

Schwartz JH. 1995. *Skeleton Keys: An Introduction to Human Skeletal Morphology, Development and Analysis*. New York: Oxford University Press.

Slice DE. 2007. Geometric Morphometrics. *Annual Review of Anthropology 36*:261-281.

Slice DE. 2005. Modern Morphometrics. Pp. 1-45 in *Modern Morphometrics in Physical Anthropology* (DE Slice, ed.). New York: Kluwer Academic/Plenum Publishers.

Smith KK. 1996. Integration of craniofacial structures during development in mammals. *American Zoology 36*:70-79.

Sperber GH, Sperber SM & Guttmann GD. 2010. *Craniofacial Embryogenetics & Development, 2nd edition*. People's Medical Publishing House - USA

Spoor F. 1997. Basicranial architecture and relative brain size of Sts 5 (*Australopithecus africanus*) and other Plio-Pleistocene hominids. *South African Journal of Science 93*:182-186.

White TD & Folkens PA. 2005. *The Human Bone Manual*. Elsevier Academic Press.

Young NM, Chong HJ, Hu D, Hallgrímsson B & Marcucio RS. Quantitative analyses link modulation of sonic hedgehog signaling to continuous variation in facial growth and shape. *Development 137:*3405-3409.

Zelditch ML, Swidersdki DL & Sheets HD. 2012. Geometric Morphometrics for Biologists: A Primer (2nd Edition). St. Louis: Academic Press.

Zelditch ML, Lundrigan BL & Garland T Jr. 2004. Developmental regulation of skull morphology. I. Ontogenetic dynamics of variance. *Evolution and Development 6*(3):194-206.

Appendix A: JFREB Human Ethics Approval Certificate

UNIVERSITY OF MANITOBA | Research Ethics and Compliance
Office of the Vice-President (Research and International)

Human Ethics
208-194 Dafoe Road
Winnipeg, MB
Canada R3T 2N2
Phone +204-474-7122
Fax +204-269-7173

APPROVAL CERTIFICATE

February 13, 2014

TO: **Joshua Lindal** (Advisor M. Roksandic)
Principal Investigator

FROM: **Susan Frohlick, Chair** [redacted]
Joint-Faculty Research Ethics Board (JFREB)

Re: **Protocol #J2013:172**
"The Role of the nasal cavity in patterns of human craniofacial covariation and integration"

Please be advised that your above-referenced protocol has received human ethics approval by the **Joint-Faculty Research Ethics Board**, which is organized and operates according to the Tri-Council Policy Statement (2). **This approval is valid for one year only**.

Any significant changes of the protocol and/or informed consent form should be reported to the Human Ethics Secretariat in advance of implementation of such changes.

Please note:

- **If you have funds pending human ethics approval, please mail/e-mail/fax (261-0325) a copy of this Approval (identifying the related UM Project Number) to the Research Grants Officer in ORS in order to initiate fund setup. (How to find your UM Project Number: http://umanitoba.ca/research/ors/mrt-faq.html#pr0)**

- **if you have received multi-year funding for this research, responsibility lies with you to apply for and obtain Renewal Approval at the expiry of the initial one-year approval; otherwise the account will be locked.**

The Research Quality Management Office may request to review research documentation from this project to demonstrate compliance with this approved protocol and the University of Manitoba *Ethics of Research Involving Humans*.

The Research Ethics Board requests a final report for your study (available at: http://umanitoba.ca/research/orec/ethics/human_ethics_REB_forms_guidelines.html) **in order to be in compliance with Tri-Council Guidelines.**

Appendix B: Sample Consent Form

Informed Consent

Study Title: The role of the nasal cavity in patterns of human craniofacial integration and covariation

Principle Investigator: Joshua Lindal, Master's student, Department of Anthropology, UofM
--**** **********@gmail.com

Sponsor: NSERC

This consent form, a copy of which will be left with you for your records and reference, is only part of the process of informed consent. It should give you the basic idea of what the research is about and what your participation will involve. Participation is voluntary and declining to participate will not influence your medical care nor will it have any negative consequences. If you would like more detail about something mentioned here, or information not included here, you should feel free to ask. Please take the time to read this carefully.

The study in which you are invited to participate is a Master's thesis, to be completed by Joshua Lindal, the principal investigator. Dr. Mirjana Roksandic is the thesis supervisor, and this study has been supported by a National Sciences and Engineering Research Council (NSERC) Canadian Graduate Student grant. The purpose of this research is to investigate the relationship between the shape of bones in the face and the shape of the base of the skull (the area around the ears and the joint of the jawbone). It is known that the shape of people's nasal airways is related to the climate in which their ancestors lived – people from cold climates have taller airways to warm and humidify the air they breathe; it is also known that people from cold climates tend to have wider skull bases. By looking for patterns in the shapes of these two structures, it should help us to understand how forces of genetics and evolution have shaped the differences in skull shape between different human populations. As a student of paleoanthropology, I intend to use these interpretations as a foundation for future research into a group of ancient humans, the Neanderthals, who lived in cold climates and who have uniquely-shaped skulls. The skulls of living people are shaped differently from those of Neanderthals, but the growth and development of their bones would have followed the same general rules as humans living today. Therefore, the shapes of modern humans' skulls cannot be directly compared to those of Neanderthals; instead, the patterns I hope to find in living human skulls will help to understand the rules of how skulls grow, and these rules will be relevant information for future studies trying to find out why Neanderthal skulls grew in different shapes from our own.

The project will consist of a statistical analysis of measurements taken on Computed Tomography (CT) scans of skulls provided by Dr. F.G. Osler obtained in the course of medical practice. These scans consist of series of two-dimensional X-ray images that can be used to recreate a 3D model of a patient's skull. By agreeing to participate in this study, you would be consenting to the secondary use of your CT scans by the principal researcher for the purposes of this study. Your participation would be limited to this one-time communication and the study does not require continued contact or communication, although you should feel free to contact the principal investigator, Joshua Lindal, if you have any followup questions.

Because there is no direct physical contact or continued communication required with participants, there are no immediate physical or psychological risks involved. Participants should not expect any

direct benefit from participation in this study. Expected benefits are theoretical: they will contribute to our general body of knowledge of human variation and evolution.

You are under no obligation to participate in this study, and declining to participate will not influence your medical care nor will it have any negative consequences. To protect the privacy of participants, the scans will be anonymized (i.e. given an anonymous number code) so the researcher will not have access to any personal information, including names, and participants' names and individual scans will not be included in the final report. As a general principle of the Tri-Council Policy Statement on Ethical Conduct for Research Involving Humans, participants have the right to withdraw consent and request that their data be removed from the study at any time; however, you should be aware that because the scans will be anonymized, once you gave given permission for your materials to be included, it may be impossible to remove them from the study if you change your mind.

This study will be submitted to relevant scholarly journals for publication. It will also be made accessible to interested researchers as a Master's thesis deposited at the University of Manitoba. The names or personal information of any participants will not be included in the report, and it will not include any reference to any individual scans; the report will only discuss the statistical averages of the shape measurements within the sample groups.

If you desire a more detailed explanation of the scientific aspects of this study, if you want clarification on any of the information presented in this form or a more detailed explanation of this research, or if you want to learn more about how this study will contribute to the field of paleoanthropology, you should feel free to contact the principal investigator, Joshua Lindal, directly.

This research has been approved by the Research Ethics Board at the University of Manitoba. If you have any concerns or complaints about this project you may contact the Human Ethics Secretariat at 204-474-7122, or by e-mail at Margaret_Bowman@umanitoba.ca.

If you consent to the use of your CT scan data in this study, your data will be obtained from Dr. Osler via a password-protected external hard drive and will be transferred to a computer at the University of Manitoba. The data will be anonymized and stored on a password-protected computer in the private locked lab of Dr. Robert Hoppa (N304, Duff Roblin) at the University of Manitoba. The hard drive will be returned to Dr. Osler and the study will be completed using the anonymized data only. In addition to this CT scan data, this study will require knowledge of participants' sex, because of size and shape differences between males and females, and ancestry, in order to determine participants' ancestral climates. No other personal information that would allow the identification of participants is required. All data will be deleted from the computer upon completion of the study. Individual participants' data may be excluded from the study in the event of skeletal pathologies or abnormalities that obscure the measurement of critical structures.

Your signature on this form indicates that you have understood to your satisfaction the information regarding participation in the research project and agree to participate as a subject. In no way does this waive your legal rights nor release the researchers, sponsors, or involved institutions from their legal and professional responsibilities.

Participant's Signature Date

Researcher and/or Delegate's Signature Date

- -

If you wish to receive a summary of the results, please leave your email address or other preferred means of contact below. This information will be stored separately from your experimental data.